Check for updates

Porphyrin-based frameworks for oxygen electrocatalysis and catalytic reduction of carbon dioxide

Zuozhong Liang, [ID] † Hong-Yan Wang, [ID] † Haoquan Zheng, [ID] Wei Zhang [ID] and Rui Cao [ID] *

Porphyrin-based frameworks, as specific kinds of metal–organic frameworks (MOFs) and covalent organic frameworks (COFs), have been widely used in energy-related conversion processes, including the oxygen reduction reaction (ORR), oxygen evolution reaction (OER) and CO_2 reduction reaction (CO_2RR), and also in energy-related storage technologies such as rechargeable Zn–air batteries. This review starts by summarizing typical crystal structures, molecular building blocks, and common synthetic procedures of various porphyrin-based frameworks used in energy-related technologies. Then, a brief introduction is provided and representative applications of porphyrin-based frameworks in ORR, OER, Zn–air batteries, and CO_2RR are discussed. The performance comparison of these porphyrin-based frameworks in each field is also summarized and discussed, which pinpoints a clear structure–activity relationship. In addition to utilizing highly active porphyrin units for catalytic conversions, regulating the porous structures of porphyrin-based frameworks will enhance mass transfer and growing porphyrin-based frameworks on conductive supports will accelerate electron transfer, which will result in the improvement of the electrocatalytic performance. This review is therefore valuable for the rational design of more efficient porphyrin-based framework catalytic systems in energy-related conversion and storage technologies.

Key Laboratory of Applied Surface and Colloid Chemistry, Ministry of Education, School of Chemistry and Chemical Engineering, Shaanxi Normal University, Xi'an 710119, China. E-mail: ruicao@snnu.edu.cn

† These authors contributed equally to this work.

Dr Zuozhong Liang is currently an associate research fellow in the School of Chemistry and Chemical Engineering at Shaanxi Normal University. He received his BS (2011) from Qufu Normal University and PhD (2016) from Beijing University of Chemical Technology under the supervision of Professor Jian-Feng Chen. In July 2016, he joined the research group of Professor Rui Cao. His research interests focus on the design and development of novel functional nanomaterials for application in renewable-energy-related fields.

Zuozhong Liang

Dr Hong-Yan Wang received her PhD in organic chemistry in Chinese Academy of Sciences in 2011. In 2014, she joined the School of Chemistry and Chemical Engineering at Shaanxi Normal University as an associate professor. Her research interest concerns artificial photosynthesis using supramolecular systems, coordination compounds, and semiconductors. Now, she is working on the design of a photochemical device for water splitting, CO_2 reduction and organic synthesis.

Hong-Yan Wang

2540 | *Chem. Soc. Rev.*, 2021, **50**, 2540–2581

This journal is © The Royal Society of Chemistry 2021

1. Introduction

1.1 Porphyrin catalysis in biological systems

Porphyrins are a class of heterocyclic molecules connected with four pyrrole subunits and methylene bridges. In nature, porphyrins exist in coordination with metal ions. These metal porphyrins and their derivatives are commonly found in organelles related to energy transfer and play important roles in diverse biological functions, such as light-harvesting, electron transfer, oxygen (O_2) transport and activation, and many catalytic transformations.[1–4] For example, in plants, chlorophyll is an Mg porphyrin compound, which can absorb light. In animals, hemocyanin is a Cu porphyrin compound, which can carry and transport O_2.

In particular, heme is an Fe porphyrin compound.[5,6] It is not only a cofactor of hemoglobin, but also a cofactor of myoglobin, cytochrome, peroxidase, catalase, *etc.* Therefore, heme has multiple uses. For example, hemoglobin transports O_2 in red blood cells. Myoglobin transports and stores O_2 in muscle cells. Cytochromes *b* and *c* can transfer electrons. Peroxidase and catalase can catalyze the degradation of hydrogen peroxide (H_2O_2). It is worth mentioning that cytochrome *c* oxidase and cytochrome P450 can promote the activation and utilization of O_2.[7,8] Above all, Fe porphyrins play crucial roles in diverse O_2 and H_2O_2 related biological processes. Although these heme structures have the same Fe porphyrin unit, their functions can be fine-tuned by regulating the surrounding environment of metal porphyrins. For example, cytochrome *c* oxidase binds and activates O_2 at its heme Fe porphyrin site.[9] Upon O–O bond cleavage, a Fe^{IV}-oxo porphyrin cation radical is suggested to be formed, which is the key intermediate of the ORR for the selective four-electron (4e) reduction of O_2 to H_2O. The redox-active dianionic porphyrin structure is very effective in stabilizing this high-valent Fe^{IV}-oxo unit. In addition to the heme Fe porphyrin site, its surrounding environments, including the proximate Cu ion, Tyr^{244} residue, axial ligand and distal pocket environment, are suggested to play crucial roles in the 4e ORR process.[10–14]

1.2 Catalysis of synthetic porphyrin complexes

Inspired by nature, metal-coordinated porphyrin molecules have been extensively studied as catalysts for small molecule activation reactions.[15–22] The use of metal porphyrins as molecular catalysts has the following advantages from the aspect of coordination chemistry. First, porphyrin ligands can provide rigid and stable coordination environments for the incorporated metal ions. The resulting metal porphyrins are stable in both acidic and alkaline solutions. This unique stability feature provides the possibility for their practical application. Second, porphyrin ligands are redox-active, and thus can participate in redox processes. This feature can enrich the redox chemistry of metal porphyrins, making them beneficial for multielectron catalytic processes. Third, the porphyrin molecules can be modified systematically with different functional groups at

Haoquan Zheng

Dr Haoquan Zheng is currently an associate professor in the School of Chemistry and Chemical Engineering at Shaanxi Normal University. He received his BS (2006) and PhD (2011) in applied chemistry from Shanghai Jiao Tong University under the supervision of Professor Shunai Che. He worked as a postdoctoral fellow in the group of Professor Xiaodong Zou at Stockholm University. He moved to his current position in July 2016. His research interest lies in the development of hierarchical porous materials with novel structures and functions for drug delivery and heterogeneous catalysis.

Wei Zhang

Prof. Wei Zhang received his BS (2007) in chemistry from Peking University in Beijing, China and PhD degree (2012) from Nanyang Technological University in Singapore with Professor Rong Xu. After postdoctoral work in photocatalytic CO_2 reduction with Professor Rong Xu, he joined the School of Chemistry and Chemical Engineering at Shaanxi Normal University in 2014. His current research focuses on catalytic reactions of water splitting.

Rui Cao

Prof. Rui Cao received his BS (2003) in chemistry from Peking University in Beijing, China and his PhD (2008) from Emory University in Atlanta, Georgia, USA, with Professor Craig L. Hill. He worked as a Postdoctoral Fellow (2008–2009) at Emory University and was the Dreyfus Postdoctoral Fellow (2009–2011) at Massachusetts Institute of Technology with Professor Stephen J. Lippard. In 2011, he became a professor at Renmin University of China, and transferred to Shaanxi Normal University in 2014. His main research interests lie in bioinorganic chemistry and catalysis for energy-related small molecule activation reactions. He served on the Advisory Board of Chemical Society Reviews since 2019.

This journal is © The Royal Society of Chemistry 2021

Chem. Soc. Rev., 2021, **50**, 2540–2581 | **2541**

the *meso*- and β-positions. This feature will result in the diversity of metal porphyrins with different chemical and physicochemical properties. Fourth, due to the stable coordination environments, the second coordination spheres of metal porphyrins can be fine-tuned to further improve catalytic efficiency. Therefore, metal porphyrins have been widely used as electrocatalysts for oxygen electrocatalysis, including ORR and OER, and for CO_2RR.[23–26]

For catalytic ORR by metal porphyrins, it is generally proposed that O_2 first binds at the axial vacant site of metal centers and is subsequently reduced to H_2O_2 (two-electron (2e) pathway), H_2O (4e pathway) or a mixture of H_2O_2 and O_2 with transfer of electrons and protons in a concerted manner. The catalytic activity, long-term stability and selectivity of products depend on the nature of the molecular catalysts, especially metal active sites and functional substituents of porphyrin macrocycles. Inspired by cytochrome *c* oxidase present in nature, Chidsey, Collman, and co-workers synthesized Fe porphyrin model molecules and confirmed the high activity and selectivity of Fe porphyrins for the 4e ORR process.[12] Many other synthetic Fe porphyrins have been designed and synthesized as ORR catalysts by Nocera,[27] Dey,[28–31] Mayer,[32–35] Savéant,[36] *etc.*

In addition to Fe porphyrins, Co porphyrins have also attracted great attention for ORR catalysis and have been extensively investigated by Fukuzumi,[37,38] Kadish,[39] Girault,[40] and Nocera.[41] It is worth mentioning that unlike Fe porphyrins, mononuclear Co porphyrins display poor selectivity for the 4e ORR, and binuclear Co porphyrins are usually required to promote the 4e reduction of O_2 to H_2O.[42–44] Peroxo-bridged binuclear species are usually proposed as key intermediates involved in this 4e ORR process. Beyond that, a series of other transition metal porphyrins,[45–47] as well as other metal-N_4 coordination molecules, such as metal corroles and phthalocyanines,[48–55] have also been investigated as electrocatalysts for ORR. Based on these results, one can conclude that the activity and selectivity of porphyrins are largely determined by the nature of metal centers and surrounding environments.[56,57]

For catalytic OER, metal porphyrins have attracted increasing interest because of their ability to stabilize high-valent metal-oxo intermediates, which are generally considered to be involved as key intermediates during the O–O bond formation step.[58–64] Among these porphyrin molecules, water-soluble Ni and Cu complexes of 5,10,15,20-tetra(4-*N*-methylpyridyl)porphyrin have been reported by Cao and co-workers to be able to catalyze OER in neutral aqueous solutions with very low overpotentials.[65,66] Importantly, in addition to the 4e water oxidation to O_2 at neutral pH, the Cu porphyrin can catalyze the 2e water oxidation to H_2O_2 in acidic solutions. As structural analogues of metal porphyrins, metal corroles have also been studied as OER catalysts.[67–69] By introducing intramolecular acid/base functional groups, hangman Co corroles showed significantly improved efficiency, as compared to the non-hangman counterparts, for electrocatalytic OER by Nocera[70] and by Cao.[71] The hanging acid/base groups are suggested to have multiple roles in facilitating the O–O bond formation: they may pre-organize water molecules within the hangman cleft,[70] and they may also function as an intramolecular

proton acceptor to accelerate proton transfer during the water nucleophilic attack to form the O–O bond.[72]

In the past decade, porphyrins have attracted increasing interest as catalysts for electrochemical CO_2RR.[73–78] In particular, Fe porphyrins have been widely and extensively studied for CO_2RR by Costentin,[79] Robert,[80] Savéant,[81] Dey,[82–84] Nocera,[85,86] Cao,[87,88] Naruta,[89] and others.[90–93] Notably, Fe tetra-(*ortho*-trimethylanilinium)porphyrin displayed a state-of-the-art catalytic efficiency by reaching a turnover frequency (TOF) of 10^6 s^{-1} at an overpotential of 220 mV.[80] Other metal porphyrins, phthalocyanines, and other molecular catalysts such as Ni(cyclam) have also been synthesized and investigated as CO_2RR electrocatalysts by Shinobu,[94,95] Wang,[96] Fujita,[97] Kubiak,[98,99] and others. Based on these studies, it has been shown that high local proton concentrations and positive charges, which can be realized by introducing substituents at the *meso*-phenyl groups of porphyrin macrocycles, can significantly boost the CO_2RR performance.[79,82] In addition to the benefits of investigating the structure–function relationships, metal porphyrins have unique advantages for reaction mechanism studies owing to their stable and rigid coordination structures and also their suitable binding affinity with both CO_2 and CO.[73,100–102]

1.3 Porphyrin-based frameworks: a bridge between homogeneous and heterogeneous catalysts

Although porphyrin-based catalysts have shown high activity for ORR, OER, and CO_2RR in homogeneous catalysis,[3,103] their applications in electrocatalytic devices are limited because of the following facts. First, molecular complexes have very poor electrical conductivity and usually have very weak interactions with electrodes, leading to low electron transfer efficiency between molecular catalysts and electrodes. Second, for homogeneous electrocatalysis, only molecules close to the electrode surfaces can be oxidized or reduced for subsequent catalytic reactions. As a consequence, most of molecules dissolved in the solution do not participate in electrocatalytic processes. This results in low atom-utilization efficiency. Third, in homogeneous catalysis, difficulties in the recovery and reuse of molecular catalysts are also encountered. Therefore, transformation of homogeneous molecular catalysts into heterogeneous electrocatalysts is desired.

In the past decade, several strategies have been developed to transfer molecular catalysts into heterogeneous ones.[104–109] First, drop-casting molecular complexes onto conductive supports is simple and straightforward. However, molecular catalysts will aggregate, and only those at the outermost layers can be exposed for the reaction with substrates. In addition, due to the weak physical contact between molecular catalysts and electrode surfaces, loaded molecules are easy to be exfoliated particularly under strong gas evolution conditions. Second, introduction of large conjugated substituents, such as pyrene groups, into porphyrin backbones can lead to increased π–π interaction with carbon-based materials.[110,111] However, this noncovalent immobilization still suffers from the disadvantage of insufficient catalyst stability of molecular catalysts on supporting materials. Third, grafting molecular catalysts on supports such as carbon-based

2542 | *Chem. Soc. Rev.*, 2021, **50**, 2540–2581

This journal is © The Royal Society of Chemistry 2021

materials and metal oxides through covalent bonds can largely improve electron transfer efficiency and atom-utilization efficiency and can also significantly increase the stability of molecular catalysts on supporting electrode materials,[112–116] although functionalizing both molecular catalysts and supports for their connection is challenging from the design and synthesis points of view.

Alternatively, molecular catalysts, especially porphyrins, can be integrated into frameworks, such as MOFs and COFs, to realize the transformation from homogeneous catalysis to heterogeneous catalysis.[117–119] MOFs are a class of crystalline porous materials prepared with metal ions or metal clusters and organic linkers through coordination bonds with periodic network structures. MOFs have unique and appealing features, such as regular and adjustable pore size, large specific surface area, and diverse topologies and morphologies.[120–124] On the other hand, COFs are a new class of porous materials constructed by organic molecules through covalent bonds with ordered crystal structures.[125–128] Compared with MOFs, COFs have three additional features.[129] First, the building units of COFs are all organic small molecules, which have a wide range of sources and make building units extremely diversified. Second, the periodic network structure of COFs is formed by covalent bonds, which have much higher thermal and chemical stability as compared to coordination bonds in MOFs. Third, COFs are composed of light elements (*e.g.* C, H, O, N, B, *etc.*), which lead to low density. For both MOFs and COFs, their periodically ordered structures of porous frameworks make all active sites uniformly distributed, which benefits structure–activity and mechanism studies. In addition, their large specific surface areas and permanent porosities are beneficial for active site exposure and mass transportation, making them highly attractive in electrocatalysis and other fields.[130–153] Generally speaking, porphyrin-based frameworks are a special kind of MOFs and COFs, and their constituent units must contain porphyrin molecules.

Recently, great efforts have been dedicated to preparing porphyrin-based frameworks with stable structures, diverse functionalities, different morphologies and porous properties. These frameworks exhibit promising applications in many energy-related conversion and storage technologies.[154–161] Constructing frameworks with porphyrin molecules has several advantages. First, the rigid and robust porphyrin backbones enable straightforward and systematic design and synthesis of porphyrin-based frameworks. Second, many functional groups can be installed on porphyrin backbones. These functional groups play critical roles not only in improving catalysis but also in controlling framework structure and morphology. Third, porphyrins can be employed as both structural units and catalytic sites in porphyrin-based frameworks. Bimetallic and polymetallic porphyrin-based frameworks can be readily constructed for synergistic catalysis. Therefore, porphyrin-based frameworks provide a very attractive platform and make porphyrin molecular catalysts promising for electrocatalytic applications. In other words, porphyrin-based frameworks have become a bridge between homogeneous catalysts and heterogeneous catalysts. In particular, the periodic structure of porphyrin-based frameworks makes these active centers uniformly distributed in the whole porous framework, which is characteristic of homogeneous catalysts. The solid properties of porphyrin-based frameworks in nano/micro-scales make them efficient heterogeneous catalysts. Therefore, based on molecular catalytic reaction mechanisms and structure–activity relationships, the rational design and development of porphyrin-based frameworks can take into account advantages of both homogeneous and heterogeneous catalysts. It is worth noting that porphyrin-based frameworks have also been broadly applied in other fields such as acid catalysis,[162,163] sensing,[164] oxidation,[165,166] capacitor,[167] photocatalysis,[168–171] environmental and biomedical applications,[172,173] and so on.[174]

1.4 Scope of this review

Recently, many reviews have been published to summarize the progress made in MOFs and COFs and their derivatives for energy-related applications. However, a deep understanding of the relationship between structures of porphyrin-based MOFs and COFs and their electrocatalytic activities is highly desirable for the rational design of porphyrin-based catalysts. This review starts by summarizing specific porphyrin-based frameworks to date in the chronological order. A series of porphyrin molecules with different functional features for ORR, OER, Zn–air batteries, and CO$_2$RR are summarized. Furthermore, several typical preparation strategies for porphyrin-based frameworks also have been summed up, including the hydrothermal method, Schiff base reaction, and electrochemical polymerization. Next, we focus on demonstrating the electrocatalytic applications, such as ORR, OER, bifunctional ORR and OER, Zn–air batteries, and CO$_2$RR, of these porphyrin-based frameworks systematically, and on discussing the theoretical basis for electrocatalysis. Furthermore, the catalytic activity and selectivity of porphyrin-based frameworks used in these energy-related fields have been summed up and discussed. At present, the research in porphyrin-based frameworks mainly focuses on the development and synthesis of new structures. However, the design and synthesis of novel frameworks, based on the knowledge of catalytic reaction mechanisms and structure–activity relationships of molecular catalysis, are highly valuable to further improve catalytic activity and selectivity. Finally, conclusions and outlooks of future developments are discussed for novel porphyrin-based frameworks as more efficient electrocatalysts. In general, combining porphyrin-based frameworks and conductive supports and constructing mesoporous and macroporous frameworks can greatly enhance electrochemical activity. The rapid development and application of *in situ* and *ex situ* technologies and theoretical calculations make it possible for reaction mechanism-based activity optimization and selectivity improvement for porphyrin-based frameworks due to their uniform active sites and precise molecular structures. This review may provide an inspiration for researchers to design more efficient porphyrin-based framework materials for practical applications in energy-related fields.

This journal is © The Royal Society of Chemistry 2021

Chem. Soc. Rev., 2021, **50**, 2540–2581 | **2543**

2. Porphyrin-based frameworks in energy-related fields

2.1 Timely update on porphyrin-based frameworks

During the last decade, many porphyrin-based MOFs and COFs were prepared. Porphyrin molecules can be used as both organic linkers of MOFs and component monomers of COFs. Due to the diversity of porphyrin molecules with different functional groups, porphyrin-based MOFs and COFs have been constructed with different topological structures and tunable porous structures. MOFs and COFs provide a suitable platform for porphyrin molecules to realize their heterogeneous catalysis. Currently, porphyrin-based frameworks have become one of the most widely investigated porous structures. Herein, several typical porphyrin-based frameworks are described in Fig. 1 in the chronological order.

In 2010, several porphyrin-based frameworks were prepared and evaluated as electrocatalysts. However, their precise structures and molecular packing styles were not well characterized.[175] Therefore, it is difficult to address the structure–activity relationship to further promote the development of porphyrin-based frameworks. The rapid development of synthetic methods and characterization technologies in the past decade has resulted in the expansion of diverse porphyrin-based frameworks. Since then, more and more porphyrin-based framework materials have been synthesized and widely used in the field of electrocatalysis, including ORR, OER, Zn–air batteries, and CO_2RR.

Among porphyrin-based MOFs, 5,10,15,20-tetra(4-carboxyphenyl) porphyrin (TCPP) is a commonly used organic linker.[176] TCPP is a tetratopic linker with a D_{4h}-symmetry and a rigid square-planar geometry. A variety of metals and metal clusters can act as nodes to form porphyrin-based MOFs with different packing structures. The porous coordination network (PCN) is one class of widely studied porphyrin-based MOFs. For example,

MOF-525 is a typical porphyrin MOF with an **ftw** topology, which has similar packing structure to PCN-221.[177] Herein, the metal cluster of MOF-525-Fe is Zr_6O_8 and the porphyrin linker coordinates with an Fe ion. Furthermore, by changing the synthetic conditions, PCN-224-Ni, PCN-223-Fe, and PCN-222-Fe were crystallized with obviously different packing structures, as displayed in Fig. 1. In particular, PCN-224-Ni has a D_{3d} symmetric Zr_6 cluster with an **she** topology.[178] In contrast, PCN-223-Fe has a D_{6h} symmetrically 12-connected Zr_6 cluster with an **shp** topology.[179] PCN-222-Fe is constructed with four 8-connected Zr_6 clusters and Fe TCPP with a **csq** topology.[180] Note that the above mentioned four porphyrin-based MOFs show completely different crystal structures although the organic linkers (TCPP molecules) and metal clusters (Zr_6 cluster) are the same. Importantly, MOF-525-Fe and PCN-222-Fe exhibit electrocatalytic CO_2RR activity,[181,182] while PCN-224-Ni and PCN-223-Fe show electrocatalytic OER and ORR activity, respectively.[183,184] Thus, electrocatalytic activities of porphyrin-based MOFs strongly depend on their crystal structures. In addition, Co–Al-based TCPP MOF (Co–Al-PMOF) is also a special MOF constructed with Co TCPP as the organic linker and AlO cluster as the metal node.[185] This Co–Al-PMOF exhibits both electrocatalytic CO_2RR and ORR activity owing to the similar molecular packing of MOF-525-Fe and PCN-224-Ni.[186,187]

In addition to porphyrin-based MOFs, COF-366 is a typical COF used for CO_2RR with an **sql** topology.[188] COF-366-Co is assembled with Co 5,10,15,20-tetra(4-aminophenyl)porphyrin (TAPP) as one component and 1,4-benzenedicarboxaldehyde (BDA) as the other component. When replacing the component BDA with 4,4′-biphenyldicarboxaldehyde (BPDA), COF-367-Co was obtained with a larger pore diameter. Through regulation of molecular structures of BDA with different substituents such as –F and –OCH_3, a series of COF-366-X-Co can be obtained with similar topological structures.[189] In addition, Co porphyrin COF
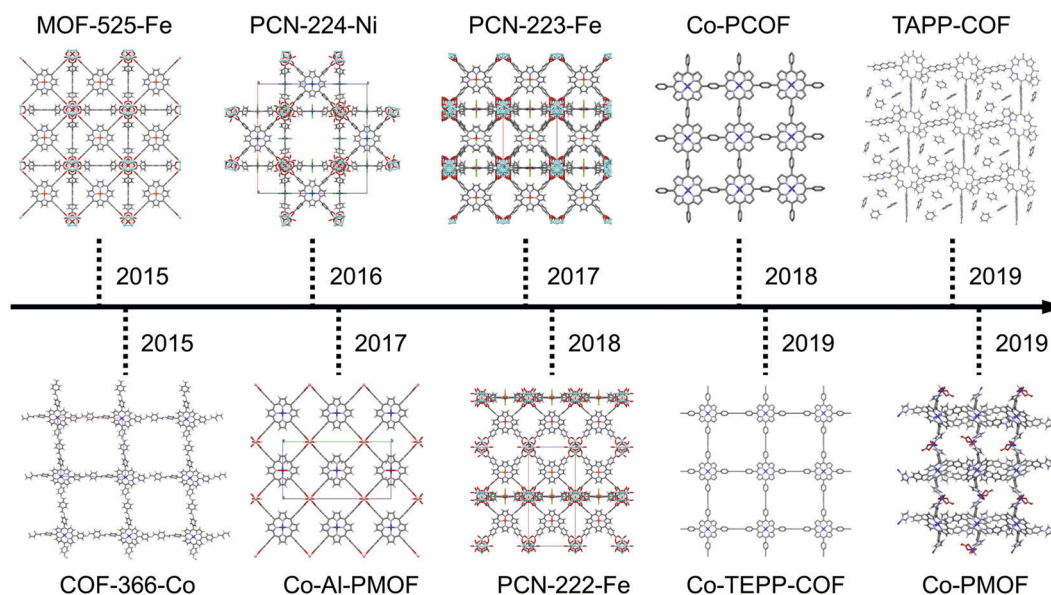
Fig. 1 Typical crystal structures of porphyrin-based frameworks used as catalysts for ORR, OER, Zn–air batteries, and CO_2RR to date.

2544 | Chem. Soc. Rev., 2021, **50**, 2540–2581

This journal is © The Royal Society of Chemistry 2021

(Co-PCOF) can be prepared using a one-pot strategy. Herein, Co porphyrins are connected with benzene rings. This Co-PCOF can also grow on carbon nanotubes (CNTs) and graphene directly.[190,191] Co-PCOF shows obvious bifunctional ORR and OER activity and has been applied in flexible and rechargeable Zn–air batteries. Co 5,10,15,20-tetra(4-ethynylphenyl)porphyrin (TEPP) COF can grow on Cu foam.[192] Similar porphyrin-based COFs assembled using 5,10,15,20-tetraethynylporphyrin (TEP) without phenyl groups can also be obtained.[193,194] These Co- or Fe-based porphyrin COFs grow directly on CNTs. These kinds of COFs can be applied as catalysts for ORR and OER. Recently, a metal-free TAPP-COF was prepared on a glassy carbon (GC) electrode through electrochemical polymerization.[195] By controlling the temperature of the electrolyte, scanning rates, and electrode materials, the growth mechanism of cocrystallization with pyridine was systematically studied. This strategy offers a suitable platform to study the formation process of porphyrin-based frameworks. More recently, a series of metal-coordinated porphyrin MOFs were prepared with metal TCPP molecules as organic linkers and polyoxometalate Zn-ε-Keggin clusters (ε-PMo$_8^V$Mo$_4^{VI}$O$_{40}$Zn$_4$) as nodes.[196] A typical Co porphyrin MOF (Co-PMOF) is shown in Fig. 1. This porphyrin molecular packing of the new crystal structure is different from those of previous PCN crystals. Co porphyrin MOF has an **mog** topology with two Zn–O bonds connected with Co TCPP. Herein, electron-rich Zn-ε-Keggin clusters can offer electrons easily when the redox reaction occurs. The resulting Co porphyrin MOF exhibited excellent CO$_2$RR performance.

Above all, the crystal structures of porphyrin-based MOFs greatly depend on the synthetic conditions. Regulating metal clusters is an effective strategy to obtain porphyrin-based MOFs with different topologies such as PCN-222-Co, PCN-223-Fe, PCN-224-Co, and Co-PMOF. Various kinds of porphyrin-based MOFs and COFs can be obtained by tuning porphyrin monomers and other components as listed in Table 1. Building units, including porphyrin molecules, metal active centers, and metal nodes/organic linkers, are compared. The corresponding topologies and applications of these porphyrin-based MOFs and COFs are also summarized.

2.2 Common porphyrin building blocks of porphyrin-based frameworks

Porphyrin molecules can act as both organic linkers for MOFs and organic components for COFs. Herein, most reported porphyrin molecular structures for ORR, OER, Zn–air batteries and CO$_2$RR are summarized (Fig. 2). Many porphyrin-based MOFs and COFs have been constructed using porphyrin building blocks due to the rigid structure and convenient substituent modification. Diverse porphyrin linkers lead to the formation of frameworks with different topologies, pore structures, morphologies, and functionalities. Subsequently, these special structural features of frameworks result in diverse applications in energy-related fields.

The *meso*-substituent groups of porphyrins can be tuned using simple –C≡N, thiophene and pyridine groups. Porphyrins with four *meso*-substituted benzoic acid, benzaldehyde and aniline groups can also be easily obtained. Among these porphyrin molecules, TCPP has been widely used as an organic linker for MOFs, while TAPP is a widely applied component for COFs. Using the same TCPP organic linker, many PCN MOFs, including MOF-525, 535, 545, PCN-222, 223, and 224, with different topologies have been constructed.[177–180,204] The different connectivities of Zr clusters result in diverse porphyrin-based MOFs.

Furthermore, 5,10,15,20-tetra(3,4,5-trihydroxyphenyl)porphyrin and 5,10,15,20-tetra(3,4,5-trihydroxybiphenyl)porphyrin have also been used as organic linkers to connect Zr clusters and form porphyrin-based MOFs with new topologies.[205] TAPP can be used as one component and aldehyde compounds such as BDA and BDA derivatives can be used as the other component. Schiff base reaction between amines and aldehydes takes place and leads to the formation of the corresponding COFs (named COF-366). By using BPDA, which has an elongated phenyl group as compared to BDA, COF-367 could be formed. Based on this strategy, the pore

Table 1 Summary of porphyrin-based frameworks and their applications

Frameworks	Porphyrin linker	Metal	Node/organic linker	Topology	Application	Ref.
Co–Al-PMOF	TCPP	Co	AlO cluster	—	ORR	187
PCN-223-Fe	TCPP	Fe	ZrO cluster	**shp**	ORR	184
PCN-222-Co	TCPP	Co	ZrO cluster	**csq**	ORR	197
TAPP-COF	TAPP	—	—	**sql**	ORR	195
Pb-TCPP-MOF	TCPP	—	PbO chain	—	OER	198
Co-TAPP-COF	TAPP	Co	TFBM	**pts**	OER	199
Co-TABPP-COF	TABPP	Co	TFBM	**pts**	OER	199
PCN-224-Ni	TCPP	Ni	ZrO cluster	**she**	OER	183
Co-TEPP-COF	TEPP	Co	—	—	OER	192
Co-PCOF	TPP	Co	—	—	ORR/OER	191
PCN-224-Co	TCPP	Co	ZrO cluster	**she**	ORR/OER	200
PCN-226-Co	TCPP	Co	ZrO cluster	**ztt**	ORR/OER	201
COF-366-Co	TAPP	Co	BDA	**sql**	CO$_2$RR	188
COF-367-Co	TAPP	Co	BPDA	**sql**	CO$_2$RR	188
Co–Al-PMOF	TCPP	Co	AlO cluster	—	CO$_2$RR	186
MOF-525-Fe	TCPP	Fe	ZrO cluster	**ftw**	CO$_2$RR	181
Co-PMOF	TCPP	Co	Zn-ε-Keggin cluster	**mog**	CO$_2$RR	196
MOF-545-Co	TCPP	Co	ZrO cluster	**csq**	CO$_2$RR	202
PCN-222-Fe	TCPP	Fe	ZrO cluster	**csq**	CO$_2$RR	182
Fe-TAPP-COF	TAPP	Fe	2,5-dihydroxyterephthalaldehyde	**sql**	CO$_2$RR	203
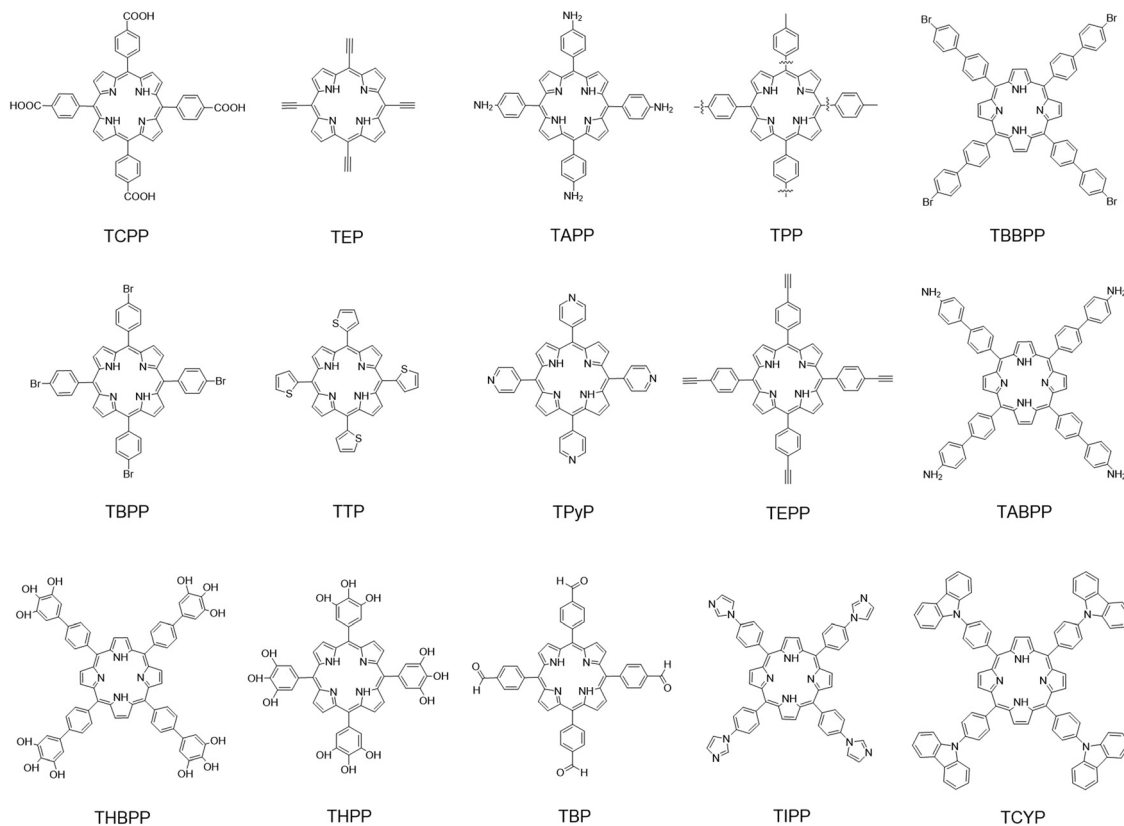
Fig. 2 Molecular structures of porphyrin building blocks used for ORR, OER, Zn–air batteries, and CO₂RR. Abbreviations: TCPP = 5,10,15,20-tetra(4-carboxyphenyl)porphyrin; TEP = 5,10,15,20-tetraethynylporphyrin; TAPP = 5,10,15,20-tetra(4-aminophenyl)porphyrin; TPP = 5,10,15,20-tetraphenylporphyrin; TBBPP = 5,10,15,20-tetra(4-bromobiphenyl)porphyrin; TBPP = 5,10,15,20-tetra(4-bromophenyl)porphyrin; TTP = 5,10,15,20-tetra(2-thienyl)porphyrin. TPyP= 5,10,15,20-tetra(4-pyridyl)porphyrin; TEPP = 5,10,15,20-tetra(4-ethynylphenyl)porphyrin; TABPP = 5,10,15,20-tetra(4-aminobiphenyl)porphyrin; THBPP = 5,10,15,20-tetra(3,4,5-trihydroxybiphenyl)porphyrin; THPP = 5,10,15,20-tetra(3,4,5-trihydroxyphenyl)porphyrin; TBP = 5,10,15,20-tetra(4-formylphenyl)porphyrin; TIPP = 5,10,15,20-tetra(4-(imidazol-1-yl)phenyl)porphyrin; TCYP = 5,10,15,20-tetra(carbazol-9-ylphenyl)porphyrin.

diameter and porosity can be tuned precisely. As a result, COF-367 has much larger accessible surface area and more exposed active sites than COF-366.

In addition, TAPP molecules can also be used as monomers to form COFs through electrochemical polymerization. Similarly, 5,10,15,20-tetra(2-thienyl)porphyrin (TTP) and 5,10,15,20-tetra(carbazol-9-ylphenyl)porphyrin (TCYP) can be used as monomers to synthesize COFs through electrochemical polymerization. The alkynyl coupling reaction of TEP has also been applied to prepare COFs with or without templates, such as CNTs. Herein, TEP can also be extended to TEPP. Therefore, diverse porphyrin-based frameworks can be obtained by precisely tuning the size and substituent of linkers. As a result, regulation of *meso*-substituents of porphyrin linkers is mainly used to construct coordination bonds and covalent bonds to form porphyrin-based MOFs and COFs. Suitable metal nodes and organic components will lead to the formation of different topological and porous structures of porphyrin-based MOFs and COFs.

2.3 Synthetic procedures for porphyrin-based frameworks

There are several strategies reported for synthesizing porphyrin-based frameworks.[206] Herein, several representative

synthetic procedures of porphyrin-based frameworks are summarized in Fig. 3. In particular, there are two common synthetic procedures for porphyrin-based MOFs. Usually, metal coordinated porphyrin molecules were first prepared by refluxing metal salts and porphyrin ligands at high temperatures (>100 °C). Then the hydrothermal strategy was applied to construct porphyrin-based MOFs (Fig. 3a). This is a commonly used method to synthesize porphyrin-based MOFs, especially a series of PCN crystalline compounds. It is very easy to tune coordinated metals of porphyrin molecules before the formation of MOFs. By controlling different synthetic conditions and using different metal porphyrin linkers and metal cluster nodes, a large variety of porphyrin-based MOFs can be obtained with different topological structures. In addition to this strategy, porphyrin-based MOFs can also be obtained by firstly using the hydrothermal method and then coordinating the metals into porphyrins to give the corresponding MOFs (Fig. 3b).[185] The bimetal Co–Al–PMOF was obtained using this method. The unusual formation process of Co–Al–PMOF may be ascribed to the unique topological structure and specific AlO chains.

For porphyrin-based COFs, several commonly used methods were also described. The first method is a one-pot strategy (Fig. 3c).

2546 | *Chem. Soc. Rev.*, 2021, **50**, 2540–2581

This journal is © The Royal Society of Chemistry 2021
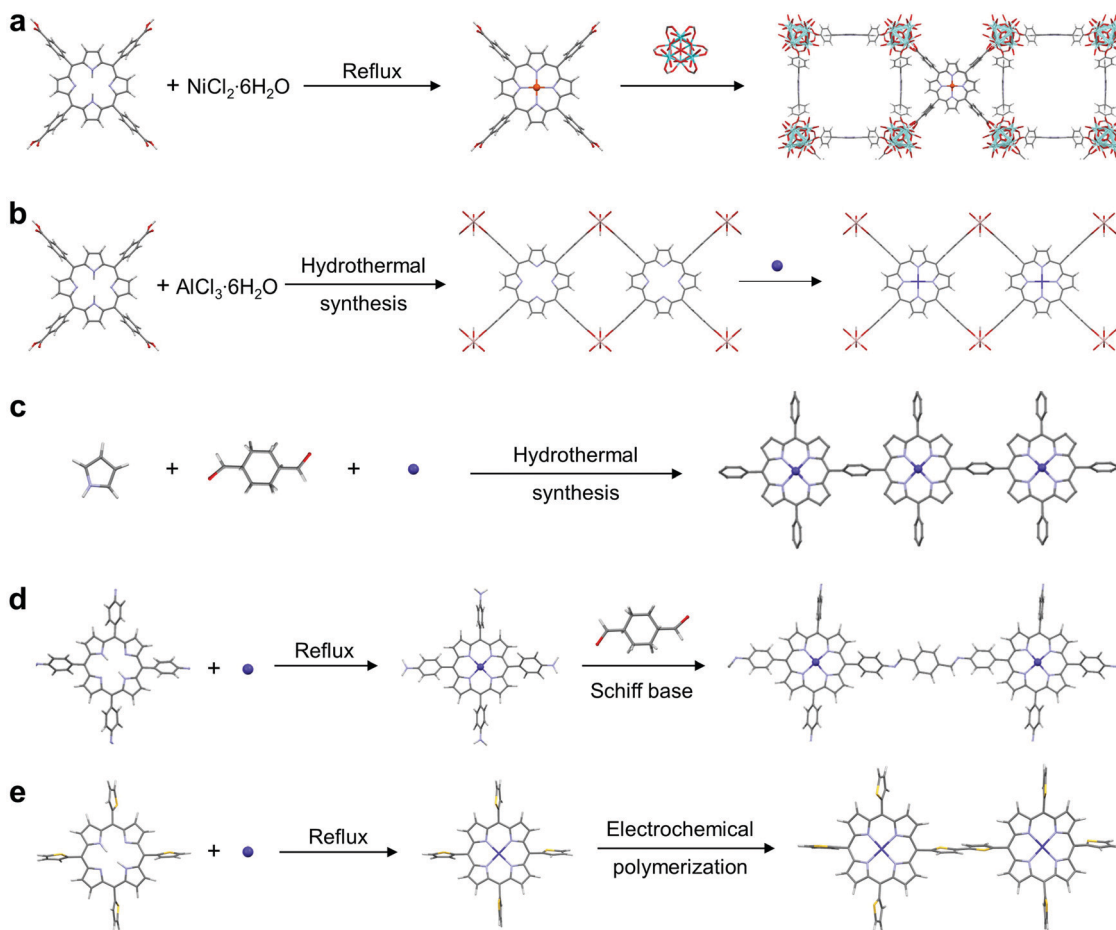
Fig. 3 Representative synthetic procedures for porphyrin-based frameworks.

Typically, pyrrole, BDA, and the corresponding metal salt were mixed together to form two dimensional (2D) porphyrin-based COFs through dehydration polymerization. The corresponding porphyrin-based COFs with different transition metals can be synthesized. Furthermore, supporting templates such as graphene and CNT can also be introduced into the system to form COF/support hybrids to enhance conductivity. The unique advantage of this strategy is that it reduces the synthetic procedure by omitting the synthesis of porphyrin monomers. The other strategy uses the Schiff base condensation reaction between aldehyde groups and amino groups (Fig. 3d). For example, the metal coordinated TAPP porphyrin molecule was synthesized and used as one component. Then, BDA was selected to form porphyrin-based COFs. This strategy is commonly used to prepare COFs.[207] This is mainly because the condensation reaction can form covalent imine bonds between the aldehyde group of organic linkers and amino group of porphyrin molecules. Diverse porphyrin-based COFs can be obtained based on Schiff base reaction through regulation of porphyrin molecules with different functional amino groups and the corresponding aldehydes with different molecular structures and *vice versa*.[208,209] In addition, electrochemical polymerization is also a simple strategy to prepare porphyrin-based COFs, as displayed in Fig. 3e.[175] Electrochemical polymerization of Co TTP was carried out *via* cyclic voltammetry (CV). The conductive

support can be the GC electrode and indium tin oxide glass. Furthermore, electrochemical polymerization has been used to prepare other COFs such as Co TCYP and TAPP COFs.[195,210]

In addition to these above-mentioned procedures, many other strategies were also reported.[211] For example, the Yamamoto polycondensation is an effective strategy to construct COFs through C–C coupling. Specifically, 5,10,15,20-tetra(4-bromophenyl)-porphyrin (TBPP) and 5,10,15,20-tetra(4-bromobiphenyl)porphyrin (TBBPP) COFs have been synthesized using this method.[212,213] Similarly, 5,10,15,20-tetra(4-(imidazol-1-yl)phenyl)porphyrin (TIPP) and α,α′-dibromo-*p*-xylene can also form porphyrin-based COFs according to the quaternization reaction.[214] In addition, Kitagawa, Makiura, and co-workers reported a layer-by-layer assembling strategy.[215] By using Co TCPP and pyridine in chloroform/methanol and CuCl$_2$ in aqueous solution, a 2D MOF was deposited on the substrate with Co TCPP as porphyrin linkers and Cu as nodes. Several strategies have also been reported to construct surface-supported MOF or COF thin films.[216,217] Zhang and co-workers constructed a 2D porphyrin-based MOF Zn-TCPP using a surfactant-assisted synthetic strategy.[218] Polyvinylpyrrolidone was selected as the surfactant. Furthermore, by using this method, 2D bimetallic Co/Fe-TCPP MOF nanosheets have also been prepared with a thickness of 5.6 ± 1.8 nm.[219]

2.4 Electrochemical energy conversion and storage of porphyrin-based frameworks

Inspired by nature, molecular porphyrin catalysts have been generally applied for ORR, OER, and CO_2RR in homogeneous solutions. However, because electrocatalytic reactions only take place at electrode surfaces, molecular catalysts are required to be heterogenized by immobilization on supporting materials or construction of framework materials. In this review, we look at the development of porphyrin-based frameworks as well as derived hybrids for practical applications in fuel cells (ORR), water splitting electrolytic cells (OER), rechargeable Zn–air batteries (ORR/OER), and CO_2 reduction flow cells (CO_2RR) (Fig. 4).

ORR is a broadly investigated reaction of porphyrin-based frameworks due to the high intrinsic activity of porphyrin molecules. ORR plays a vital role in many energy-related devices, including fuel cells and metal–air batteries.[220] Fuel cells are a class of power generation devices.[221–223] In fuel cells, chemical energy is converted into electrical energy. The proton exchange membrane fuel cell (PEMFC) is a typical fuel cell.[224,225] In PEMFC (Fig. 4a), hydrogen (H_2) is oxidized at the anode to form protons (H^+) and electrons (e^-) (eqn (1)).

$$HOR: H_2 \rightarrow 2e^- + 2H^+ \tag{1}$$
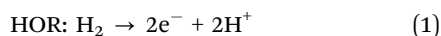
The generated electrons will transfer from the anode to the cathode to participate in the ORR, while protons will penetrate through proton exchange membrane (PEM) and finally diffuse into the electrolyte of the cathode. Then, O_2 reacts with protons and electrons to give H_2O (eqn (2)). Therefore, a typical PEMFC is constructed using a H_2 diffusion layer, catalyst layer on the anode, PEM, catalyst layer on the cathode, and air diffusion layer. Particularly, the ORR process at the cathode involves multi-step reactions with the participation of protons and electrons. Generally speaking, there are two major possible pathways (4e pathway *versus* 2e pathway) in both acidic and alkaline solutions.[226]

ORR can be carried out in acidic solution through the 4e pathway (eqn (2)),

$$O_2 + 4H^+ + 4e^- \rightarrow 2H_2O \tag{2}$$

and 2e pathway (eqn (3) and (4)).

$$O_2 + 2H^+ + 2e^- \rightarrow H_2O_2 \tag{3}$$

$$H_2O_2 + 2H^+ + 2e^- \rightarrow 2H_2O \tag{4}$$
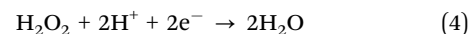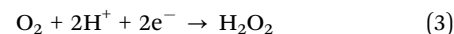
In addition, ORR can also be carried out in alkaline solution through the 4e pathway (eqn (5)),

$$O_2 + H_2O + 4e^- \rightarrow 4OH^- \tag{5}$$

and 2e pathway (eqn (6) and (7)).

$$O_2 + H_2O + 2e^- \rightarrow HO_2^- + OH^- \tag{6}$$

$$HO_2^- + H_2O + 2e^- \rightarrow 3OH^- \tag{7}$$
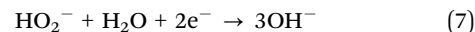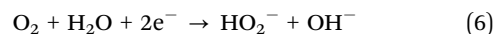
PEMFC is a zero-emission device with the product of only H_2O. The byproduct H_2O_2 generated in the 2e reduction process is also an important energy carrier, which has also attracted great
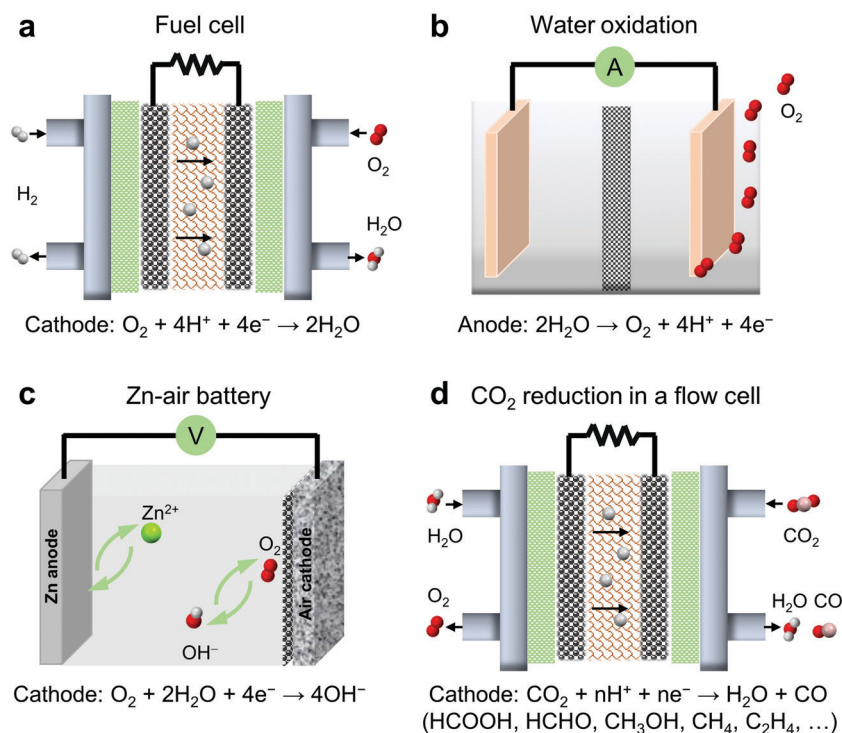
Fig. 4 Schematic illustration of electrochemical energy conversion and storage devices assembled using porphyrin-based frameworks. (a) H_2–O_2 fuel cell. (b) Water splitting electrolytic cell. (c) Rechargeable Zn–air battery. (d) Membrane reactor of CO_2 reduction.

2548 | *Chem. Soc. Rev.*, 2021, **50**, 2540–2581

This journal is © The Royal Society of Chemistry 2021

attention recently.[227,228] Therefore, PEMFC has been considered as one of the cleanest power generation technologies.

OER, as the reverse reaction of ORR, is one half reaction of water splitting. Water splitting can be divided into two half reactions: water reduction (the so called hydrogen evolution reaction, HER) and water oxidation (the so called OER) (Fig. 4b). The water oxidation reaction can provide four electrons and four protons and meanwhile generate one O_2 molecule in acidic solution (eqn (8)).

$$2H_2O \rightarrow O_2 + 4H^+ + 4e^- \qquad (8)$$
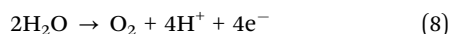
In addition, H_2O can also be oxidized to O_2 in alkaline solution (eqn (9)).

$$4OH^- \rightarrow O_2 + 2H_2O + 4e^- \qquad (9)$$
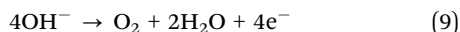
The oxidation of water requires an endothermic energy of 237 kJ mol^{-1} and significant rearrangements of several atoms. As a consequence, OER is very slow in kinetics.

Metal–air batteries have attracted growing attention from countries around the world due to high theoretical energy density.[229–232] Metal–air batteries combine the characteristics of a traditional battery and a fuel cell. The anode is made of metal like a traditional battery. O_2 from air diffuses into the cathode as a reactant for ORR, and its efficiency has a great influence on the battery voltage and energy density. For a rechargeable metal–air battery, the conversion between oxygen and water occurs in the process of discharge (ORR) and charge (OER) on the cathode. Among these metal–air batteries, the Zn–air battery is appealing.[233–240] The Zn–air battery is a kind of primary battery which uses activated carbon to absorb O_2 in air as a positive active material, a Zn plate as the negative electrode, and ammonium chloride or caustic solution as the electrolyte (Fig. 4c). Electrochemical reactions of a Zn–air battery contain the following:

$$\text{Cathode: } O_2 + 2H_2O + 4e^- \rightarrow 4OH^- \qquad (10)$$

$$\text{Anode: } Zn + 2OH^- \rightarrow ZnO + H_2O + 2e^- \qquad (11)$$
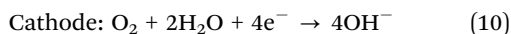
Owing to its advantages of safety, zero pollution, low cost, renewable raw materials, high energy and power density, the Zn–air battery has become an ideal power supply for electric vehicles.[241] The Zn–air battery has a high specific energy with a theoretical mass energy density of 1350 W h kg^{-1}.[234] For a rechargeable Zn–air battery, the OER is also involved and occurs on the cathode catalyst (eqn (9)). Thus, a rechargeable Zn–air battery involves both ORR and OER and requires bifunctional catalysts. Usually, a typical Zn–air battery contains a Zn anode, alkaline electrolyte, and air cathode with catalysts. A newly polished Zn plate is applied as the anode. The composition of the electrolyte is 6 M KOH and 0.2 M ZnCl$_2$. The air cathode contains the catalyst layer, carbon cloth layer and gas diffusion layer. Three layers were assembled together to form a whole air cathode.

CO$_2$RR provides a very attractive method for the utilization of renewable energy to generate synthetic fuels and chemical raw materials.[242–245] Since the industrial revolution, the emission

of CO_2 has been causing global warming. Therefore, reducing the concentration of CO_2 in the atmosphere will ameliorate the greenhouse effect. In addition, CO_2RR will produce C1 and C2 compounds as fuels and valuable chemicals. In comparison with electrolytic water oxidation for O_2 production, currently, the technology of CO_2 electrolysis remains largely unexplored.[246] CO_2RR is a thermodynamically uphill reaction and has sluggish kinetics. Electrocatalytic CO_2RR will produce a series of products, including C1 compounds (*e.g.*, CO, HCHO, CH$_3$OH, CH$_4$, *etc.*) and C2 compounds (*e.g.*, C$_2$H$_4$, C$_2$H$_5$OH, C$_2$H$_6$, *etc.*) based on the numbers of protons and electrons transferred. Therefore, developing CO_2 reduction electrocatalysts with high activity, selectivity, and stability is desired.

As for CO_2RR, the electron transfer numbers, corresponding carbon-based products, and energy changes are listed below (eqn (12)–(18)).[247,248]

$$CO_2 + e^- \rightarrow CO_2^{\bullet-} \quad E_0 = -1.90 \text{ V} \qquad (12)$$

$$CO_2 + 2H^+ + 2e^- \rightarrow HCOOH \quad E_0 = -0.61 \text{ V} \qquad (13)$$

$$CO_2 + 2H^+ + 2e^- \rightarrow CO + H_2O \quad E_0 = -0.53 \text{ V} \qquad (14)$$

$$CO_2 + 4H^+ + 4e^- \rightarrow HCHO + H_2O \quad E_0 = -0.48 \text{ V} \qquad (15)$$

$$CO_2 + 6H^+ + 6e^- \rightarrow CH_3OH + H_2O \quad E_0 = -0.38 \text{ V} \qquad (16)$$

$$CO_2 + 8H^+ + 8e^- \rightarrow CH_4 + 2H_2O \quad E_0 = -0.24 \text{ V} \qquad (17)$$

$$2CO_2 + 12H^+ + 12e^- \rightarrow C_2H_4 + 4H_2O \quad E_0 = -0.34 \text{ V} \qquad (18)$$

$$2H^+ + 2e^- \rightarrow H_2 \quad E_0 = -0.42 \text{ V} \qquad (19)$$
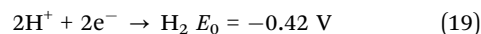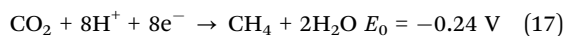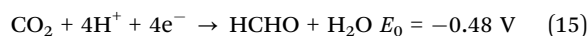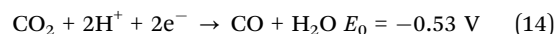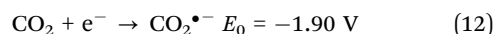
CO_2 molecule can experience a direct one electron reduction with a potential energy of -1.90 V *versus* a normal hydrogen electrode (NHE, eqn (12), pH = 7). During this reduction process, the linear CO_2 molecule will be adsorbed on the active site and form bent $CO_2^{\bullet-}$. The reduction potentials of 2e, 4e, 6e, 8e and 12e transfer processes (-0.24 to -0.61 V *versus* NHE) are quite close to each other (eqn (13)–(18), pH = 7). Moreover, the reduction potential of H^+ to H_2 is -0.42 V *versus* NHE (eqn (19), pH = 7), which is located in the area of CO_2RR with different reduction electron numbers. It is thus clear that the production of H_2 is a competitive reaction compared to CO_2RR. Therefore, the development of electrocatalysts with extraordinary selectivity still remains a great challenge. Currently, the most extensively studied device of CO_2RR is the membrane containing reactor.[249] In a typical flow cell of CO_2RR, CO_2 reduction reaction occurs at the cathode while water oxidation occurs at the anode (Fig. 4d). This kind of reactor is similar to PEMFC. Specifically, CO_2 gas passes to the cathode through the gas diffusion layer. The gas diffusion layer will ensure full contact between CO_2 and catalysts. CO_2RR occurs on the surface of the catalyst layer immersed in the electrolyte. The cathodic and anodic reactions are separated by the PEM, which enables the flow of ions. All of these parts including gas diffusion layer, catalyst layer, and PEM composites will affect the activity, selectivity and stability of CO_2RR.

3. Applications of porphyrin-based frameworks

3.1 Oxygen reduction reaction (ORR)

3.1.1 Evaluation of activity and selectivity for ORR. In the past decade, catalysts for ORR have been extensively investigated.[250–254] Ideally, the ORR performance should be evaluated by encapsulating catalysts in the cathode of a membrane electrode assembly. However, the effect of the assembly process of the membrane electrode on catalytic activity is complicated and is challenging to eliminate. Therefore, ORR activity is usually evaluated under rotating conditions using a rotating disk electrode (RDE).[255] Catalysts are coated on the surface of RDE. CV data are first measured in N_2- and O_2-saturated electrolytes. Then linear sweep voltammetry (LSV) data are measured in the O_2-saturated electrolyte at a specific rotating speed (e.g., 1600 rpm). The onset potential (E_{onset}) and half-wave potential ($E_{1/2}$) are two key parameters used to evaluate and compare ORR performance. E_{onset} is obtained at the inflection point of the LSV curve, while $E_{1/2}$ is the potential when current density reaches the half-value of diffusion-limited current density. The activity of catalyst materials is usually compared with E_{onset} and $E_{1/2}$ obtained at a specific rotation speed (e.g., 1600 rpm). Both acidic and alkaline solutions have been applied to evaluate catalytic activity.

The electron transfer number n is a key parameter to determine the 2e versus 4e reduction pathway. The measurement of n has two methods. One method is measuring LSV data under different rotating speeds ranging from 400 to 2500 rpm with RDE. Then, n can be calculated using the Koutecky–Levich equation (eqn (20) and (21)).[256]

$$\frac{1}{j} = \frac{1}{j_L} + \frac{1}{j_K} = \frac{1}{B(2\pi R)^{1/2}} + \frac{1}{nFkC_{O_2}} \tag{20}$$

$$B = 0.62nFC_{O_2}D_{O_2}^{2/3}\nu^{-1/6} \tag{21}$$

Herein, j_L and j_K are diffusion-limited and kinetic current density (j), respectively. j_L is proportional to the square root of rotating speed (R). F represents the Faraday constant, and k represents electron transfer rate constant. C_{O_2} is the concentration of dissolved O_2 in the electrolyte. D_{O_2} represents the diffusion coefficient of O_2 in the electrolyte. ν is the kinetic viscosity of the electrolyte.

In addition, n can also be calculated by performing LSV using a rotating ring-disk electrode (RRDE) at a specific rotating speed (e.g., 1600 rpm) (eqn (22)).

$$n = 4\frac{I_d}{I_d + I_r/N} \tag{22}$$

Herein, I_d and I_r stand for the current obtained at disk electrode and ring electrode, respectively. N represents the collection efficiency of the Pt ring, which is an inherent characteristic of an RRDE. For a 4e reduction process, the n value of a catalyst is close to 4. In contrast, the value of n is close to 2 for a 2e process. In most instances, the value of n is between 2 and 4. This indicates that both 2e and 4e pathways

occur during the ORR process. Therefore, a certain amount of H_2O_2 will be produced. In particular, the yield of H_2O_2 can be calculated using the following equation (eqn (23)).

$$\%H_2O_2 = 200\frac{I_r/N}{I_d + I_r/N} \tag{23}$$

At present, precious metal Pt-based materials are the best ORR catalysts due to the high catalytic activity with an $E_{1/2}$ of >0.86 V versus a reversible hydrogen electrode (RHE) and the excellent selectivity for the 4e reduction process in alkaline electrolytes.[257–259] However, the long-term stability of Pt-based materials is not satisfactory.[260] Furthermore, Pt takes almost half of the total cost of practical new energy vehicles.[261] Therefore, the scarcity and high price of Pt still remain a bottleneck of commercial development. In addition, the poor resistance of methanol for Pt/C of direct methanol fuel cells is also a serious problem that needs to be solved.

3.1.2 ORR reaction mechanisms with metal porphyrins. As mentioned above, the ORR selectivity of porphyrins coordinated with different transition metals is different. In general, mononuclear early and middle transition metal porphyrin molecules (e.g., Fe porphyrin) can catalyze O_2 to H_2O through a 4e reduction process, while mononuclear late transition metal porphyrin molecules (e.g., Co porphyrin) catalyze O_2 to H_2O_2 through a 2e reduction process (Fig. 5).[3] This difference is caused by the ease of formation of terminal metal-oxo species during the ORR process.

It is suggested that terminal metal-oxo species are key intermediates generated from the heterolytic cleavage of an O–O bond. For late transition metal elements, due to the repulsion between electrons of metal d orbitals and oxo ligand p orbitals, their terminal metal-oxo species are high in energy. Nevertheless, late transition metal compounds can also catalyze O_2 via a 4e reduction process through the formation of bimetallic peroxo species (Fig. 5).[44] Subsequent cleavage of the O–O bond will result in the reduction of O_2 to H_2O. Therefore, the nature of metal active sites is of great importance for ORR selectivity.

To further confirm this conclusion, theoretical calculations have been carried out. A typical 4e reduction process of O_2 involves three main intermediates: *OOH, *O, and *OH. The * stands for active sites of catalysts. Usually, the reaction mechanism of a catalyst depends mainly on the energy barrier of oxygen dissociation. Particularly, an associative mechanism is shown below.

$$* + O_2 + H^+ + e^- \rightarrow {}^*OOH \tag{24}$$

$$^*OOH + H^+ + e^- \rightarrow {}^*O + H_2O \tag{25}$$

$$^*O + H^+ + e^- \rightarrow {}^*OH \tag{26}$$

$$^*OH + H^+ + e^- \rightarrow * + H_2O \tag{27}$$
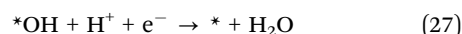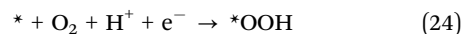
Accordingly, *OH, *O and *OOH intermediates play crucial roles during the ORR process. Therefore, adsorption energy of these intermediates on metal active sites can reflect ORR activity and selectivity. For example, Rossmeisl and co-workers calculated the adsorption energy of *OH (ΔG_{OH}) for porphyrins coordinated

2550 | Chem. Soc. Rev., 2021, **50**, 2540–2581

This journal is © The Royal Society of Chemistry 2021
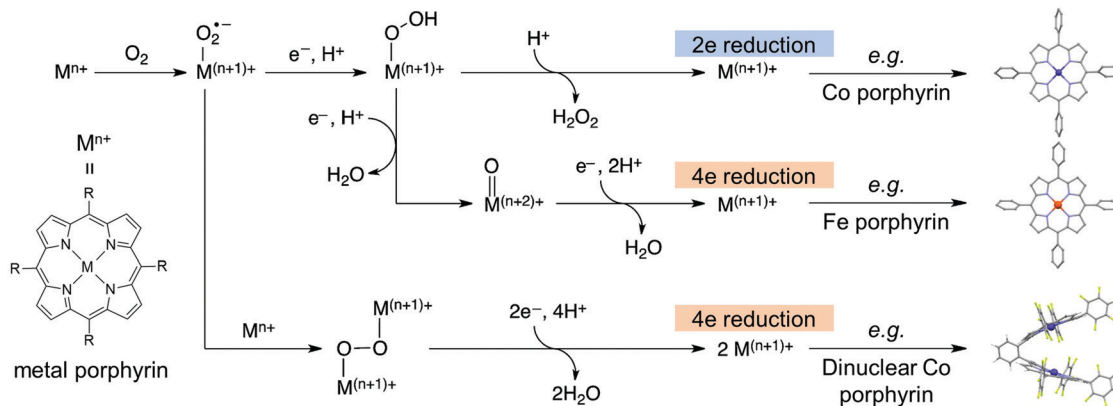
Fig. 5 Possible reaction mechanisms of ORR catalyzed by metal porphyrins through 2e and 4e pathways.

with different metal elements, including Mn, Fe, Co, Ni, and Cu.[262] Their results demonstrated that ΔG_{OH} increases with the increase of d electrons of transitional metals in porphyrin molecules. Furthermore, the removal of *OH from the active site of Fe porphyrin is potential limiting (< 0.86 eV), while Co porphyrin has a high selectivity for the 2e pathway due to weak ΔG_{OH}. To solve this problem, binuclear porphyrin catalysts such as diporphyrin anthracene and diporphyrin dibenzofuran coordinated with different metals were designed. Computational screening results indicated that Co-based diporphyrin anthracene complex exhibited an extremely low energy barrier to dissociate O_2 molecules. This is consistent with the cleavage process of homolytic O–O bond through the formation of a binuclear peroxo species as discussed above. These theoretical calculations shed light on the development of porphyrin-based frameworks. To experimentally investigate the reaction mechanisms of ORR, Wan, Wang and co-workers introduced an *in situ* electrochemical scanning tunneling microscopy (ECSTM) technology.[263] Co 5,10,15,20-tetraphenylporphyrin (TPP) was selected as the subject. A highly ordered thin layer of Co TPP molecules was grown on the Au(111) electrode. They observed the formation of Co TPP–O_2 complexes during the ORR process using ECSTM.

3.1.3 Porphyrin-based framework composites for ORR. Currently, porphyrin-based frameworks have been widely used as catalysts for ORR due to the high intrinsic activity of porphyrin molecules. However, the conductivity of porphyrin-based frameworks is poor and thus limits their ORR performance. The most widely applied strategy is introduction of conductive materials such as carbon black and CNT *etc.* to the catalyst ink. For example, Zhang, Liu and co-workers designed a Co-TEPP-COF and mixed with carbon black to evaluate the catalytic activity.[264] The resulting Co-TEPP-COF/C composite exhibited an E_{onset} of 0.63 V (*versus* RHE) in 0.5 M H_2SO_4 and 0.86 V (*versus* RHE) in 0.1 M KOH, respectively. Moreover, the n value of Co-TEPP-COF/C was 3.88 and 3.80 in 0.5 M H_2SO_4 and 0.1 M KOH, respectively, measured with RRDE. Co-TEPP-COF/C also exhibited excellent durability and enhanced methanol resistance as compared to the composite of porphyrin molecules and carbon black. Therefore, constructing porphyrin-based frameworks does improve catalytic activity and stability of

porphyrin molecules. In addition, Fateeva and co-workers prepared Co–Al-PMOF with Co TCPP as the organic linker and AlO cluster as the coordination node.[187] Co–Al-PMOF mixed with carbon black (Vulcan XC72) exhibited an $E_{onset} = 0.75$ V (*versus* RHE) in 0.1 M H_2SO_4. More recently, Bao, Jaramillo, and co-workers prepared a series of PCN-222-Co with different particle sizes ranging from 200 nm to 1000 nm.[197] Conductive Vulcan carbon was introduced to prepare the catalyst ink. PCN-222-Co with the smallest size exhibited the highest mass activity for ORR in 0.1 M $HClO_4$. PCN-222-Co also showed excellent stability during electro-
catalysis with the remaining structure and morphology. In addition, Huang, Zhou, Zheng and co-workers prepared a new kind of porphyrin MOF, named PCN-226.[201] Different from other Zr-based PCN MOFs, PCN-226 has a Zr-oxide chain structure, which enhances the overall stability of MOFs and forms a close packing structure of porphyrin molecules. Carbon black was mixed with MOFs when carrying out the evaluation of ORR. PCN-226-Co exhibited the best ORR performance with an $E_{1/2} = 0.75$ V (*versus* RHE) as compared to previously reported PCN-221-Co ($E_{1/2} = 0.70$ V *versus* RHE) and PCN-222-Co ($E_{1/2} = 0.69$ V *versus* RHE) measured in 0.1 M KOH. Theoretical calculations demonstrated that PCN-226-Co has suitable packing distance (~ 7 Å) of porphyrin molecules, which is beneficial for the adsorption of *O, *OH, and *OOH intermediates. All the above results confirm that ORR active porphyrin molecular catalysts are suitable building blocks for preparing COFs or MOFs with efficient heterogeneous activity.

3.1.4 Porphyrin-based frameworks grown on supports for ORR. To further improve the ORR performance of porphyrin-based frameworks, carbon-based materials and metal oxides were usually selected as templates/supports to grow frameworks. Different from physical mixing of frameworks and carbon materials, the ordered and close combination of porphyrin-based frameworks and conductive supports will further improve conductivity and thus electron transfer efficiency. Graphene and reduced graphene oxide (rGO) are commonly used carbon material supports due to their high surface areas.[265] Graphene can be used as a support to grow frameworks directly. For example, Zhang and co-workers prepared several M-PCOF/

This journal is © The Royal Society of Chemistry 2021

Chem. Soc. Rev., 2021, **50**, 2540–2581 | **2551**
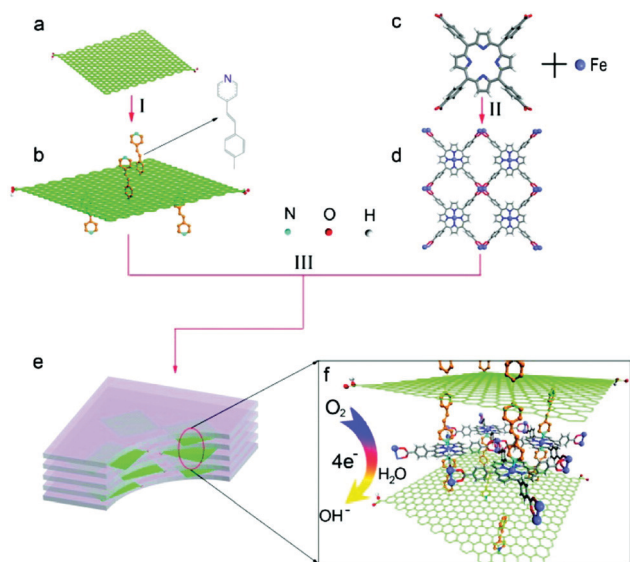
Fig. 6 Schematic procedure of Fe-TCPP-MOF/py-G.[268] Reproduced from ref. 268 with permission from American Chemical Society, copyright 2012.

graphene composites through a one-pot method with graphene as the substrate, and metal salts, pyrrole, and BDA as raw materials.[266] Screening of the results indicated that Co-PCOF/graphene showed improved activity with an $E_{1/2} = 0.81$ V (versus RHE) for ORR in 0.1 M KOH, outperforming other metal COF catalysts (Mn, Fe, Ni, Cu, and Zn). The Tafel slope of Co-PCOF/graphene was 53 mV dec^{-1}. In addition, Xiang, Xia and co-workers assembled a series of porphyrin-based COFs and rGO hybrids.[267] Porphyrin-based COFs were first synthesized with TBBPP. Differently from common porphyrin-based frameworks, the β-positions of these porphyrin-based COFs were substituted with –SO$_3$H groups (named PCOF-SO$_3$H) to improve the solubility. Metal ions M and rGO were successively introduced into the system when self-assembling porphyrin-based COFs and rGO to give PCOF-SO$_3$-M-rGO. Using this strategy, the conductivity of PCOF-SO$_3$-Co-rGO (0.256 S m^{-1}) can be greatly improved as compared to PCOF (3.06 × 10^{-8} S m^{-1}). PCOF-SO$_3$-Co-rGO exhibited boosted catalytic

activity of ORR with an $E_{onset} = 0.88$ V (versus RHE) and an n value of 3.70 in 0.1 M KOH.

Moreover, pyridine-functionalized graphene (py-G) and pyridine-functionalized rGO (py-rGO) have also been widely used as supports. Pyridine groups may form strong interaction with the metal active sites of porphyrin molecules and promote ordered assembly of porphyrin-based frameworks. For example, Loh and co-workers prepared an active composite for ORR with py-G and a porphyrin-based MOF (Fig. 6).[268]

Herein, a porphyrin-based MOF was constructed with Fe TCPP as an organic linker and Fe^{3+} as node to give Fe-TCPP-MOF. Fe-TCPP-MOF/py-G presented an E_{onset} of 0.93 V (versus RHE) and a 4e ORR process with an electron transfer number of 3.82 in 0.1 M KOH. Similarly, Luo and co-workers applied py-rGO as the support to assemble Co porphyrin COFs.[269] Co TAPP was also selected as the porphyrin building unit. BDA was selected as the organic linker. The resulting COF-366-Co/py-rGO framework showed an E_{onset} of 0.84 V (versus RHE) and an $E_{1/2}$ of 0.765 V (versus RHE) in 0.1 M KOH. The n value of the COF-366-Co/py-rGO framework was around 3.8. Furthermore, Dehghanpour and co-workers found that PCN-222-Fe assembled with py-G also exhibited ORR activity in acidic solution.[270]

CNTs are another widely used conductive carbon materials due to high conductivity. In 2014, Campidelli and co-workers prepared a porphyrin-based framework coated on CNT materials by covalently linking Co TEP on the surface of CNT (named Co-TEP-COF/CNT, Fig. 7).[193] A porphyrin monomer Co TEP was synthesized by deprotecting alkyne functional groups using tetrabutylammonium fluoride. Then a polymerization reaction was carried out. The resulting Co-TEP-COF/CNT exhibited a large electrocatalytic ORR wave with an $E_{onset} = 0.75$ V (versus RHE) and an $E_{1/2} = 0.65$ V (versus RHE) in 0.5 M H$_2$SO$_4$. RRDE measurements demonstrated that Co-TEP-COF/CNT displayed an n value of 3.93, indicating a dominant 4e pathway. More importantly, Co-TEP-COF/CNT exhibited only a 5% current drop after 24 h stability test. As a result, the introduction of CNT can increase the activity and stability of porphyrin-based COFs.
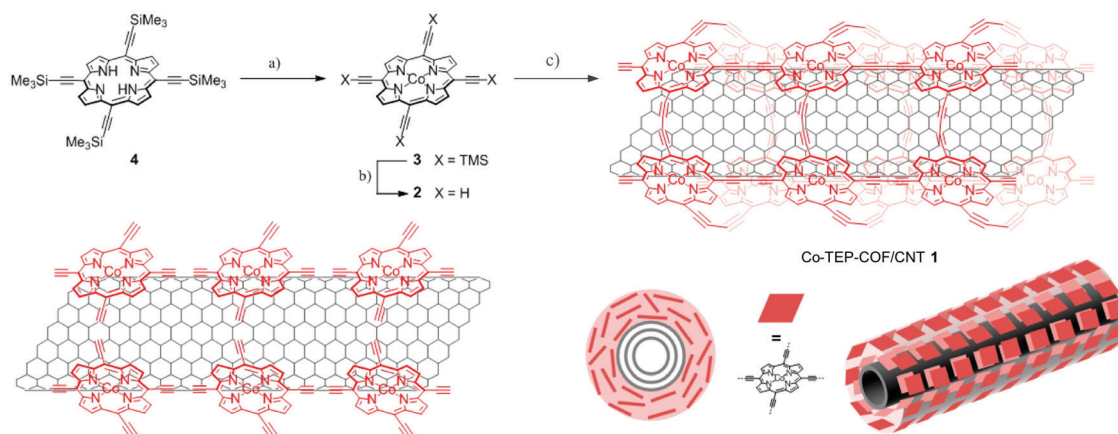
Fig. 7 Synthetic procedure of Co-TEP-COF/CNT.[193] Reproduced from ref. 193 with permission from American Chemical Society, copyright 2014.

2552 | Chem. Soc. Rev., 2021, 50, 2540–2581

This journal is © The Royal Society of Chemistry 2021

Similarly, Du and co-workers prepared a hybrid material with Fe-TEP-COF supported on CNT (named Fe-TEP-COF/CNT) for ORR.[194] Hybrid Fe-TEP-COF/CNTs exhibited an ORR wave with an $E_{onset} = 0.88$ V (versus RHE) and an $E_{1/2} = 0.76$ V (versus RHE) in 0.1 M KOH. Meanwhile, the n value of Fe-TEP-COF/CNT was 3.79, demonstrating a 4e reduction process. Therefore, this is a very effective strategy to enhance ORR performance and 4e selectivity not only in acidic electrolyte but also in alkaline solution. In addition, the stability of porphyrin-based frameworks and CNT hybrids has been greatly enhanced using this strategy.

In addition to carbon materials, conductive fluorine-doped tin oxide (FTO) electrodes have also been selected as substrates. For instance, Morris and co-workers prepared a PCN-223-Fe catalyst grown on FTO for ORR.[184] PCN-223-Fe with a plate-like morphology was fabricated with metal ZrO clusters and Fe TCPP organic linkers. The PCN-223-Fe/FTO composite showed excellent 4e ORR selectivity with less than 6% H_2O_2 production. Therefore, porphyrin-based frameworks are usually loaded onto conductive supports for electrocatalytic applications. Recently, Nejati and co-workers prepared several metal-free porphyrin COFs using TAPP as building units through the electrodeposition method grown on the GC electrode (Fig. 8).[195] The simulated crystal structure of TAPP-COF with six pyridine molecules is shown in Fig. 8a. TAPP-COF has an obvious packing structure of porphyrin molecules with pyridines dispersed in the channel. Scanning electron microscopy (SEM) images of TAPP-COFs obtained at 25 °C with different scan rates, such as 2 mV s^{-1} (i), 10 mV s^{-1} (ii), and 50 mV s^{-1} (iii), demonstrated that the morphology of porphyrin-based COFs could be regulated by scan rates (Fig. 8b–d). In addition, the growth process of TAPP-COFs demonstrated that porphyrin crystals prefer to grow from the edges of the (110) planes of COFs. The CV data of samples were measured in O_2-saturated phosphate buffer solution (PBS) with

different scan rates (Fig. 8e). An obvious O_2 reduction peak at 0.54 V (versus RHE) was observed for sample iii, as compared to samples i and ii, demonstrating its better ORR performance. By combining SEM images of samples i and ii, it was found that porphyrin framework films with larger crystalline dendrites displayed better ORR activity.

The above-mentioned experiments confirmed that electrochemical polymerization is also an effective strategy to construct COFs. Lei and co-workers also prepared a Co-TTP-COF on the GC electrode through electrochemical polymerization.[175] The CV data presented an obvious peak of O_2 reduction for Co-TTP-COF at $\sim$0.41 V (versus RHE) measured in PBS (0.01 M, pH = 7). The electron transfer numbers of Co-TTP-COF were 3.9, 3.82, and 4.03 in buffers of pH = 2, 7, and 13, respectively. Furthermore, Co-TTP-COF showed excellent stability after running 100 cycles in 0.1 M KOH and good methanol resistance.

3.1.5 Porphyrin-based framework derivatives for ORR.
Transition metal–nitrogen–carbon (M–N–C, M = Fe and Co, etc.) materials have become promising candidates for ORR due to their high activity and excellent stability.[271–277] However, the exact active site structure of M–N–C materials, which are usually generated through high temperature pyrolysis processes, is difficult to be determined, leading to the difficulty in investigating reaction mechanisms and also structure–activity relationships. With the development of characterization technologies, the active site of the M–N–C material is considered to have the M–N_4 coordination structure.[278–280] The resulting M–N_4 active site is structurally similar to that of biological heme units for O_2 activation and reduction. Because of their precise structures, many porphyrin-based MOFs and COFs have recently been used as precursors to prepare M–N–C materials with M–N_4 active site structures.[281] In addition, the chemical and catalytic features of M–N_4 active sites can be readily regulated by tuning structures of porphyrin-based MOFs and COFs. The uniform distribution of
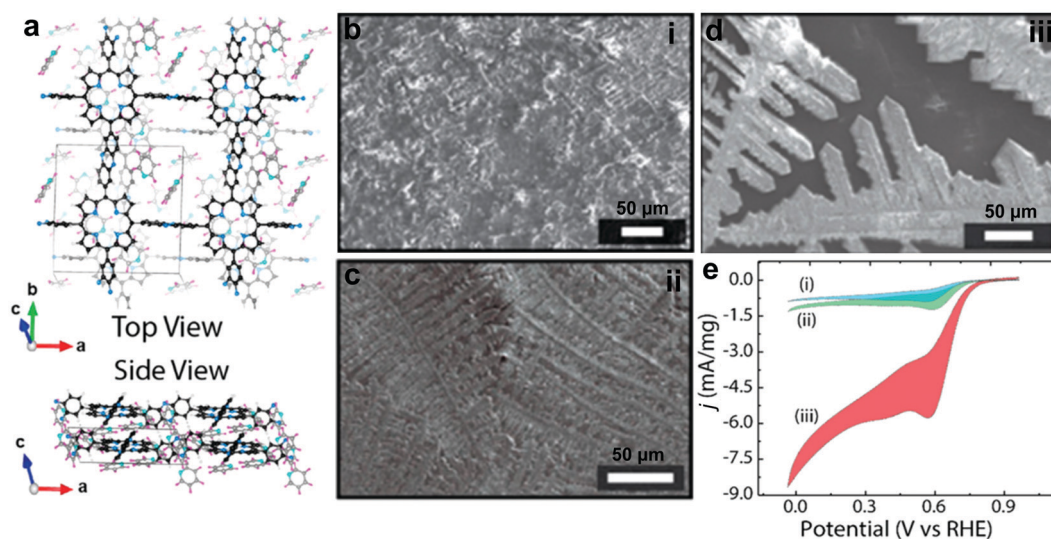
Fig. 8 (a) Calculated crystal structure of TAPP-COFs with six pyridine molecules. (b–d) SEM images of TAPP-COFs electrodeposited on the GC electrode obtained at 25 °C with different scan rates: 2 mV s^{-1} (i), 10 mV s^{-1} (ii), and 50 mV s^{-1} (iii), and (e) the corresponding normalized CV data measured in O_2-saturated phosphate buffer solution (pH = 13).[195] Reproduced from ref. 195 with permission from American Chemical Society, copyright 2019.

This journal is © The Royal Society of Chemistry 2021

Chem. Soc. Rev., 2021, 50, 2540–2581 | 2553

M–N$_4$ active sites can be maintained during the pyrolysis process. Porous carbon materials have relatively good conductivity, which will enhance electron transfer during the ORR process. Therefore, porphyrin-based frameworks are appealing precursors to make M–N–C materials, whose catalytic properties can be fine-tuned and studied. In 2011, Li and co-workers prepared a Co-TPP-COF.[282] The resulting mixture of Co-TPP-COF and Vulcan XC-72 was further heated at 600 °C. Electrochemical measurements showed that Co-TPP-COF-600 exhibited an E_{onset} = 0.80 V (*versus* RHE) and an $E_{1/2}$ = 0.73 V (*versus* RHE) in 0.5 M H$_2$SO$_4$. Furthermore, porphyrin-based framework composites exhibited better activity and stability for ORR than porphyrin molecule composites, demonstrating the benefits of porphyrin-based frameworks. Dai, Cao and co-workers also prepared several M–N–C materials by heating different metal porphyrin-based COFs constructed with metal coordinated TBBPP through self-polycondensation.[213] Carbonized metal porphyrin COF materials were obtained at 950 °C. The resulting Fe–N–C-950 exhibited significantly boosted ORR activity with an E_{onset} = 0.98 V (*versus* RHE), which was similar with that of commercial Pt/C 20 wt% in 0.1 M KOH. In contrast, E_{onset} of Fe–N–C-950 was 0.89 V (*versus* RHE) in 0.1 M HClO$_4$, while the E_{onset} value is 0.96 V (*versus* RHE) for Pt/C in this acidic solution. Similarly, Müllen, Feng and co-workers synthesized a Co-TBPP-COF *via* the Yamamoto polycondensation.[212] Then, Co-TBPP-COF was pyrolyzed at 800 °C. The resulting Co-TBPP-COF-800 exhibited ORR wave with an $E_{1/2}$ = 0.78 V (*versus* RHE) in 0.1 M KOH and an $E_{1/2}$ = 0.64 V (*versus* RHE) in 0.5 M H$_2$SO$_4$. The n of Co-TBPP-COF-800 was 3.94 in acidic solution. Mao and co-workers also obtained a series of Co–N–C materials by heating porphyrin COFs synthesized with Co TAPP and terephthalaldehyde at different temperatures (600 to 1000 °C).[283]

In addition, porphyrin-based frameworks have been regarded as suitable platforms or precursors to prepare single-atom catalysts.[284] Porphyrin molecules can coordinate with precious metals (*e.g.*, Pt) or nonprecious metals (*e.g.*, Fe) to realize uniform distribution of single atoms on porphyrin-based frameworks.[285–287] Recently, Cao, Huang and co-workers prepared a single-atom-based Fe–N–C material through pyrolyzation of Fe porphyrin-based COFs constructed with Fe^{III} 5,10,15,20-tetra(4-cyanophenyl)porphyrin (TCyPP) chloride through trimerization reaction.[288] Fe single-atoms distributed frameworks were heated at 600 °C. The resulting Fe–N–C-600 showed an E_{onset} = 1.01 V (*versus* RHE) and an $E_{1/2}$ = 0.87 V (*versus* RHE) for electrocatalytic ORR in 0.1 M KOH. Furthermore, the n value of Fe–N–C-600 was 3.88, which indicated a 4e reduction process. The current loss of Fe–N–C-600 was about 10% after running the 8 h stability test, indicating relatively good durability. In addition, Fe–N–C-600 also exhibited excellent activity and durability for ORR in 0.1 HClO$_4$. Compared to other catalysts, single-atom-based materials exhibited high intrinsic electrocatalytic activity.[289–291] Jiang and co-workers designed a series of single-atom Fe doped N–C materials (Fe$_{SA}$–N–C) by heating porphyrin-based MOF PCN-222-Fe constructed with different molar ratios of Fe TCPP and metal-free TCPP (Fig. 9a and b).[287] The Fe$_{SA}$–N–C obtained at 800 °C had an Fe content of 1.76 wt% with uniformly
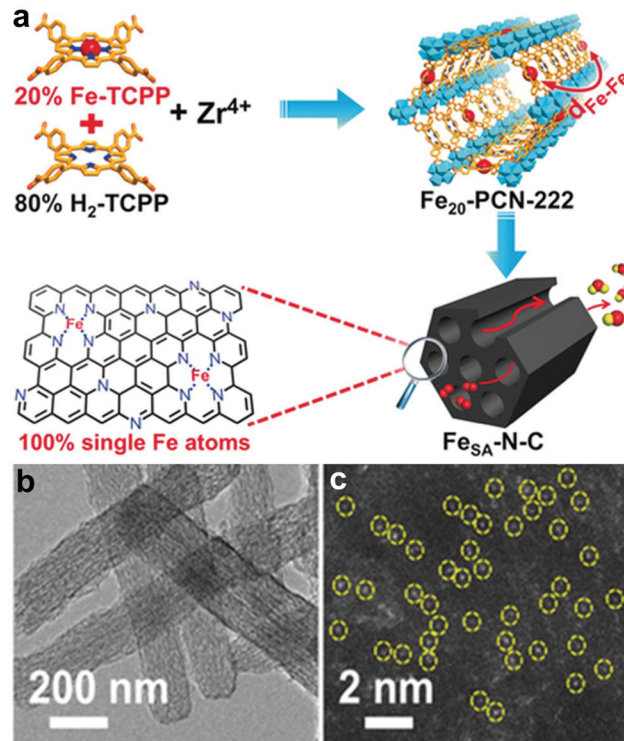
Fig. 9 (a) Schematic illustration of the preparation procedure for Fe$_{SA}$–N–C derived from the porphyrin-based framework PCN-222-Fe. (b) TEM image and (c) aberration-corrected high-angle annular dark field scanning transmission electron microscopy image of Fe$_{SA}$–N–C.[287] Reproduced from ref. 287 with permission from the Wiley-VCH, copyright 2018.

distributed single-atoms (Fig. 9c). Fe$_{SA}$–N–C exhibited ORR activity with an $E_{1/2}$ = 0.891 V (*versus* RHE) in 0.1 M KOH and an $E_{1/2}$ = 0.776 V (*versus* RHE) in 0.1 M HClO$_4$. More recently, the same group introduced SiO$_2$ into this porphyrin MOF system to prevent the aggregation of Fe atoms during the pyrolysis process.[292] The resulting Fe$_{SA}$–N–C exhibited a much higher content of Fe loading (3.46 wt%) and further enhanced ORR activity with an $E_{1/2}$ = 0.90 V (*versus* RHE) in 0.1 M KOH and an $E_{1/2}$ = 0.80 V (*versus* RHE) in 0.1 M HClO$_4$.

Furthermore, porphyrin-based frameworks are also suitable precursors to obtain uniform dual-metal-based catalysts.[293] For example, Feng, Bu and co-workers constructed several porous PCN materials with Fe 5,10,15,20-tetra(4-iodophenyl)porphyrin and Co TEPP as components.[294] PCN-FeCo COF materials were heated at 800 °C to give PCN-FeCo/C-800. Porous PCN-FeCo/C-800 showed superior ORR performance with an E_{onset} = 1.0 V (*versus* RHE) in 0.1 M KOH as compared to PCN-FeFe/C-800 (E_{onset} = 0.97 V *versus* RHE) and PCN-CoCo/C-800 (E_{onset} = 0.92 V *versus* RHE), respectively.[294] PCN-FeCo/C-800 also exhibited excellent catalytic activity of ORR in 0.1 M HClO$_4$ with an $E_{1/2}$ = 0.76 V (*versus* RHE).

Based on the above discussion, M–N–C catalysts derived from porphyrin-based frameworks showed relatively higher catalytic activity for ORR as compared to pyrolysis-free frameworks. This may be ascribed to the high conductivity of M–N–C materials after heat treatment. Furthermore, porphyrin-based

2554 | *Chem. Soc. Rev.*, 2021, **50**, 2540–2581

This journal is © The Royal Society of Chemistry 2021

framework precursors are beneficial for the preparation of single-atom based materials, which have become a promising candidate for ORR in PEMFC.

3.1.6 Comparison of porphyrin-based frameworks for ORR. Catalytic ORR activities of porphyrin-based frameworks, composites, and their derived M–N–C materials reported in the literature have been summarized and listed in Table 2. Several conclusions can be drawn from these results.

First, for pyrolysis-free porphyrin-based frameworks, Co-TEP-COF/CNT and Co-PCOF/graphene have the largest ORR $E_{1/2}$ with a value of 0.65 V (*versus* RHE) in 0.5 M H_2SO_4 and 0.81 V (*versus* RHE) in 0.1 M KOH, respectively. Carbon materials such as carbon black, graphene, rGO, py-rGO, and CNT have been generally used in hybrid systems owing to the relatively poor conductivity of porphyrin-based frameworks. However, catalytic activity of porphyrin-based frameworks is still unsatisfactory for practical applications as compared to commercial Pt/C (20 wt%), which exhibited an $E_{1/2}$ = 0.84 V (*versus* RHE) in 0.1 M $HClO_4$ and $E_{1/2}$ = 0.86 V (*versus* RHE) in 0.1 M KOH. In contrast, porphyrin-based frameworks-derived M–N–C materials exhibit higher ORR catalytic activity due to the enhanced conductivity. For example, Fe–N–C-600 exhibits an E_{onset} = 1.01 V (*versus* RHE) and an $E_{1/2}$ = 0.87 V (*versus* RHE) in 0.1 M KOH. Furthermore, ORR performance of the single-atom based M–N–C material will be enhanced due to the

intrinsic catalytic activity. Fe_{SA}–N–C exhibited an $E_{1/2}$ = 0.891 V (*versus* RHE) in 0.1 M KOH. In addition, pyrolyzation of porphyrin-based frameworks has become an effective strategy to prepare single-atom based materials due to the unique advantages of frameworks and precise and tunable coordination environments of metal active sites.

Second, the electron transfer number n for most porphyrin-based frameworks is close to 4, indicating a 4e reduction process with the main product of H_2O. For example, Co porphyrin-based framework composites Co-TEP-COF/CNT exhibited an electron transfer number of 3.93 in 0.5 M H_2SO_4. As mentioned above, mononuclear Co porphyrin molecule usually displays an n value of 2 for ORR. Thus, porphyrin-based frameworks have beneficial effects on the 4e reduction process due to the unique packing structures of porphyrin molecules. In contrast, PCN-222-Co/C had an n value of 2.3 in 0.1 M KOH due to the large distance between porphyrin molecules in frameworks. Therefore, developing porphyrin-based frameworks with a suitable packing distance of porphyrin molecules can regulate the selectivity of ORR.

3.2 Oxygen evolution reaction (OER)

3.2.1 Evaluation of activity for OER. Usually, catalysts were coated on GC electrodes to evaluate OER performance. In addition, other electrodes, such as carbon fiber paper (CFP), Cu foam (CF) and FTO, have also been applied as working electrodes due to their large surface areas. The most important evaluation criterion is the overpotential η_{10}, which is the overpotential required to yield a catalytic current density j = 10 mA cm^{-2}. Correspondingly, the E_{10} strands for the potential at j = 10 mA cm^{-2}. The overpotential η_{10} can be calculated using eqn (28) and (29), by taking the Ag/AgCl reference electrode ($E_{Ag/AgCl}$ = 0.197 V at 25 °C) as an example.

$$E_{10} = E_{Ag/AgCl} + 0.197 + 0.059 \times pH \text{ V} \qquad (28)$$

$$\eta_{10} = E_{10} - 1.23 \text{ V} \qquad (29)$$

Herein, the theoretical potential required for water oxidation is 1.23 V. At the same j (10 mA cm^{-2}), the smaller of η_{10}, the better of as-prepared electrocatalysts. The Tafel slope is another parameter used to reflect the growth rate of j. The smaller the Tafel slope, the better the as-prepared catalysts. Stability is also a significant parameter for practical application by carrying out controlled potential/current electrolysis.

At present, precious metal-based RuO_2 and IrO_2 compounds are the most promising catalysts for OER.[299] However, the high price and limited reserves restrict their wide applications. Currently, transition metal-based hydroxides, oxides, and phosphides have been extensively studied as catalysts for OER due to their excellent catalytic activity.[300–305] Recently, MOFs and COFs were also reported for OER.[129,150,306] This is mainly because MOFs and COFs have clear active sites and surrounding coordination environments, which are helpful to study the OER process and reaction mechanisms, and then to build the structure–activity relationships. Porphyrin-based frameworks as a

Table 2 Comparison of the ORR performance for porphyrin-based composites, frameworks and their derived M–N–C materials

Catalysts	Electrolyte	E_{onset} (V *versus* RHE)	$E_{1/2}$ (V *versus* RHE)	n	Ref.
Co–Al-PMOF/C	0.1 M H_2SO_4	0.75	0.50	3.65	187
Co-TPP-COF-600	0.5 M H_2SO_4	0.80	0.73	—	282
Co-TEPP-COF/C	0.5 M H_2SO_4	0.62	0.52	3.88	264
Co-TEP-COF/CNT	0.5 M H_2SO_4	0.75	0.65	3.93	193
Co-TBPP-COF-800	0.5 M H_2SO_4	0.80	0.64	3.94	212
PCN-222-Co/C	0.1 M $HClO_4$	0.64	0.48	—	197
PCN-FeCo/C-800	0.1 M $HClO_4$	0.90	0.76	4.2	294
Fe–N–C-950	0.1 M $HClO_4$	0.89	0.80	3.82	213
Fe_{SA}–N–C	0.1 M $HClO_4$	0.88	0.776	4.0	287
Pt/C (20 wt%)	0.1 M $HClO_4$	1.0	0.84	4.0	292
Co TPP cage/CNT	PBS (pH = 7)	0.72	0.65	2.0	295
TAPP-COF	PBS (pH = 13)	0.75	0.68	3.97	195
Co-TAPP-COF-Fe	1.0 M KOH	0.95	0.84	2.1	296
Co TPP/CNT	0.1 M KOH	0.86	0.81	—	297
Co TPFPP/CNT	0.1 M KOH	0.80	0.76	—	297
Fe-TCPP-MOF/py-G	0.1 M KOH	0.93	0.76	3.82	268
Co-PCOF/graphene	0.1 M KOH	0.90	0.81	—	266
Cu phthalocyanines MOFs/CNT	0.1 M KOH	0.90	0.83	3.93	298
Fe-TEP-COF/CNT	0.1 M KOH	0.88	0.76	3.79	194
COF-366-Co/py-rGO	0.1 M KOH	0.84	0.765	3.80	269
PCOF-SO_3-Co/rGO	0.1 M KOH	0.88	0.72	3.70	267
Co-TEPP-COF/C	0.1 M KOH	0.86	0.80	3.80	264
PCN-221-Co/C	0.1 M KOH	0.80	0.70	2.6	201
PCN-222-Co/C	0.1 M KOH	0.80	0.69	2.3	201
PCN-226-Co/C	0.1 M KOH	0.83	0.75	3.3	201
Fe–N–C-600	0.1 M KOH	1.01	0.87	3.88	288
Fe–N–C-950	0.1 M KOH	0.98	0.82	3.81	213
Co-TBPP-COF-800	0.1 M KOH	0.86	0.78	3.85	212
Fe_{SA}-N-C	0.1 M KOH	0.97	0.891	4.0	287
PCN-FeCo/C-800	0.1 M KOH	1.0	0.85	4.2	294
Pt/C (20 wt%)	0.1 M KOH	1.0	0.86	4.0	292

This journal is © The Royal Society of Chemistry 2021

Chem. Soc. Rev., 2021, **50**, 2540–2581 | **2555**

specific kinds of framework material have also been reported as catalysts for OER.

3.2.2 OER reaction mechanisms with metal porphyrins.

Currently, the OER mechanism of transition metal based oxides and hydroxides has been studied.[307,308] Typically, an OER mechanism in alkaline electrolytes is displayed below (eqn (30)–(34)).

$$* + OH^- \rightarrow *OH + e^- \tag{30}$$

$$*OH + OH^- \rightarrow *O + e^- + H_2O \tag{31}$$

$$*O + OH^- \rightarrow *OOH + e^- \tag{32}$$

$$*OOH + OH^- \rightarrow *O_2 + e^- + H_2O \tag{33}$$

$$*O_2 \rightarrow * + O_2 \tag{34}$$
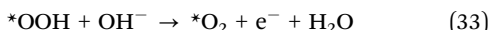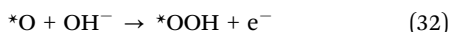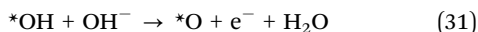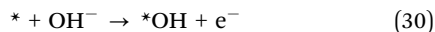
However, the OER mechanism is rarely reported for porphyrin-based frameworks. As for porphyrin molecules in homogenous catalysis, a similar reaction mechanism had been proposed and suggested.[66,309] For example, Groves and co-workers synthesized the cationic Co 5,10,15,20-tetra(1,3-dimethylimidazolium-2-yl)porphyrin.[60] OER mechanism studies demonstrated that the formation of O–O bond is the rate determining step. Specifically, Co^{II} porphyrin experienced two oxidation processes and formed Co^{III}–OH and Co^{IV}–O, respectively. Then the nucleophilic attack process of Co^{IV}–O by water molecule occurred and formed the peroxo intermediate. Finally, the peroxo intermediate was further oxidized to release O_2.

Recently, ECSTM has been regarded as an effective technology for the study of the reaction mechanism, especially for capture of intermediates. Wan, Wang and co-workers investigated the OER mechanism of porphyrin molecules using the ECSTM technology.[310] Co TPP was selected as the model molecule. Co TPP molecules were assembled on the Au(111) electrode to form a thin layer. During the OER process, the change of the Co TPP–OH^- to the Co TPP molecule was directly observed using *in situ* ECSTM, further confirming the OER mechanism. Therefore, it is possible to further study OER mechanism of porphyrin-based frameworks.

3.2.3 Porphyrin-based frameworks for OER.

Porphyrin-based frameworks can be used as catalysts for OER directly. For example, Sun, Dai and co-workers designed a porphyrin-based MOF connected with a polymeric chain (Fig. 10).[198] Metal-free TCPP was selected as the porphyrin organic linker (Fig. 10a). An obvious three dimensional (3D) porous structure of Pb-TCPP-MOF was observed with one dimensional (1D) channels as shown *via* ball and stick representation (Fig. 10b). The chain was made up of carboxyl oxygen coordinated Pb ions (Fig. 10c). The space filling diagram of Pb-TCPP-MOF further confirmed the porous structure (Fig. 10d). Simulated and experimental X-ray diffraction (XRD) patterns confirmed the formation of this topological structure (Fig. 10e). Pb-TCPP-MOF showed obvious gas adsorption selectivity for CO_2 compared to CH_4 at 298 K. In addition, the OER performance of Pb TCPP was carried out without adding conductive carbon materials. Pb TCPP
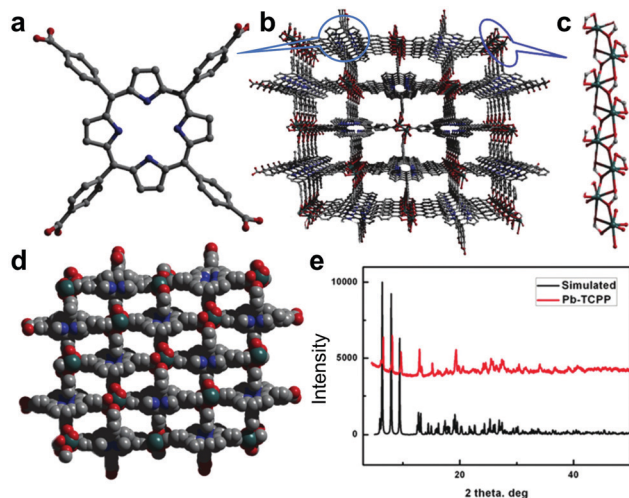
Fig. 10 Metal-free TCPP molecule (a), ball and stick crystal structure (b), polymeric chain constructed with carboxyl oxygen coordinated Pb ions (c) and space filling diagram (d) of Pb-TCPP-MOF. Simulated and experimental XRD pattern of Pb-TCPP-MOF (e).[198] Reproduced from ref. 198 with permission from the Royal Society of Chemistry, copyright 2016.

exhibited an $\eta_{10} = 470$ mV with a Tafel slope of 106.2 mV dec^{-1} in 1.0 M KOH.

Metal porphyrins have also been applied as building blocks to prepare frameworks for OER. For example, Dai, Wang and co-workers prepared Zn and Cu coordinated TCyPP.[311] Metal-free TCyPP molecules exhibited an $\eta_{10} = 510$ mV in 1.0 M KOH. In contrast, Cu TCyPP and Zn TCyPP showed an enhanced OER activity with lower η_{10} values of 430 and 480 mV, respectively. The Tafel slope of Cu TCyPP and Zn TCyPP was 83.9 and 87.5 mV dec^{-1}, respectively, while metal-free TCyPP had a Tafel slope of 90.1 mV dec^{-1}. These results demonstrated that the metal centers of porphyrins were the real active sites for OER. Tuning crystal structure of frameworks can further improve the OER performance.

In addition to porphyrin-based MOFs, Gu and co-workers recently synthesized two porphyrin-based COFs (Fig. 11).[199] The 3,3′,5,5′-tetra(4-formylphenyl)bimesityl (TFBM) was selected as a rigid tetrahedral aldehyde. The Co-based planar porphyrin TAPP and 5,10,15,20-tetra(4-aminobiphenyl)porphyrin (TABPP) were applied as porphyrin units. The overpotential to reach OER current density $j = 10$ mA cm^{-2} for Co-TAPP-COF and Co-TABPP-COF in 1.0 M KOH was 473 and 487 mV, respectively. The relatively larger η_{10} of Co-TABPP-COF is ascribed to the smaller Brunauer–Emmett–Teller surface area (234 m^2 g^{-1}) compared to that of Co-TAPP-COF (316 m^2 g^{-1}). In a similar manner, Zhu, Zhao, Wang and co-workers constructed a Co porphyrin-based COF with Co TAPP as the porphyrin building unit and 2-hydroxyterephthalaldehyde as the organic linker.[312] The resulting Co-TAPP-COF particle has a BET surface area of 289 m^2 g^{-1}. The overpotential and Tafel slope of Co-TAPP-COF particle for OER is 350 mV at $j = 10$ mA cm^{-2} and 151 mV dec^{-1} in 1.0 M KOH. Furthermore, Zhang and co-workers prepared a series of metal coordinated TAPP COFs with ferrocene-1,1′-dicarbaldehyde as organic linkers.[296] The results demonstrate
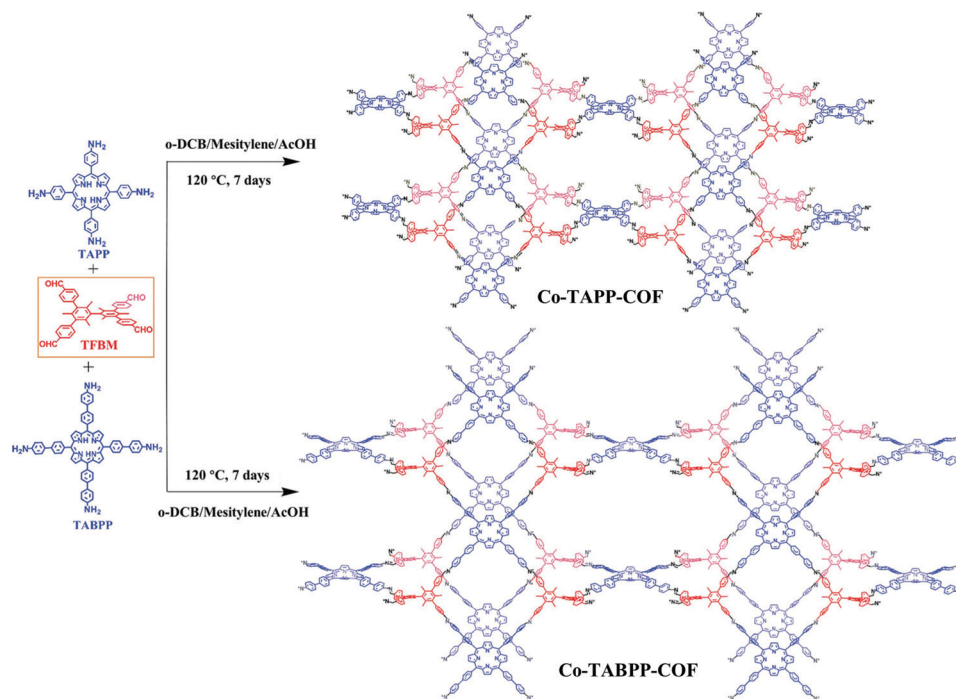
Fig. 11 Synthetic procedure and crystal structure of Co–TAPP-COF and Co–TABPP-COF prepared with TFBM as the monomer and TAPP and TABPP as porphyrin linkers, respectively.[199] Reproduced from ref. 199 with permission from the Royal Society of Chemistry, copyright 2019.

that Co-based TAPP COFs exhibited excellent OER performance compared to Ni-, Zn-, and Pd-based TAPP COFs. The Co-TAPP-COF-Fe exhibited an η_{10} of 416 mV for OER in 1.0 M KOH compared to Ni-TAPP-COF-Fe (486 mV).

Similarly, Bhattacharya, Pradhan, Bhaumik and co-workers constructed a Co-based porphyrin COF through the Suzuki C–C cross-coupling reaction using Co 5,10,15,20-tetra(4-bromophenyl)-porphyrin and 1,3,6,8-tetra(4,4,5,5-tetramethyl-1,3,2-dioxaborolan-2-yl)pyrene as components.[313] The resulting Co COF exhibited an η_{10} = 420 mV for OER measured in 1.0 M NaOH. The excellent OER performance may be ascribed to the efficient electron transfer between Co porphyrin (donor) and pyrene (acceptor). Differently from these metal porphyrins, Zhu, Wang and co-workers prepared a metal free porphyrin-based COF with catechol porphyrin and titanium tetraisopropoxide as reactants.[314] The resulting PCOF-Ti exhibited an η_{10} = 310 mV and a Tafel slope of 117 mV dec^{-1} for OER in 1.0 M KOH.

3.2.4 Porphyrin-based frameworks grown on supports for OER. At present, the OER performance of porphyrin-based frameworks is still unsatisfied. To further improve their catalytic activity, conductive supports were introduced into these systems. For example, Morris and co-workers obtained a thin MOF film grown on FTO with PCN-224-Ni.[183] The OER performance was evaluated in neutral pH with an onset overpotential of 450 mV and a Tafel slope of 150 mV dec^{-1}. Du and co-workers constructed Co-TEP-COFs supported on CNT materials (named Co-TEP-COF/CNTs) (Fig. 12a).[315] Transmission electron microscopy (TEM) image confirmed the formation of Co-TEP-COF/CNTs with COFs on the surface of CNTs (Fig. 12b). LSV measurements showed that the overpotential of Co-TEP-COF/CNTs was

410 mV at j = 10 mA cm^{-2} in 1.0 M KOH (Fig. 12c). Co-TEP-COF/CNTs exhibited a Tafel slope of 60.8 mV dec^{-1}. Durability test performed at j = 10 mA cm^{-2} further confirmed the stability of Co-TEP-COF/CNTs (Fig. 12d). Therefore, the introduction of CNTs greatly improves OER performance and stability of porphyrin-based frameworks.

Similarly, Co TEPP with an additional phenyl was also selected as porphyrin building units to construct COFs. For example, Chen, Zhang and co-workers obtained a Co-TEPP-COF
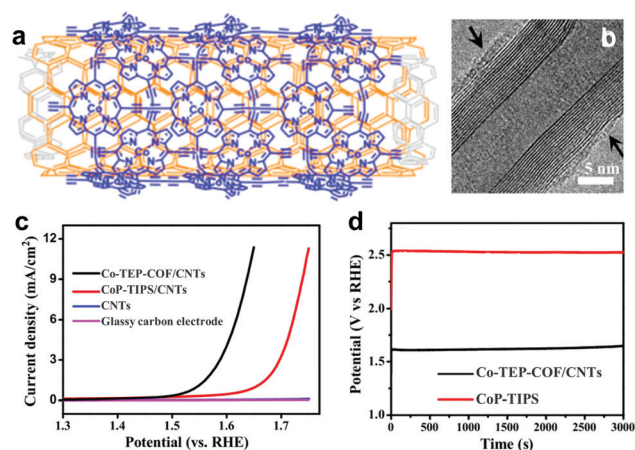
Fig. 12 (a) Schematic illustration of Co-TEP-COF/CNTs. (b) TEM image, (c) LSV curve and (d) controlled current density electrolysis measurement at j = 10 mA cm^{-2} for Co-TEP-COF/CNTs in 1.0 M KOH.[315] Reproduced from ref. 315 with permission from American Chemical Society, copyright 2015.

This journal is © The Royal Society of Chemistry 2021

Chem. Soc. Rev., 2021, **50**, 2540–2581 | **2557**
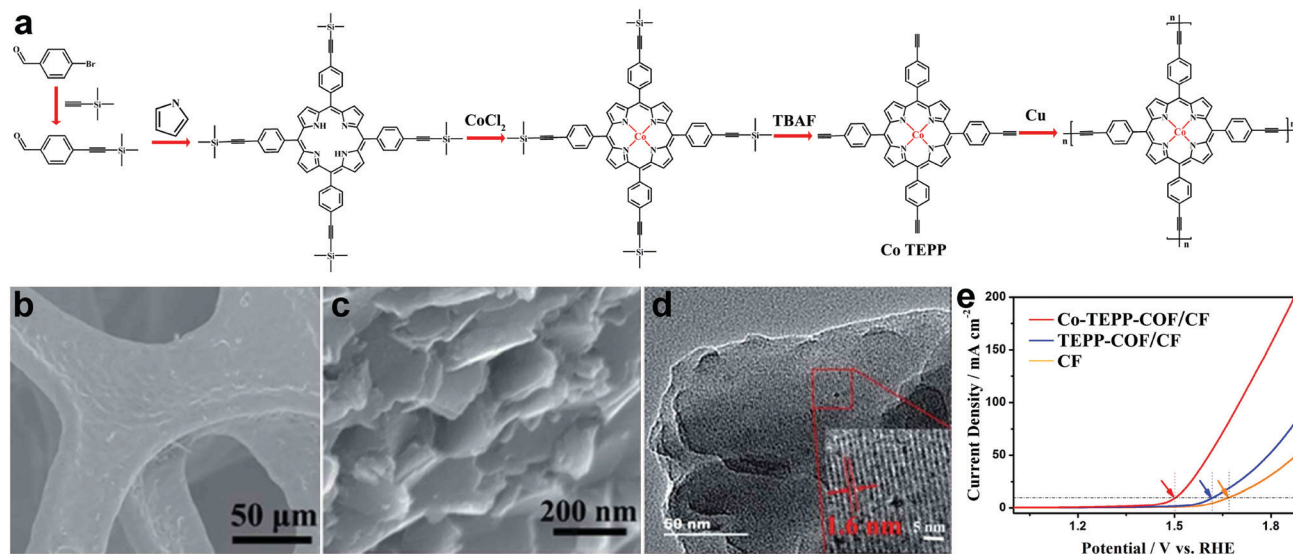
Fig. 13 (a) Synthetic routes, (b and c) SEM images, (d) TEM image and (e) LSV data of Co-TEPP-COF on the Cu foam (CF). Inset in Fig. 13d: high-resolution TEM image.[192] Reproduced from ref. 192 with permission from the Royal Society of Chemistry, copyright 2019.

nanosheet grown directly on Cu foam (Fig. 13).[192] The synthetic procedure of Co-TEPP-COF is similar with that reported by Campidelli and co-workers (Fig. 13a),[193] which afforded Co-TEPP-COF as 2D nanosheet with a lattice distance of 1.6 nm (Fig. 13b–d). Herein, the Cu foam is a 3D porous conductive substrate, which will improve the conductivity of the resulting hybrid material. Furthermore, Cu foam can catalyze the polymerization reaction of Co TEPP to form Co-TEPP-COF. Co-TEPP-COF/CF material exhibited an η_{10} = 270 mV and a Tafel slope of 99 mV dec^{-1} for OER in 1.0 M KOH (Fig. 13e). In contrast, TEPP-COF/CF without Co coordination and pure CF exhibited an overpotential of 381 and 442 mV at j = 10 mA cm^{-2}, respectively. Thus, Co is the real active site for OER.

Different from monometallic porphyrin-based frameworks, Grumelli and co-workers assembled a thin layer of dual-metal porphyrin MOF M^{1}TPyP-M^2 (M^{1}TPyP = metal-5,10,15,20-tetra(4-pyridyl)-porphyrin; M^1, M^2 = Fe, Co) on Au(111) electrode.[316] Electrochemical results demonstrated a dramatic OER enhancement for heterobimetallic catalysts compared to metal porphyrins. Specifically, FeTPyP-Co exhibited the best OER performance among this series of catalysts. Wan and co-workers also prepared a bimetallic Co–Cu porphyrin MOF/rGO hybrid with TCPP molecules. Optimized Co–Cu-TCPP-MOF/rGO showed an η_{10} = 396 mV and a Tafel slope of 58 mV dec^{-1} in 1.0 M KOH.[317] Therefore, porphyrin-based frameworks also provide a suitable platform to study the synergistic effect of dual-metals on electrocatalytic activity.

Table 3 Comparison of the OER performance for porphyrin-based composites, frameworks, and other typical catalysts

Catalysts	Electrode	Electrolyte (KOH)	Loading (mg cm^{-2})	η_{10} (mV)	Tafel (mV dec^{-1})	Ref.
Co TPP/CNT	GC	1.0 M	0.25	407	60.3	297
Co TPFPP/CNT	GC	1.0 M	0.25	480	71.6	297
Pb-TCPP-MOF	GC	0.1 M	0.2	560	124.5	198
Pb-TCPP-MOF	GC	1.0 M	0.2	470	106.2	198
TCyPP	GC	1.0 M	0.2	510	90.1	311
Cu TCyPP	GC	1.0 M	0.2	430	83.9	311
Zn TCyPP	GC	1.0 M	0.2	480	87.5	311
PCN-226-Co/C	GC	1.0 M	0.08	445	111	201
Co-TEP-COF/CNTs	GC	1.0 M	0.14	410	60.8	315
TEPP-COF/CF	CF	1.0 M	—	381	113	192
Co-TEPP-COF/CF	CF	1.0 M	—	270	99	192
PCOF-Ti	CFP	1.0 M	330	310	117	314
Co-TAPP-COF	GC		0.643	473	89	199
Co-TABPP-COF	GC	1.0 M	0.643	487	95	199
Co-TAPP-COF-Fe	GC	1.0 M	0.42	416	68	296
Ni-TAPP-COF-Fe	GC	1.0 M	0.42	486	81	296
Co-TAPP-COF particle	CFP	1.0 M	290	350	151	312
Co–Cu-TCPP-MOF/rGO	GC	1.0 M	0.13	396	58	317
Ni phthalocyanines-MOF	FTO	1.0 M	0.0076	350	74	318
Commercial RuO$_2$	GC	1.0 M	0.2	330	48	319
Commercial IrO$_2$	GC	1.0 M	1.0	338	50	320

2558 | Chem. Soc. Rev., 2021, 50, 2540–2581

This journal is © The Royal Society of Chemistry 2021

3.2.5 Comparison of porphyrin-based frameworks for OER.

As discussed above, the catalytic activities for OER of reported porphyrin-based composites and frameworks are listed in Table 3.

In conclusion, the Co-based porphyrin COF grown on CF, named Co-TEPP-COF/CF, has the smallest overpotential of 270 mV to reach $j = 10$ mA cm^{-2} in 1.0 M KOH. Co–Cu-TCPP-MOF/rGO exhibited the smallest Tafel slope with a value of 58 mV dec^{-1}. Porphyrin-based frameworks with conductive supports usually have superior catalytic activity for OER compared to pure frameworks due to the enhanced electron transfer efficiency. However, the overpotential η at $j = 10$ mA cm^{-2} of most porphyrin-based frameworks for OER is between 400 and 500 mV, which is still larger than that of commercial RuO$_2$ (330 mV) and IrO$_2$ (338 mV) measured in 1.0 M KOH. Therefore, the OER performance of porphyrin-based framework catalysts is unsatisfactory and requires further improvement.

3.3 Rechargeable Zn–air battery

3.3.1 Evaluation of Zn–air battery performance.

Bifunctional electrocatalysts for ORR and OER are required for rechargeable metal–air batteries. The potential difference (ΔE) of $E_{1/2}$ for ORR and E_{10} for OER is usually selected as a key parameter to evaluate catalytic activity of bifunctional ORR and OER catalysts (eqn (35)).

$$\Delta E = E_{10} - E_{1/2} \tag{35}$$

Porphyrin molecules coordinated with transitional metals such as Co and Fe have been shown to be highly active for both electrocatalytic ORR and OER. Therefore, the rational design and development of porphyrin-based frameworks will realize bifunctional ORR and OER.

Zn–air battery is one of the prevailing metal batteries for energy storage.[321] In general, the Zn–air battery contains Zn anode, electrolyte, and catalyst cathode. Several parameters, including open circuit voltage, discharge and charge voltage gap, and power density, are commonly reported to evaluate performance of the Zn–air battery. Herein, the open circuit voltage refers to the difference between the positive electrode potential and the negative electrode potential of a battery when the battery is open (e.g., when no current passes through two poles). Discharge and charge voltage gap represents the voltage difference between charge voltage and discharge voltage. For a Zn–air battery, the power density equals current density times voltage.

3.3.2 Porphyrin-based composites for Zn–air batteries.

From what has been discussed above, metal porphyrins are promising alternative catalysts for both ORR and OER. Recently, Cao, Wang and co-workers compared the bifunctional ORR and OER performance of Co TPP and Co 5,10,15,20-tetra(pentafluorophenyl)porphyrin (TPFPP) by drop-coating molecular catalysts on CNTs.[297] Substituent groups of these two porphyrin molecules exhibited obvious different electron-withdrawing properties. Electrochemical results indicated that Co TPP/CNTs exhibited a larger $E_{1/2}$ (0.81 V versus RHE) compared to Co TPFPP/CNTs ($E_{1/2}$ = 0.76 V versus RHE) measured in 0.1 M KOH for ORR. Furthermore, the

overpotential of OER for Co TPP/CNT is 407 mV, which is smaller than that of Co TPFPP/CNT (480 mV) at $j = 10$ mA cm^{-2} measured in 1.0 M KOH. Therefore, the ΔE of Co TPP/CNT is about 0.827 V. Based on the bifunctional ORR and OER performance, practical application of Zn–air batteries was evaluated. Co TPP/CNT exhibited a peak power density of 155.7 mW cm^{-2}, while the value of Co TPFPP/CNT is 84.5 mW cm^{-2}. As a result, Co porphyrin molecules exhibit excellent performance in Zn–air batteries. Therefore, porphyrin-based frameworks have been investigated and regarded as bifunctional ORR an OER electrocatalysts.

3.3.3 Porphyrin-based framework composites for Zn–air batteries.

In addition to porphyrin-based composites, porphyrin-based frameworks also have been used as catalysts for Zn–air batteries. For example, Dehghanpour and co-workers prepared a Co porphyrin-based MOF (named PCN-224-Co).[200] Cubic particles of PCN-224-Co were obtained with microscale diameters. CNTs were introduced and mixed with PCN-224-Co to improve conductivity. SEM image demonstrated the uniform distribution of CNTs and PCN-224-Co. The resulting PCN-224-Co/CNT hybrid displayed bifunctional ORR and OER performance with high stability and good methanol resistance, which specifies the broad application prospect of porphyrin-based PCN porous materials. More recently, a series of porphyrin-based PCN-226 MOFs have been prepared with M
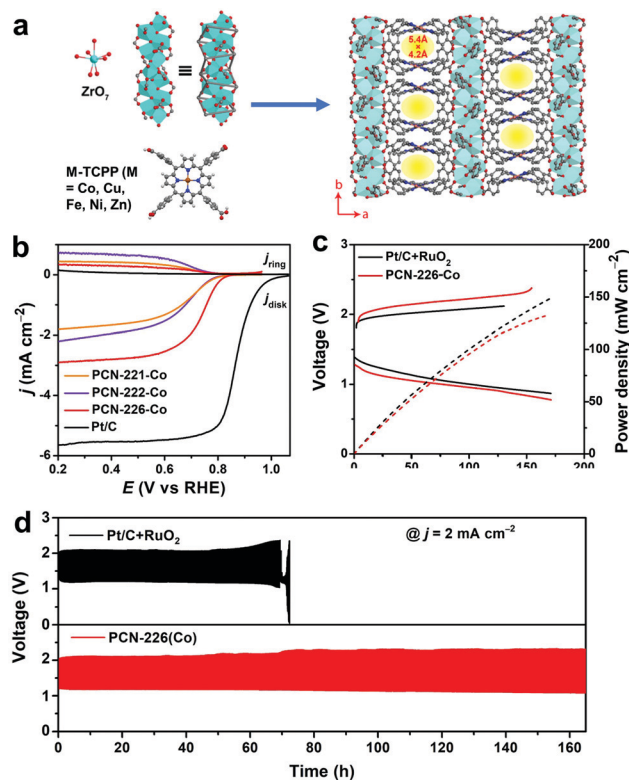
Fig. 14 (a) Crystal structure of PCN-226-M (M = Co, Cu, Fe, Ni, and Zn). (b) LSV data of PCN-221-Co, PCN-222-Co, PCN-226-Co, and Pt/C measured with RRDE. (c) Charge–discharge LSV data and the corresponding power density and (d) long-term charge–discharge cycling test of PCN-226-Co and Pt/C + RuO$_2$.[201] Reproduced from ref. 201 with permission from American Chemical Society, copyright 2020.

This journal is © The Royal Society of Chemistry 2021

Chem. Soc. Rev., 2021, 50, 2540–2581 | 2559

TCPP (M = Co, Cu, Fe, Ni, and Zn) as porphyrin building units and ZrO_7 clusters as chain nodes (Fig. 14a).[201] The obtained PCN-226-M has obvious porous structures with a size of 5.4 Å × 4.2 Å. PCN-226-Co exhibited the best ORR performance compared to other transition metal-based PCN-226 MOFs and previous reported MOFs such as PCN-221 and PCN-222 (Fig. 14b). PCN-226-Co also exhibited an overpotential of 445 mV for OER at $j = 10$ mA cm^{-2} in 1.0 M KOH. A Zn–air battery assembled with PCN-226-Co showed comparable peak power density with a value of 133 mW cm^{-2} as compared to commercial Pt/C + RuO$_2$ (150 mW cm^{-2}) (Fig. 14c). PCN-226-Co also exhibited outstanding long-term charge–discharge cycling stability over 160 h with a voltage gap of 0.97 V at $j = 2$ mA cm^{-2} (Fig. 14d). In contrast, the voltage gap of Pt/C + RuO$_2$ increases after running for 60 h at the same conditions. Therefore, porphyrin-based frameworks showed great potential as bifunctional ORR and OER catalysts for Zn–air batteries.

In addition to porphyrin-based frameworks, phthalocyanine-based frameworks also exhibited comparable activity for Zn–air batteries. Recently, Xiang and co-workers constructed a conjugated Fe phthalocyanines COF/graphene hybrid.[322] This pyrolysis-free Fe-based single-atom catalysts exhibited an $E_{1/2} = 0.91$ V (*versus* RHE) for ORR in 0.1 M KOH, which was much larger than that of benchmark commercial Pt/C 20 wt% ($E_{1/2} = 0.86$ V *versus* RHE). A Zn–air battery assembled using this catalyst showed a power density of 123.43 mW cm^{-2}. Typically, the discharge/charge cycling test demonstrated exceptional durability for more than 300 h. Similarly, Feng, Dong and co-workers prepared a Cu phthalocyanine-based MOF connected with Co–O$_4$ nodes.[298] Cu phthalocyanines MOFs were mixed with CNT to serve as electrocatalysts for ORR and Zn–air batteries. The resulting Cu phthalocyanines MOFs/CNT exhibited an $E_{1/2} = 0.83$ V (*versus* RHE) and a $n = 3.93$ in 0.1 M KOH. Herein, the Co–O$_4$ nodes are real active sites for ORR as confirmed by theoretical calculations

and *in situ* Raman spectro-electrochemistry. The Zn–air battery assembled with Cu phthalocyanines MOFs/CNT exhibited an open circuit voltage of 1.37 V and a peak power density of 94 mW cm^{-2}. Therefore, phthalocyanine-based frameworks also exhibited excellent Zn–air battery performance.

3.3.4 Porphyrin-based frameworks grown on supports for Zn–air batteries. As discussed above, porphyrin-based frameworks can easily grow on conductive supports, which are more suitable to construct Zn–air batteries using these composites. For example, Zhang and co-workers prepared a Co-PCOF material by using a one-pot synthesis with introduced graphene (Fig. 15).[191] Co porphyrins were covalently connected through benzene units to give Co-PCOF (Fig. 15a). Then, hybrid Co-PCOF/graphene was obtained. SEM image indicated that the morphology of 2D graphene nanosheets still remained (Fig. 15b). Scanning transmission electron microscopy (STEM) images further confirmed the existence of single Co atoms (Fig. 15c). This 2D hybrid nanosheet exhibited a thickness of 45.53 nm as proved by atomic force microscopy (AFM) image (Fig. 15d). Co-PCOF/graphene showed an $\eta_{10} = 430$ mV for OER and an $E_{1/2}$ of 0.81 V (*versus* RHE) for ORR in 0.1 M KOH, respectively (Fig. 15e). Therefore, the ΔE is 0.85 V. This performance of Co-PCOF/graphene is better than that of most reported materials, including M–N–C catalysts and commercial Pt/C (Fig. 15f).

To further increase the bifunctional ORR and OER performance, Co_3O_4 was introduced into the Co-PCOF system due to its excellent OER performance ($\eta_{10} = 430$ mV).[323] The resulting Co_3O_4@Co-PCOF had a $\Delta E = 0.74$ V. A Zn–air battery assembled with Co_3O_4@Co-PCOF exhibited a voltage gap of 1.0 V at $j = 5$ mA cm^{-2} and a peak power density of 222.2 mW cm^{-2}. In addition, the above mentioned Co-TAPP-COF-Fe also exhibited excellent OER performance.[296] ORR performance of this Co-TAPP-COF-Fe has also been evaluated in 1.0 M KOH.
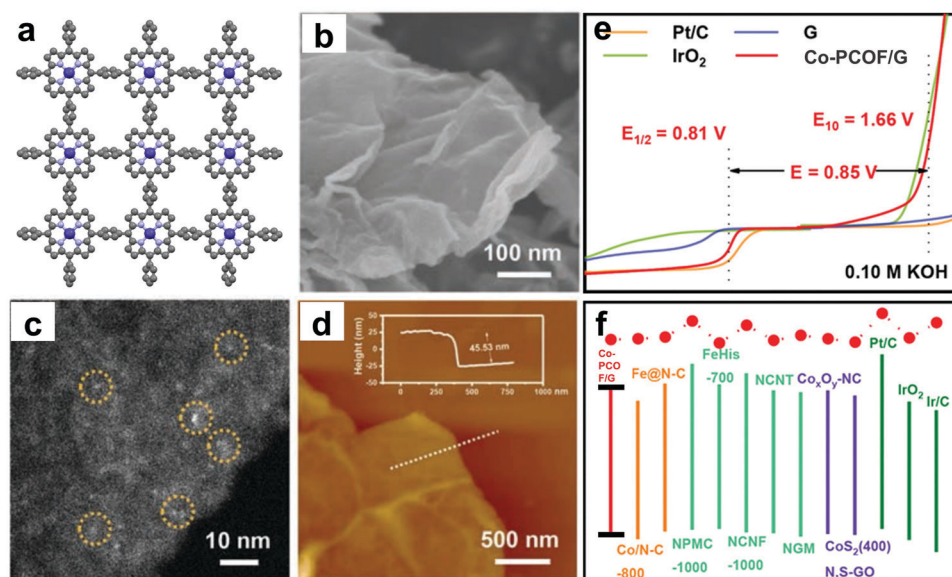
Fig. 15 (a) Schematic crystal structure of porphyrin COF. (b) SEM image, (c) STEM image, (d) AFM image, (e) LSV data, and (f) comparison of ORR/OER activity for Co-PCOF/graphene.[191] Reproduced from ref. 191 with permission from the Wiley-VCH, copyright 2019.

2560 | *Chem. Soc. Rev.*, 2021, **50**, 2540–2581

This journal is © The Royal Society of Chemistry 2021
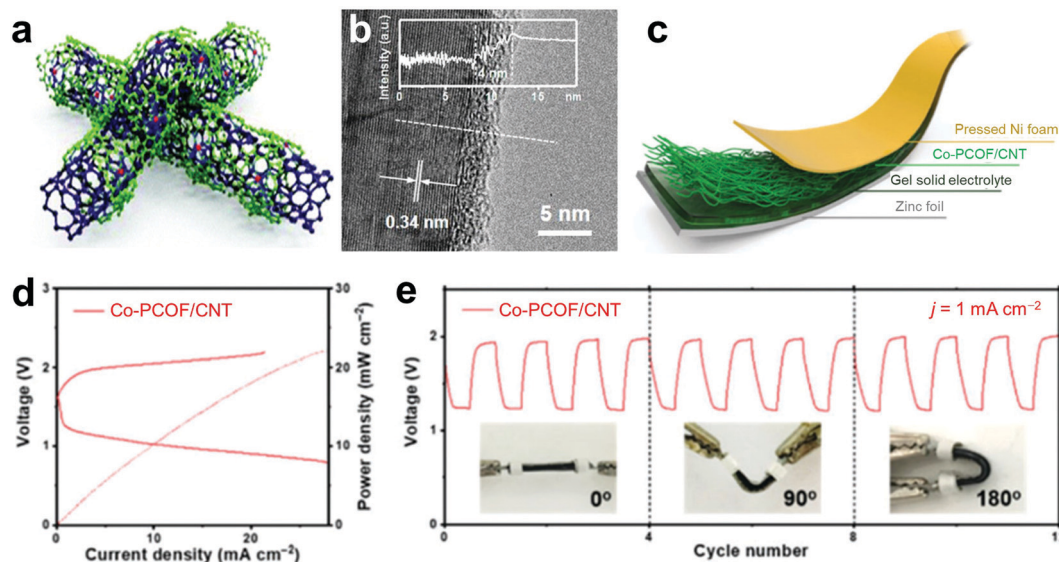
Fig. 16 (a) Structural sketch and (b) TEM image of Co-PCOF/CNT. (c) A typical Zn–air battery assembled with Co-PCOF/CNT. (d) Polarization discharge/charge data and corresponding power density curve and (e) discharge/charge cycling test of a flexible Zn–air battery constructed with Co-PCOF/CNT.[190] Reproduced from ref. 190 with permission from the Royal Society of Chemistry, copyright 2018.

Co-TAPP-COF-Fe had an E_{onset} = 0.95 V (*versus* RHE) and an $E_{1/2}$ = 0.84 V (*versus* RHE). Furthermore, the electron transfer number of Co-TAPP-COF-Fe was 2.1 as determined using the Koutecky–Levich equation, demonstrating a 2e catalytic ORR process.

To further improve the performance of the Zn–air battery, Zhang and co-workers fabricated Co-PCOF coated CNTs (named Co-PCOF/CNT, Fig. 16a).[190] TEM images confirmed the successful encapsulation of CNTs with a characteristic lattice distance of 0.34 nm for CNTs and a very thin layer of 4 nm for Co-PCOF (Fig. 16b). The Zn–air battery assembled with Co-PCOF/CNT exhibits a voltage gap of 0.78 V at j = 2 mA cm^{-2} and a peak power density of 237 mW cm^{-2}. Furthermore, Co-PCOF/CNT was used to assemble a flexible solid Zn–air battery, which was constructed with Zn foil, gel solid electrolyte, Co-PCOF/CNT catalysts, and pressed Ni foam (Fig. 16c). The resulting flexible Zn–air battery exhibited a power density of 22.3 mW cm^{-2} (Fig. 16d). Discharge/charge cycling test demonstrated that the voltage gap of the battery was 0.76 V at j = 1.0 mA cm^{-2}. Furthermore, the stability of this flexible Zn–air battery remained very good when the battery was bent for different angles (Fig. 16e). This work sheds light on the design and development of other flexible all-solid-state Zn–air batteries.

3.3.5 Porphyrin-based framework derivatives for the Zn–air battery. To further enhance the performance of the Zn–air battery, porphyrin-based frameworks were usually heated at high temperature.[324] For example, Zhang and co-workers heated Co-PCOF and assembled catalysts into a Zn–air battery (Fig. 17).[325] This 2D graphene-like nanosheet has uniformly distributed single-atoms Co–N$_x$–C (Fig. 17a and b). Co–N$_x$–C exhibited improved activity with an $E_{1/2}$ = 0.83 V (*versus* RHE) for ORR and a η_{10} = 470 mV for OER in 0.1 M KOH. Therefore,

the ΔE of Co–N$_x$–C was 0.87 V, which was slightly larger than that of Co-PCOF/G (ΔE = 0.85 V), demonstrating the excellent bifunctional performance of porphyrin-based framework derivatives. This Co–N$_x$–C was assembled into a Zn–air battery by coating catalysts on carbon cloth (Fig. 17c). Co–N$_x$–C showed a discharge/charge voltage gap of 1.04 V at 2.0 mA cm^{-2} and a power density of 78.0 mW cm^{-2} in a Zn–air battery, which was better than that of Pt/C + Ir/C (1.34 V; 17.7 mW cm^{-2}), indicating the promising practical application (Fig. 17d and e).

More recently, Wang, Lv, and co-workers obtained a dual-metal COF with Co TAPP, Fe 5,10,15,20-tetra(4-aminophenyl)-phthalocyanine, and BDA as components.[326] CoFe COF was used as the precursor and heated at high temperature. The resulting CoFe–N–C catalyst exhibited an $E_{1/2}$ of 0.777 V (*versus* RHE) for ORR in 0.1 M KOH and an η_{10} of 360 mV for OER in 1.0 M KOH. Therefore, the ΔE was about 0.813 V. The performance of the Zn–air battery assembled with CoFe–N–C was evaluated. The maximum power density was 53.4 mW cm^{-2}, which was smaller than that of the mixture of commercial Pt/C + RuO$_2$ (73.5 mW cm^{-2}).

In addition to the Zn–air battery, Li and co-workers prepared a porphyrin-based COF with Fe TCPP as the organic linker for an Al-air battery.[327] The resulting Fe-based porphyrin COF exhibited comparable catalytic activity with commercial Pt/C. The ORR n value of this COF was 3.84, demonstrating a 4e reduction process. In addition to metal–air batteries, porphyrin-based frameworks can also be applied in Li–S batteries. For example, Zhang and co-workers constructed a hollow porphyrin-based COF sphere using the template method.[328] Similarly, hollow metal-free PCOFs were prepared using a one-pot method by introducing a SiO$_2$ hard template. This hollow PCOF sphere showed excellent Li–S battery performance with high capacity and long-term durability. This is mainly ascribed to the specific

This journal is © The Royal Society of Chemistry 2021

Chem. Soc. Rev., 2021, **50**, 2540–2581 | **2561**
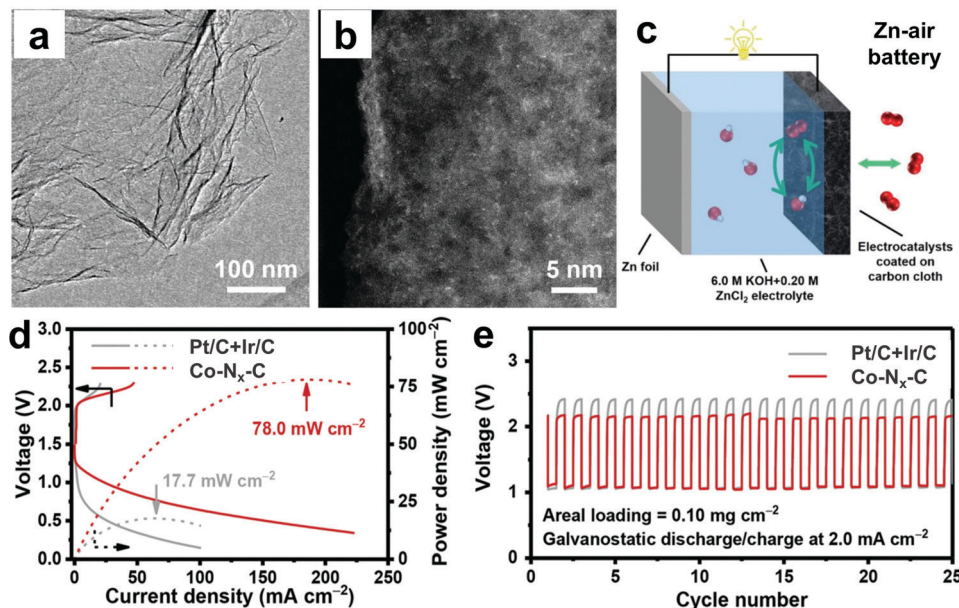
Fig. 17 (a) TEM image, and (b) STEM image of Co$-N_x-$C. (c) Schematic illustration of a typical Zn$-$air battery with Zn foil, electrolyte, and electrocatalysts coated on carbon cloth. (d) Polarization charging and discharging data and the corresponding power density data of Co$-N_x-$C and Pt/C + Ir/C. (e) Long-term discharge/charge cycling test of Co$-N_x-$C and Pt/C + Ir/C at j = 2.0 mA cm^{-2}.[325] Reproduced from ref. 325 with permission from the Wiley-VCH, copyright 2019.

hollow structure of PCOF, which provides a suitable host for S cathode. Similarly, Yu, Chen, Zhang and co-workers also applied porphyrin-based COFs for Li–S batteries.[329] Obtained porphyrin-based COFs exhibited microflower morphology with porous structures and ultrathin nanosheets (4 nm). Furthermore, porphyrin units have strong binding power to polysulfide.

3.3.6   Comparison of porphyrin-based frameworks for Zn–air batteries. According to the performance of reported catalysts for Zn–air batteries, porphyrin-based frameworks are a class of competitive materials (Table 4). Porphyrin-based frameworks were usually constructed with conductive CNTs or graphene to enhance conductivity and then to improve catalytic activity. First, Co-PCOF/CNT exhibited a superior peak power density of 237 mW cm^{-2}, which is larger than that of most pyrolyzed M–N–C materials (Co–N$_x$–C: 78 mW cm^{-2}) and precious metal materials (PdMo: 154.2 mW cm^{-2}). Second, porphyrin-based composites exhibited high voltage gap at the same conditions as compared to porphyrin-based framework composites. This

result demonstrated the unique advantages of frameworks. The voltage gap of Co-PCOF/CNT is 0.78 V at j = 2 mA cm^{-2}, which is smaller than that of most reported porphyrin-based composites and frameworks. Third, the open circuit voltage of reported porphyrin-based frameworks is still much smaller than precious metals such as PdMo nanosheets.

3.4   CO$_2$ reduction reaction (CO$_2$RR)

3.4.1   Evaluation of activity and selectivity for CO$_2$RR. With increasing CO$_2$ emission, electrochemical CO$_2$ reduction to CO and other carbon-based chemicals provides a possibility for long-term energy storage.[331–333] To evaluate the performance of electrochemical CO$_2$RR, several key parameters, including overpotential, faradaic efficiency (FE), turnover number (TON), and turnover frequency (TOF) were used. Herein, overpotential η can be calculated using the following equation.

$$\eta = E^0 - E_{\text{onset}} \tag{36}$$

Table 4 Comparison of the Zn–air battery performance for porphyrin-based composites, frameworks, and their derivatives

Catalysts	Open circuit voltage (V)	Specific current density (mA cm^{-2})	Voltage gap at specific current density (V)	Peak power density (mW cm^{-2})	Ref.
Co TPP/CNT	—	2	1.03	155.7	297
Co TPFPP/CNT	—	2	1.73	84.5	297
PCN-226-Co	1.37	2	0.97	133	201
Co-PCOF/CNT	1.39	2	0.78	237	190
Fe phthalocyanines COF/graphene	1.41	5	0.78	123.43	322
Cu phthalocyanines MOFs/CNT	1.37	—	—	94	298
Co–N$_x$–C	1.33	2	1.04	78.0	325
CoFe–N–C	—	10	1.02	53.4	326
Co$_3$O$_4$@Co-PCOF	—	5	1.0	222.2	323
PdMo bimetallene/C	1.48	10	0.75	154.2	330

E^0 is the standard potential for the reduction of CO_2 to CO (−0.11 V *versus* RHE).[79] Catalysts, which can drive CO_2 reduction with small overpotentials, are required. For CO_2RR, since several carbon-based compounds will be obtained during reduction, the selectivity of a specific catalyst is of great importance. FE is usually used to evaluate the efficiency for CO_2RR, which is the fraction of electrons consumed to produce a specific product. In other words, it is the needed moles of electrons divided by total moles of electrons transferred from anode to cathode during the electrocatalytic reduction process. Therefore, FE can be calculated using the following equation:

$$FE = anF/Q \tag{37}$$

Herein, a is the transferred number of electrons for a given product ($a = 2$ for H_2, CO and HCOOH), n is the number of moles of a product, and Q is the overall charge passing through the cell. TON and TOF are the parameters applied to evaluate the intrinsic catalytic activity of the active site. TON is the number of products divided by the number of catalysts (eqn (38)). TOF is the number of molecules converted per unit active site per unit time (eqn (39)).

$$TON = n/n_{catalyst} \tag{38}$$

$$TOF = n/tn_{catalyst} \tag{39}$$

Herein, $n_{catalyst}$ is the number of moles of catalysts, and t is the time of electrocatalysis.

3.4.2 Porphyrin-based composites for CO_2RR. For homogeneous catalysis, porphyrins have been widely applied as molecular catalysts for CO_2RR.[74,334] However, homogeneous CO_2 reduction is considered to be less practically applicable due to the poor water solubility of catalyst molecules, low utilization of catalysts, and difficult separation of products. Loading molecular catalysts onto substrates such as CNTs, graphene, Cu nanowire, and MOFs to realize heterogeneous catalysis for CO_2RR has therefore attracted great attention.[73,335–339] For example, Daasbjerg and co-workers reported that Co TPP exhibits a selectivity of >90% for CO when simply immobilizing on CNTs.[340] Han, Ye and co-workers designed a strategy for covalently grafting Co protoporphyrin IX chloride on hydroxyl-functionalized CNTs.[341] The coordination Co–O bonds formed when refluxing porphyrin molecules and CNTs. The resulting hybrid exhibited an FE of 98.3% for CO generation at an overpotential of 490 mV. Similarly, Robert and co-workers designed a Fe porphyrin–CNT composite connected through covalent bonds.[342] This Fe porphyrin has six –OH groups in *ortho* positions of three phenyl rings. The resulting Fe porphyrin–CNT exhibits a FE of 90% for CO with an overpotential of 510 mV. Officer, Wallace, and co-workers constructed a Fe porphyrin/graphene hybrid.[343] The porphyrin linker is Fe tetraphenyltrimethylammonium porphyrin (TPTAP). The resulting hybrid exhibited CO_2RR with an FE of 97.0% for CO production at an overpotential of 480 mV. This catalyst also showed high long-term durability after running 24 h electrocatalysis. Porphyrins can also be immobilized on MOFs through covalent grafting. For example, Lin, Wang and co-workers grafted Co protoporphyrin IX on MOFs, which exhibited a FE of 92.2% for CO at −0.86 V (*versus* RHE) with a TOF of 0.40 s^{-1}.[344]

In addition, Cu surface has also been applied as a support to immobilize Fe TPP, named Fe TPP/Cu, which exhibits outstanding selectivity for ethanol with a FE of 41% at −0.82 V (*versus* RHE).[345] This is attributed to the high selectivity of C2 compounds of Cu materials for CO_2RR.[346]

In addition to porphyrins, Wang, Liang and co-workers prepared a hybrid of Co phthalocyanines and CNT for CO_2RR.[73] The resulting Co phthalocyanines/CNT hybrid can mediate CO_2RR to methanol with a high FE of 44% at about −0.82 V (*versus* RHE). Furthermore, four amino groups (–NH$_2$) were introduced into the ligand of Co phthalocyanines to improve the stability and long-term durability. Herein, the efficiency and selectivity may be mainly attributed to the monodisperse Co phthalocyanines, suitable carbon support, and beneficial structure modification. Recently, Berlinguette, Robert and co-workers reported that commercial Co phthalocyanines can catalyze CO_2RR with a high selectivity for CO (FE > 95%) at 150 mA cm^{-2}.[347] Molecular Co phthalocyanine catalyst was mixed with carbon powder and Nafion and was then spray coated on carbon paper. The resulting catalyst layer was assembled in a flow cell to perform CO_2RR. The immobilization of molecular catalysts on carbon materials is also one of widely studied strategies to transfer homogeneous catalysis into heterogeneous catalysis.

3.4.3 Porphyrin-based framework composites for CO_2RR. Based on the excellent electrocatalytic activity of porphyrin molecules, a series of porphyrin-based frameworks were developed for CO_2RR. Currently, porphyrin-based MOFs and COFs are usually produced using the solvothermal method. The resulting products were then drop-casted onto the surface of electrodes. During the electrocatalysis, only metal centers on the surface remain electrochemically accessible and active due to confined adsorption and diffusion of CO_2 within framework channels. In addition, electron transfer between catalysts and electrodes is limited, leading to low electrocatalytic activity. To solve the problem, carbon material was introduced into the system. Teng, Dong and co-workers prepared PCN-222-Fe, and composite catalyst PCN-222-Fe/C was drop-coated on the electrode.[182] PCN-222-Fe/C presented a good catalytic activity for CO_2RR to CO with an overpotential of 494 mV and a maximum FE of 91% for CO in CO_2-saturated 0.5 M KHCO$_3$, realizing a TOF of 0.14 s^{-1}. The stability of this composite is good with an average FE of 80.4% after running electrolysis for 10 h. In 2015, Chang, Yaghi, and co-workers constructed Co porphyrin-based COFs, namely COF-366-Co and COF-367-Co, to promote CO_2RR in a neutral solution.[188] Co-based TAPP was selected as porphyrin molecules. COF-366-Co and COF-367-Co was prepared with BDA and BPDA as the organic linker through Schiff-base condensation reactions, respectively. This strategy is extensively used to prepare porphyrin-based COFs. COF-367-Co deposited on carbon fabric demonstrated enhanced CO_2RR activity with a larger current of 27 mA at −0.87 V (*versus* RHE) compared to that of COF-366-Co (19 mA) under CO_2-saturated 0.5 M KHCO$_3$. This may be attributed to the larger pores in expanded COF-367-Co (26.5 Å) compared to that in COF-366-Co (23.5 Å), which provided more accessible active sites for CO_2 adsorption to metal active sites and thus resulted in the improvement in activity. To further improve

This journal is © The Royal Society of Chemistry 2021

Chem. Soc. Rev., 2021, **50**, 2540–2581 | **2563**
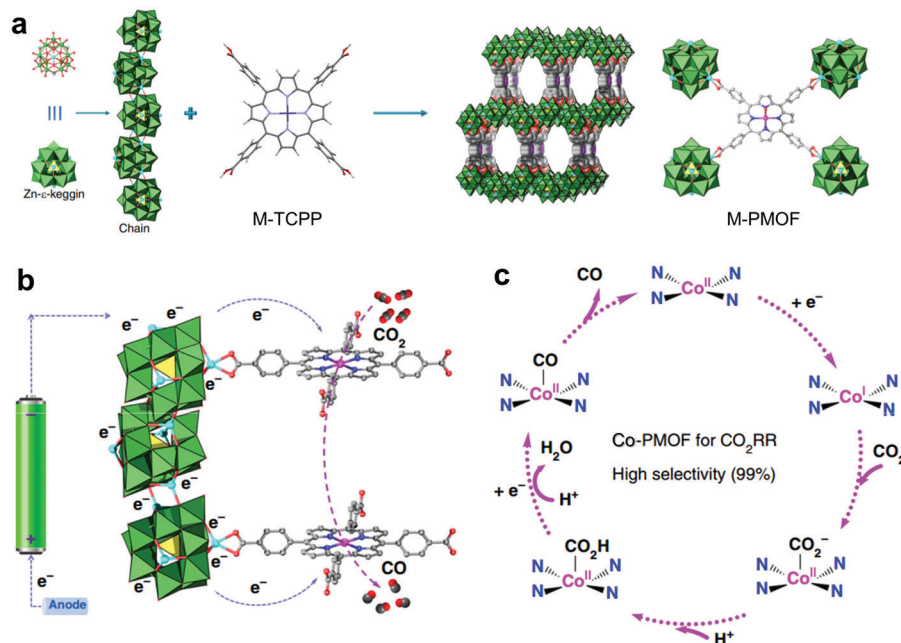
Fig. 18 (a) Synthetic procedure and crystal structure of M-PMOF (M presents transition metal). (b and c) Possible reaction mechanism of CO_2RR for Co-PMOF.[196] Reproduced from ref. 196 with permission from the Springer Nature Ltd, copyright 2018.

the performance of CO_2RR, Cu was introduced and Co content (1% and 10% mole ratio) of COF-367 was tuned. COF-367-Co(1%) showed superior activity compared to COF-367-Co(10%), COF-367-Co and COF-367-Cu, along with a highly stable operation for 136 hours. Similarly, Lan and co-workers prepared a Co-TAPP-COF nanosheet through Schiff-base condensation reaction with Co TAPP and 2,3,6,7-tetra(4-formylphenyl)-tetrathiafulvalene as reactants.[348] The resulting Co-TAPP-COF nanosheet had a porous structure with a pore diameter of 15.7 Å and a layer distance of 3.69 Å. The FE of Co-TAPP-COF nanosheet reached 91.3% for CO at -0.7 V (versus RHE) and the corresponding TOF is 1.28 s^{-1}. Zhuang, Liang, Qiu, Hou and co-workers prepared a porphyrin COF by using Ni TCyPP.[349] This Ni-TCyPP-COF exhibited an overpotential of 443 mV and a FE of $>90\%$ for CO conversion during 20 h electrolysis.

More recently, Lan and co-workers prepared several metal porphyrin-based MOFs with polyoxometalate Zn-ε-Keggin clusters as nodes (Fig. 18).[196] This cluster node is electron-rich and thus the formed cluster chain can transfer electrons effectively. The inherent macrocycle conjugated π-electron system and suitable pore size of porphyrin-based frameworks can benefit the adsorption of CO_2 and the mobility of electrons. MOFs with different metals including Co, Fe, Ni and Zn were prepared. Co-PMOF exhibited the smallest onset potential (-0.35 V versus RHE) and the largest FE (98.7%) for CO production among this series of catalysts.

In addition, the mechanism of Co-PMOF for CO_2RR was proposed (Fig. 18b and c). First, the Zn-ε-Keggin cluster node can trap electrons from electrodes and then transfer electrons to Co active sites of metal porphyrins, while Co^{II} was reduced to Co^{I} simultaneously. The resulting Co^{I} will interact with CO_2 and form a Co^{II}*COOH intermediate with the transfer of proton

in a concerted manner. Then Co^{II}*COOH will change to Co^{II}*CO with the participation of proton and electron and the formation of H_2O. Finally, CO formed and was desorbed.

In addition to the structure regulation of porphyrin-based frameworks, other strategies had also been investigated. Tang and co-workers prepared an ultra-thin MOF electrocatalyst Co-TPyP-MOF by self-assembly of Co TPyP molecules.[350] The authors found that the electrocatalytic activity of CO_2RR can be significantly promoted through increasing the energy level of the metal d_{Z^2} orbital. Due to the axial coordination of pyridine, the d_{Z^2} orbital energy level of the active Co center of Co-TPyP-MOF increases, which will result in electron transfer from Co to CO_2, thus improving selectivity and activity of CO_2 reduction. This work explored the relationship between chemical environment and catalytic activity of heterogeneous catalysts from molecular orbital levels, providing theoretical basis and design ideas for bottom-up design and construction of high-efficiency single atom catalysts. The obtained Co-TPyP-MOF had a FE of 96% for CO generation at an overpotential of 500 mV and a TOF of 4.21 s^{-1}. Similarly, Lan, Chen and co-workers proposed a new strategy to enhance the selectivity of CO_2RR by inserting metallocene into porphyrin-based frameworks using a facile chemical vapor deposition method.[202] Through optimizing the experimental conditions, Co cyclopentadienyl was selected as the metallocene, and MOF-545-Co was selected as the framework. The resulting Co cyclopentadienyl@MOF-545-Co had a FE of 97% for CO at -0.7 V (versus RHE). The introduction of metallocene may act as the electron donor and carrier. Furthermore, the strong binding-interaction between metallocene and the metal active site of porphyrin molecule can decrease the adsorption energy of CO_2. More recently, Su, Zhang and co-workers prepared a hybrid of Au@PCN-222-Ir with Au
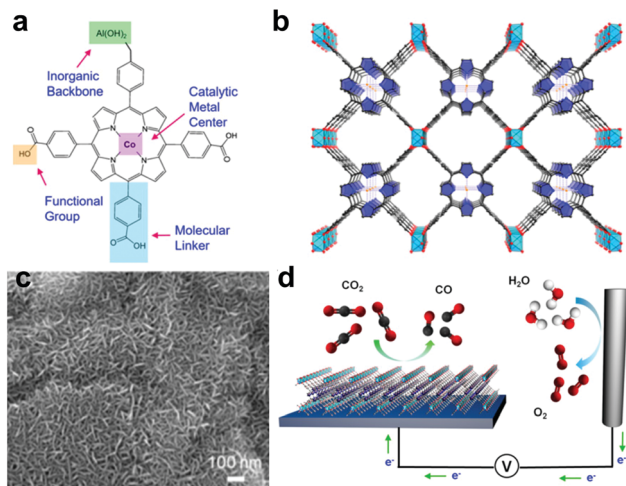
Fig. 19 (a) Molecular structure, (b) crystal structure, (c) SEM image, and (d) schematic illustration of CO₂RR for MOF thin film grown on the surface of FTO electrode.[186] Reproduced from ref. 186 with permission from American Chemical Society, copyright 2015.

Fig. 20 (a) Crystal structure, (b) SEM image, and (c) schematic structures of COF-366-Co layers with respect to the substrate.[189] Reproduced from ref. 189 with permission from American Chemical Society, copyright 2018.

nanoparticles encapsulated in inner cavities of MOF.[351] Au@PCN-222-Ir exhibited enhanced CO_2 adsorption and activation due to the synergistic effect of PCN-222-Ir and Au. Au nanoparticles not only adsorb CO_2 onto the pores of framework to increase CO_2 concentration but also transfer electrons to Ir porphyrins to increase interactions with CO_2. Following a similar strategy, Yang, Gu, Cao and co-workers prepared a novel porphyrin-based MOF with ZrO clusters as nodes and 1,4-benzenedicarboxylic acid and Fe TCPP as organic linkers.[352] The resulting MOF, named Fe TCPP@UiO-66, exhibits high chemical stability and improved proton transfer, which delivers an FE of ~100% for CO generation at the overpotential of 460 mV.

3.4.4 Porphyrin-based frameworks grown on supports for CO₂RR. Porphyrin-based frameworks can also be directly grown onto the surface of electrodes. For instance, Yang, Yaghi, and co-workers constructed a 3D Co–Al-PMOF on a conductive substrate (Fig. 19).[186] An atomic layer deposition technology was applied to deposit Al thin films onto conductive carbon disk electrodes. Then metal coordinated porphyrin linkers react directly with metal Al thin film deposited on the electrode in a dimethylformamide solvent to form the 3D Co–Al-PMOF (Fig. 19a and b). SEM images confirmed the formation of plate-like MOFs (Fig. 19c). Co–Al-PMOF showed a CO selectivity of 76% with a TON of 1400 at −0.70 V (*versus* RHE) (η = 590 mV) in 0.5 M KHCO₃ solution (Fig. 19d). Hupp, Farha, Kubiak, and co-workers constructed a MOF-525 thin film with electrophoretic deposition on the FTO electrode.[181] MOF-525 was constructed using a Zr₆-based node and Fe-TCPP linker. MOF-525-Fe exhibited an overpotential of about 650 mV and a FE of 100% for CO generation.

Similarly, Daasbjerg and co-workers constructed carbazole-functionalized Fe porphyrin-based COFs films by using an electrochemical polymerization procedure on GC and indium tin oxide electrodes.[210] Direct growth of porphyrin-based MOFs
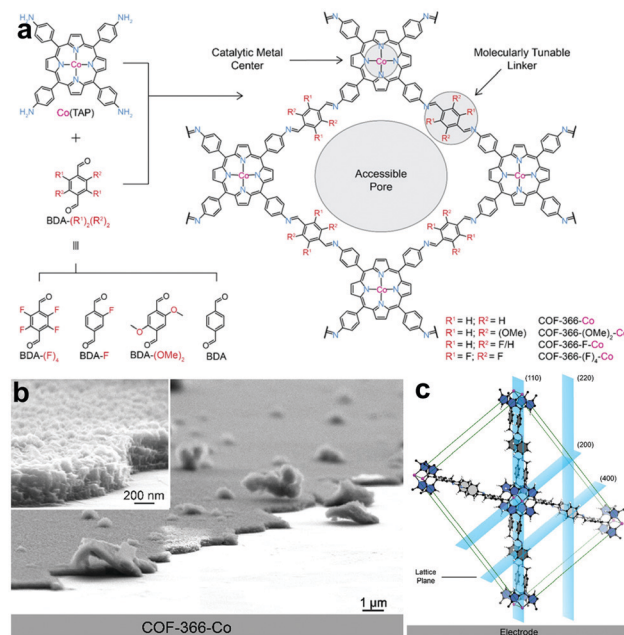
and COFs onto the substrate can avoid the usage of binders, which will promote stability and conductivity of framework films during electrocatalysis. Yaghi, Chang and co-workers further expanded COF-366 structures by regulating the linker of BDA (Fig. 20).[189] Substituted BDA derivatives, including BDA-(F)₄, BDA-F, and BDA-(OMe)₂, were selected (Fig. 20a). The COF-366 structure possesses several advantages, including large accessible pores, changeable metal centers and molecularly tunable linkers. Herein, uniform films of COF-366-Co were observed with a thickness of 250 nm (Fig. 20b). Differently from common frameworks grown on the substrate, the COF layers were oriented at a 90° angle to the substrate (Fig. 20c). The oriented thin porphyrin-based COF films had a low overpotential of 550 mV with a high FE of 87% through the reduction of CO_2 to CO. This kind of composite electrode was very stable after running more than 12 h. Furthermore, Zhu and co-workers assembled a series of COF-366-Co COFs on CNT composites with different BDA derivatives as organic linkers.[353] The resulting COF-366-(OMe)₂-Co/CNT exhibited an FE of 93.6% for CO generation at −0.68 V (*versus* RHE) compared to other COFs/CNT composites including COF-366-Co/CNT, COF-366-(OH)₂-Co/CNT, and COF-366-(F)₄-Co/CNT. Therefore, regulating the porous structures of porphyrin-based COFs through the introduction of functional groups with electron-donating ability will enhance the performance of CO₂RR. Similarly, Cao, Huang and co-workers designed a COF-366-Co with tetrathiafulvalene (TTF) as the organic linker.[354] The resulting COF-366-TTF-Co exhibited an FE of 95% for CO generation at −0.7 V (*versus* RHE). Herein, the TTF, as an electron donor, can greatly enhance electron transfer from organic linker to porphyrin center and then lower the activation energy of CO_2.

This journal is © The Royal Society of Chemistry 2021

Chem. Soc. Rev., 2021, **50**, 2540–2581 | **2565**
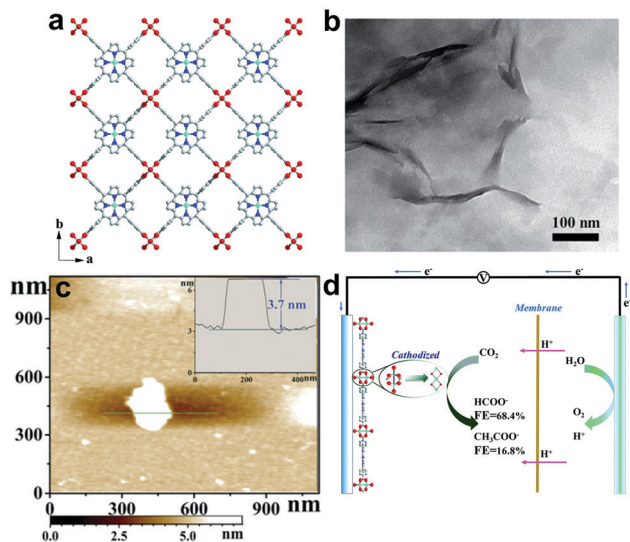
Fig. 21 (a) Molecular packing of Cu_2(CuTCPP) MOF view along c axis. (b) TEM image and (c) AFM image of Cu_2(CuTCPP) MOF nanosheets. (d) A typical two-compartment H-type cell for electrochemical CO_2RR with Cu_2(CuTCPP) MOF nanosheets as catalysts.[355] Reproduced from ref. 355 with permission from the Royal Society of Chemistry, copyright 2019.

In addition to Co porphyrin-based frameworks, other transition metal-based frameworks also have been reported for CO_2RR. For example, Kubiak and co-workers constructed a thin Fe-based porphyrin COF on a carbon cloth electrode.[203] Herein, Fe^{III} TAPP chloride and 2,5-dihydroxyterephthalaldehyde was selected as the porphyrin active site and the organic linker, respectively. The resulting Fe-TAPP-COF had a TOF of >0.17 s^{-1} and a FE of 80% for generating CO. Recently, Gu and co-workers constructed Cu porphyrin-based MOF nanosheets on the FTO electrode for CO_2RR (Fig. 21).[355] This MOF was prepared using Cu TCPP ligands and $Cu_2(COO)_4$ nodes (Fig. 21a). Cu_2(CuTCPP) MOF exhibited a 2D nanosheet morphology with a thickness of 3.7 nm (Fig. 21b and c). The Cu porphyrin MOF exhibited a selective formate HCOO$^-$ (FE = 68.4%) and acetate CH$_3$COO$^-$ (FE = 16.8%) production measured in a typical two-compartment H-type cell (Fig. 21d). Similarly, Wang and co-workers prepared two 2D porphyrin MOFs with Cu–N$_4$ and Au–N$_4$ active centers, respectively.[356] The Cu porphyrin MOF also exhibits a high selectivity for HCOO$^-$ with an FE of 80.86% at -0.7 V (*versus* RHE), while the Au porphyrin MOF has a selectivity for HCOO$^-$ with a FE of 40.90% at -0.8 V (*versus* RHE). It has been demonstrated that Cu will improve the production of C2 compounds. Recently, Jing and co-workers prepared Cu@porphyrin-based COF nanorods, which exhibits enhanced CO_2 adsorption and C2 compound production.[357]

3.4.5 Porphyrin-based framework derivatives for CO_2RR. Pyrolyzed porphyrin-based frameworks also have been used as electrocatalysts for CO_2RR. For example, Jiang and co-workers prepared a series of single-atom M–N–C materials with PCN-222-M as precursors (M = Fe, Co, Ni, and Cu).[358] Different metal porphyrins and metal-free porphyrins were selected as porphyrin building blocks to prepare PCN-222-M.

The resulting single-atom Ni–N–C material exhibited the best CO_2RR activity with an FE of 96.8% and a TOF of 3.14 s^{-1} for CO production at -0.8 V (*versus* RHE). For heterogeneous CO_2RR, there are usually three major steps: (1) CO_2 adsorption on active sites; (2) electron transfer to cleave C–O bonds and/or proton migration to form C–H bonds; and (3) desorption of products (*e.g.*, CO, CH$_4$, C$_2$H$_4$, C$_2$H$_5$OH, and CH$_3$OH).[359] Theoretical calculations demonstrated that Ni–N–C showed low energy barriers for the formation of *COOH and the desorption of CO.

In addition to porphyrin-based MOFs, porphyrin-based triazine frameworks have also been used as precursors to prepare M–N–C catalysts. For example, Hou, Wang and co-workers prepared a series of M–N–C materials with uniformly dispersed M–N$_x$ active sites (M = Mn, Fe, Co, Ni, and Cu).[360] The resulting Ni-N-C-600 exhibited a FE of 97.6% for CO generation at -0.8 V (*versus* RHE). Similarly, Cao and co-workers also prepared a series of single-atom M–N–C catalysts based on porphyrin-based triazine frameworks (M = Fe, Co, Ni, and Cu).[361] Ni–N–C exhibited the best CO_2RR performance with an FE of 98% for CO generation at -0.8 V (*versus* RHE). Furthermore, Ni–N–C also had a high TOF with a value of 3.74 s^{-1} at -1.2 V (*versus* RHE). Therefore, porphyrin-based framework derivatives, especially Ni–N–C, are also promising catalysts for CO_2RR.

3.4.6 Porphyrin-based frameworks for photocatalytic CO_2RR. In natural photosynthesis, porphyrin molecules can not only sense photons but also transfer electrons.[362] Based on this photoelectric character of porphyrin molecules, porphyrin-based frameworks also exhibit photocatalytic properties. For example, Ye and co-workers found that MOF-525-Co showed obvious visible-light-driven CO_2RR to CO and CH$_4$.[171] Recently, Cao and co-workers prepared a PCN-601-Ni with pyrazolyl Ni porphyrin.[363] The coordination structure of the pyrazolyl group and NiO cluster promotes the electron transfer of ligand-to-node and boosts the CH$_4$ production. More recently, Jiang and co-workers reported two COF-367-Co materials with different oxidation states of Co porphyrin (Co^{II} and Co^{III}).[364] COF-367-Co^{III} exhibited enhanced selectivity for HCOOH rather than CO and CH$_4$. Therefore, photocatalytic CO_2 reduction is also a promising field.[365–367]

3.4.7 Comparison of porphyrin-based frameworks for CO_2RR. For comparison, electrochemical activities of CO_2RR for porphyrin composites, porphyrin-based frameworks, and other reported catalysts are summarized in Table 5.

Currently, immobilizing porphyrin molecular catalysts on carbon materials or other supports have been widely investigated for CO_2RR due to the excellent catalytic activity of porphyrins in homogeneous solutions. However, these porphyrin-based carbon material composites usually have poor long-term stability. To improve the stability, porphyrin-based MOFs and COFs have been extensively studied. At present, COF-367-Co(1%) exhibit the best stability with 136 h electrolysis of CO_2RR. In addition, the FE of Fe TCPP@UiO-66 and Fe porphyrin cage is about 100% for CO generation. Co-TPyP-MOF exhibited the largest TOF with a value of 4.21 s^{-1}. Therefore, porphyrin-based frameworks usually catalyze CO_2 to CO with high selectivity and TOF values. In comparison, metal nanoparticles, such as Pd, Ag, and Au also exhibited excellent CO_2RR performance for CO

Table 5 Comparison of CO_2RR performance for porphyrin-based composites, frameworks, and other reported catalysts

Catalysts	Overpotential (mV)	Electrolyte	Time[a] (h)	FE (CO, %)	TOF (s^{-1})	Ref.
Co TPP/CNT	550	0.5 M KHCO$_3$	4	91	0.078	340
Fe TPTAP/rGO	480	0.1 M KHCO$_3$	24	97	0.8	343
Fe TPTAP/graphene hydrogel	280	0.1 M KHCO$_3$	20	96.2	0.8	338
Co phthalocyanines/CNT	520	0.1 M KHCO$_3$	1	92	2.7	368
Co protoporphyrin IX–CNT	490	0.5 M KHCO$_3$	12	98	1.37	341
Fe porphyrin–CNT	510	0.5 M NaHCO$_3$	3	90	0.049	342
Co protoporphyrin IX–MOF	750	0.1 M NaHCO$_3$	—	92.2	0.4	344
Fe TCPP@UiO-66	450	0.1 M KHCO$_3$	2.5	100	—	352
Co cyclopentadienyl@MOF-545-Co	590	0.5 M KHCO$_3$	24	97	0.216	202
Ni-TCyPP-COF	790	0.5 M KHCO$_3$	20	97	0.47	349
Co–Al-PMOF	590	0.5 M KHCO$_3$	7	76	0.056	186
COF-366-Co oriented film	550	0.5 M KHCO$_3$	12	87	—	189
COF-366-Co film	550	0.5 M KHCO$_3$	24	86	0.185	188
COF-366-Co	550	0.5 M KHCO$_3$	24	90	0.027	188
COF-367-Co	550	0.5 M KHCO$_3$	24	91	0.046	188
COF-367-Co(1%)	550	0.5 M KHCO$_3$	136	40	0.212	188
COF-367-Co(10%)	550	0.5 M KHCO$_3$	4	70	0.10	188
COF-366-TTF-Co	590	0.5 M KHCO$_3$	10	95	0.188	354
Co-PMOF	690	0.5 M KHCO$_3$	36	98.7	0.46	196
Co-TPyP-MOF	500	0.5 M KHCO$_3$	48	96	4.21	350
Co-TAPP-COF nanosheet	590	0.5 M KHCO$_3$	40	91.3	1.28	348
COF-366-(OMe)$_2$-Co/CNT	570	0.5 M KHCO$_3$	12	93.6	3.3	353
Fe porphyrin cage	520	0.5 M KHCO$_3$	24	100	1.74	369
Ni–N–C-600	690	0.5 M KHCO$_3$	10	97.6	0.129	360
Ni–N–C	690	0.5 M KHCO$_3$	10	98	3.74	361
Pd	780	0.1 M KHCO$_3$	—	91.2	0.16	370
Ag	390	0.5 M KHCO$_3$	2	92	0.002	371
Au	240	0.5 M KHCO$_3$	12	94	0.02	372

[a] Time of electrolysis.

generation with high FE ($>$90%). However, the TOF values of these metal particles are relatively low. Furthermore, the high price of these precious metals limits their wide applications.

4. Guidelines on further development of porphyrin-based frameworks

Though various porphyrin-based frameworks have been reported, developing more efficient porphyrin-based frameworks for ORR, OER and CO_2RR still remains a challenge. Based on above discussions, guidelines on the further development of porphyrin-based frameworks are suggested.

4.1 Guidelines for improving activity

Currently, most of reported porphyrin-based frameworks were constructed using simple porphyrin building blocks and metal nodes or organic linkers. The central active site structures, namely the metal-coordinated porphyrin macrocycles, are quite similar. Inspired from molecular catalysis with porphyrins, structural effects of porphyrins play crucial roles in regulating electrocatalytic activity. Therefore, it is valuable to consider structural effects when constructing porphyrin-based frameworks to enhance catalytic activity.

4.1.1 *meso*-Substituent effect. The *meso*-substituents have been shown to be able to regulate the redox properties of metal porphyrins by tuning the electronic structure of metal centers, which is crucial for determining the efficiency and activity of ORR.[3] It is suggested that strong electron-withdrawing *meso*-

substituents can cause metal porphyrins to be easily reduced. The anodic shift of the reduction will lead to the formation of reduced active metal species at relatively small negative potentials, leading to the decrease of ORR overpotentials. However, on the other hand, electron-donating substituents can increase the electron density on metal ions and thus increase its binding and electron transfer with O_2. This effect will improve the electrocatalytic ORR activity.[373] As a consequence, fine-tuning the electronic structure of metal ions by using different *meso*-substituents of porphyrin macrocycles is an appealing strategy to further improve ORR efficiency and activity. At present, porphyrins bearing simple phenyl-based *meso*-substituents with their *para*-positions substituted with functional groups are generally used for constructing frameworks. Recently, Cao and co-workers designed a CNT-templated porphyrin-based framework composite with Co tetra(2,3,5,6-tetrafluoro-4-ethynylphenyl)porphyrin as the organic linker, named FCoP/CNT.[118] As compared to the analogous framework prepared using the tetra(4-ethynylphenyl)porphyrin building block, the electrochemical properties of FCoP/CNT were largely improved by using strong electron-withdrawing *meso*-tetrafluoro-4-ethynylphenyl substituents. This work is significant to show the significant improvement in the electrocatalysis of porphyrin-based frameworks by using well-designed *meso*-substituents. It is necessary to note that although modifying *meso*-substituents has been well demonstrated for molecular porphyrin catalysts, this strategy has been rarely reported for porphyrin-based framework catalysts, largely due to the difficulty in the design and synthesis of porphyrin building blocks with tunable electronic structure properties.

This journal is © The Royal Society of Chemistry 2021

Chem. Soc. Rev., 2021, **50**, 2540−2581 | **2567**

4.1.2 β-Substituent effect. In addition to *meso*-substituents, β-substituents of porphyrin macrocycles also have a significant influence on the electronic structure of central metal ions, which has been demonstrated by using synthetic porphyrin molecules.[48] More significantly, it is suggested that the electronic structure effect of β-substituents for porphyrins is usually larger than that of *meso*-substituents due to the relatively closer distance to metal active centers. Therefore, the design of new porphyrin-based frameworks by regulating porphyrin β-substituents is also an effective strategy. Recently, Promarak, Wannakao, and co-workers investigated the effects of different metal centers and β-substituents using theoretical calculations (Fig. 22).[374] Free energies of all intermediates *OH, *O, and *OOH for ORR and OER were calculated based on constructed metal porphyrin-based frameworks (M-Por-X; M = Cr, Mn, Fe, Co, Ni, Cu, Zn, Ru, Rh, Pd, Ag, Ir, Pt, and Au; X = H, F, Cl, and Br) (Fig. 22a and b). M-Por-X presents the substitution of M-Por with X at the β-position. For an ideal catalyst of ORR, the ΔG_{OH} is ~1.23 eV. The plot of the calculated overpotential (η_{RHE}) of M-Por-X against $\Delta G_{*OH} - 1.23$ eV is shown in Fig. 22c. Calculated results demonstrated that Co-Por-F had the smallest overpotential of ORR compared to other metal porphyrins and was located at the top of volcano plots. In contrast, Ir-Por-F and Ir-Por exhibited the best OER performance. For non-precious metals, Co-Por-F is the best porphyrin-based framework for OER as compared to others. As a result, Co-Por-F exhibited the best bifunctional ORR and OER activity theoretically. Although the structural effect of β-substituents on electrocatalytic ORR and OER has been investigated, few experimental reports have been known in the literature to utilize this effect to tune the electrocatalytic properties of porphyrin-based frameworks.

From the perspective of synthesis, Zhou and co-workers prepared a series of PCN-224-Fe derivatives with eight ethyl, F, Cl, and Br groups substituted at the β-positions of Fe TCPP as porphyrin building blocks.[375] The 3-methylpentane oxidation catalysis was investigated with these porphyrin-based frameworks. Although the electrocatalytic performance has not been studied, these porphyrin-based frameworks provide a suitable platform to study the substituent effect of electron-donating and electron-withdrawing functional groups at the β-position of porphyrins on ORR/OER performance.

4.1.3 *Trans* axial ligand effect. Introducing *trans* axial ligands into porphyrin-based frameworks is a sound approach. In nature, the axial histidine imidazole group on Fe porphyrin in heme plays a key role in tuning the catalytic ORR process. Herein, the effect of *trans* axial ligands on the metal active center is through the "push effect". Specifically, the *trans* axial ligand coordination on the metal active center will donate electrons to unoccupied d-orbitals of the metal active center and then increase the electron density of the metal porphyrin molecule, and further affect their electrocatalytic activity. Several studies have also confirmed the *trans* axial ligand effect on ORR in activity.[13,109,376,377] For example, Xia, Wang, Ma and co-workers investigated the "push effect" of 4-mercaptopyridine, 4-aminothiolphenol, and 4-mercaptobenzonitrile on Co 5,10,15,20-tetra(4-methoxyphenyl)porphyrin.[376] The 4-mercaptopyridine coordinated Co porphyrin exhibited the best ORR performance compared to others due to the strongest coordinating ability of 4-mercaptopyridine. Recently, Hod and co-workers introduced the 2-methylimidazole group on Fe porphyrin hemin through axial ligand coordination, which greatly improves the catalytic activity of Fe porphyrin-based MOF for ORR.[377] Herein, the Fe porphyrin molecule was functionalized on UIO-66 MOF through ligand exchange. As a result, the "push effect" of the *trans* axial ligand can also be studied directly on porphyrin-based frameworks by introducing functional groups such as imidazole, phenolate and thiolate complexes. At present, the axial ligand pyridine coordinated Co-TPyP-MOF has been synthesized and used as catalyst for CO2RR, which exhibited enhanced catalytic activity for CO generation with a TOF value of 4.21 s^{-1}.[350] Therefore, applying the "push effect" of the *trans* axial ligand on porphyrin-based frameworks is an appealing strategy to further improve ORR/CO2RR activity.

4.1.4 Hydrogen bonding effect. For homogeneous catalysis of porphyrins, the second coordination sphere hydrogen bonding effect plays an important role in the electrocatalytic activity of ORR and CO2RR.[378] This is mainly because the hydrogen bond can stabilize intermediates and promote proton transfer during ORR and CO2RR.[28,379] For example, Dey and co-workers designed a series of porphyrin molecules to study the ORR activity through modification of the amino group of Fe *o*-aminophenyltris(phenyl)-porphyrin with pyridine-2-carboxaldehyde and 2-bromo-ethylamine *etc.*[28] Experimental and theoretical results demonstrated that the N$_1$H substituent surrounding the metal active center can form the hydrogen bond with Fe^{III}–OOH intermediate and activate the O–O
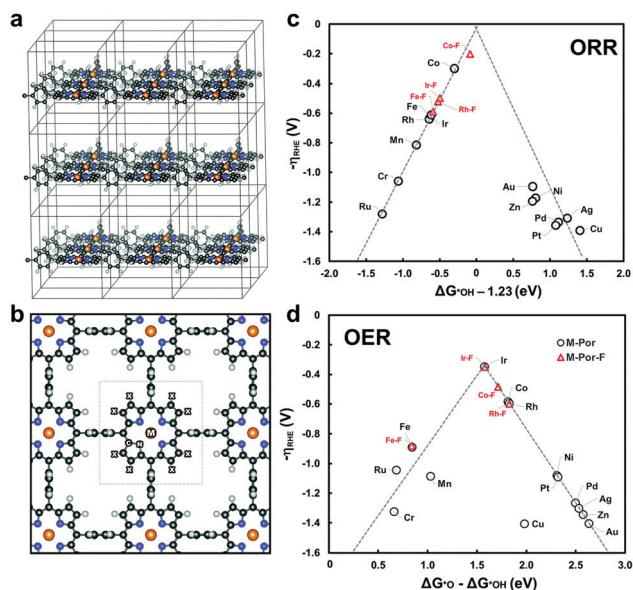
Fig. 22 (a and b) Schematic crystal structure of metal porphyrin-based frameworks M-Por-X, where M is Cr, Mn, Fe, Co, Ni, Cu, Zn, Ru, Rh, Pd, Ag, Ir, Pt, and Au; X represents H, F, Cl, and Br. Calculated overpotential of M-Por and M-Por-X for ORR plotted against $\Delta G_{*OH} - 1.23$ (eV) (c) and for OER plotted against $\Delta G_{*O} - \Delta G_{*OH}$ (eV) (d).[374] Reproduced from ref. 374 with permission from the Royal Society of Chemistry, copyright 2017.

bond of the hydroperoxide species and then promote the proton transfer to the distal O atom. As for CO_2RR, Aukauloo, Halime, and co-workers demonstrated that the introduction of urea functions around the metal porphyrin ring can significantly decrease the overpotential of CO_2RR.[92,380] This is attributed to the formation of hydrogen bonds between the urea functional group and the CO_2 adduct. More recently, Cao and co-workers also demonstrated that the introduction of phenolic groups at the second coordination sphere of Fe hangman porphyrin can greatly increase the catalytic activity of CO_2RR.[87] Herein, phenolic groups can not only form hydrogen bonds with the CO_2 adduct but also provide high local proton concentration. In general, the hydrogen bond effect plays a crucial role in improving the activity of ORR and CO_2RR for homogeneous catalysis. However, this effect has been rarely reported for heterogeneous catalysis due to the difficulty in the design and preparation of unsymmetrical porphyrin-based frameworks. Therefore, constructing porphyrin-based frameworks with unsymmetrical porphyrin building units to form hydrogen bonds by tuning the second coordination spheres of metal porphyrins is a promising strategy to enhance catalytic activity for both ORR and CO_2RR.

4.1.5   Space charge interaction effect. Similar to the hydrogen bonding effect, the space electrostatic interaction effect can also stabilize intermediates of ORR and CO_2RR. For example, Warren and co-workers demonstrated that the introduction of trimethylanilinium group $-N(CH_3)_3^+$ at the *ortho*-position of the phenyl group of Co TPP can stabilize the $CO-O_2^*$ intermediate through electrostatic interaction to promote ORR.[381] As for CO_2RR, Savéant, Robert, Costentin, and co-workers designed a specific Fe TPP, which has four positively charged trimethylanilinium groups $-N(CH_3)_3^+$ at the *ortho*-position of the phenyl group.[80] The space charge interaction can stabilize the initial $Fe-CO_2$ adduct to enhance the activity of CO_2RR. As a result, the space charge interaction effect plays a crucial role in the stabilization of reaction intermediates for both ORR and CO_2RR. Although space charge interaction substituent effect has been well demonstrated for molecular catalysts of porphyrins, synthesizing porphyrin-based frameworks with positively charged functional groups is very difficult.

4.1.6   Binuclear synergistic effect. In nature, the binuclear synergistic effect of heme Fe porphyrin and Cu_B site plays a crucial role in the O_2 reduction process with 4e selectivity. Inspired from nature, a series of binuclear porphyrin-based molecular catalysts have been synthesized to enhance the activity and selectivity for ORR. For example, Cao and co-workers reported a pacman binuclear Co bistri(pentafluorophenyl)porphyrin connected with the benzene linker for ORR.[44] Herein, the atomic distance of Co between two porphyrin molecules is about 5.76 Å. The resulting binuclear Co porphyrin exhibited high 4e selectivity of O_2 reduction reaction to H_2O. In addition to the pacman binuclear Co porphyrins, hangman cofacial binuclear Co porphyrins also attracted great interest.[43] The distance of two Co atoms can be fine-tuned by using different spacers. Furthermore, heterobimetallic Fe/Co porphyrins have also been prepared to investigate the synergistic effect for ORR.[382] As a result, binuclear metal species are favorable for oxygen binding and activation, and the formation

of the bridging superoxide species, which is the key intermediate of ORR catalysis. As for the OER, pacman binuclear Mn porphyrins had also been prepared and the formation of the O–O bond showed direct coupling of $Mn^V\!\!=\!\!O$ species.[383] Though great efforts have been dedicated to investigating the synthetic effect of binuclear metal porphyrins, rare reports were found for porphyrin-based frameworks. In future, the kind of metal centers and the distance between the metal centers of porphyrin building units for porphyrin-based frameworks can be fine-tuned to realize the regulation of activity and selectivity for oxygen electrocatalysis by controlling organic linkers, metal nodes, and coordination geometries.

4.1.7   Charge transfer effect. Conductivity of porphyrin-based frameworks still remains a bottleneck for efficient electron transfer and overall catalytic activity. One way to solve this problem is to introduce conductive materials into the catalyst ink to improve the conductivity and then enhance catalytic activity. The other way is to construct porphyrin-based frameworks on conductive substrates such as CNTs, FTO *etc.* In addition, selecting specific electron-donating organic linkers and nodes to improve electron transfer to metal porphyrin has also become a new strategy to enhance catalytic activity. Recently, a universal strategy to tune electrical conductivity of MOFs had been reported by introducing redox-active and conjugated guest molecules into pores of MOFs.[384–386] For example, Allendorf, Talin and co-workers found that the introduction of 7,7,8,8-tetracyanoquinododimethane can greatly improve the conductivity of MOF Cu_3(benzene-1,3,5-tricarboxylic acid)$_2$ (HKUST-1) from $\sim\!10^{-6}$ S m^{-1} to $\sim\!7$ S m^{-1}.[386] Note that the appearance of conductive MOFs provides a possibility to further enhance application of MOFs in electrocatalysis.[387–391] Previous studies have demonstrated that regularly arranged Cu-TCPP-MOF nanosheets prepared using Cu TCPP exhibited superior proton conductivity.[392] Therefore, constructing new conductive porphyrin-based frameworks and improving the conductivity of the reported porphyrin-based frameworks may be promising development directions in the future.

4.1.8   Mass transfer effect. Designing porphyrin-based frameworks with micro/mesopores to enhance mass transfer is an effective strategy to improve electrocatalytic activity. Usually, there are two ways to construct porous frameworks with increased micro/mesopores. One way is by increasing the length of organic linkers. The difference between COF-366 and COF-367 is caused by the difference in the length of organic linkers changed from BDA to BPDA. The other way is by prolonging the substituent of porphyrin at the *meso*-position (*e.g.*, TAPP and TABPP). Regulating the length of porphyrin building blocks or organic linkers to control the pore size of the resulting porphyrin-based frameworks is a widely applied strategy to construct various structures. As for CO_2RR, constructing porphyrin-based frameworks with suitable micropores to adsorb CO_2 is also very important. Very recently, Smit, Stylianou, Garcia, Woo and co-workers showed that $Al_2(OH)_2(H_2TCPP)$ MOF (Al-PMOF) had a larger CO_2 capture capacity than $Al_2(OH)_2$(1,3,6,8-tetra(p-benzoic acid)pyrene) MOF (Al-PyrMOF) under either dry or humid conditions after screening 325 000 frameworks with computer-aided filtering

This journal is © The Royal Society of Chemistry 2021

Chem. Soc. Rev., 2021, **50**, 2540–2581 | **2569**

and validation.[393] The results demonstrated that CO_2 molecules are preferably adsorbed in the pores of Al-PMOF, which has a suitable packing distance of 6.61 Å, compared to Al-PyrMOF with a packing distance of 6.78 Å. Therefore, the specific packing structure of porphyrin-based frameworks with suitable porous structures have unique advantages for the capture of CO_2 molecules, which is an initial and crucial step of CO_2RR. Differently from porphyrin-based frameworks, Chang, Kim and co-workers constructed a porous organic cage with porphyrin molecules.[369] The results demonstrated that Fe porphyrin cage had an FE of ~100% generating CO and a TOF of 1.74 s^{-1}, while the Fe TPP monomer had an FE of ~96% and a TOF of 0.94 s^{-1} in 0.5 M KHCO$_3$. This may be ascribed to the large porosity of the porphyrin cage, which favors the CO_2 diffusion. As a result, the suitable porous structures of porphyrin-based frameworks is of great importance for electrocatalysis.

4.2 Guidelines for improving selectivity

For ORR, controlling 4e/2e selectivity of O_2 reduction is an ongoing challenge. As for mononuclear porphyrin molecules, usually, early and middle transition metal porphyrins (*e.g.*, Fe porphyrin) can catalyze O_2 to H_2O, while late transition metal porphyrin molecules (*e.g.*, Co porphyrin) catalyze O_2 to H_2O_2. However, binuclear Co porphyrin molecules can catalyze O_2 to H_2O with 4e selectivity through the formation of Co–O–O–Co species. Inspired from binuclear Co porphyrin molecules, regulating the distance of porphyrin molecules has been regarded as a promising strategy to control 4e selectivity for ORR.[394] For example, Cook and co-workers designed a series of cofacial prism architectures with Co TPyP as the porphyrin building unit.[395] The resulting electron transfer number of this cofacial catalyst for ORR can reach up to 3.96 with 97% selectivity of H_2O. Similar to the Co porphyrin cofacial prism, porphyrin cage, as a new class of porphyrin-based architectures, also attracted increasing attention.[396] Chang, Kim and co-workers designed two porous supramolecular porphyrin boxes (PB) with Co TPP as building units (Fig. 23a–c).[295] The resulting porphyrin boxes exhibited 90–100% H_2O_2 selectivity with a 2e reduction process, while Co TPP monomer exhibited 50% H_2O_2 selectivity (Fig. 23d and e). This great 2e process selectivity as presented by cages is likely attributed to the site isolation of porphyrin molecules in each supramolecular cage. In contrast, it is very hard to make all metal active sites separated for Co TPP monomers. This result agrees well with the conclusion discussed above that mononuclear late transition metal Co porphyrin molecules prefer to catalyze O_2 to H_2O_2 through a 2e reduction process. The volume, window size and polarity of porphyrin boxes can be tuned by regulating porphyrin molecules and linkers. Therefore, constructing porphyrin-based frameworks with suitable packing distance of porphyrin molecules will enhance the adsorption of intermediates and then further improve the catalytic selectivity of ORR.

For CO_2RR, currently, selectivity of C2 compounds for porphyrin-based frameworks is very low. Most of the reported porphyrin-based frameworks have high selectivity for CO
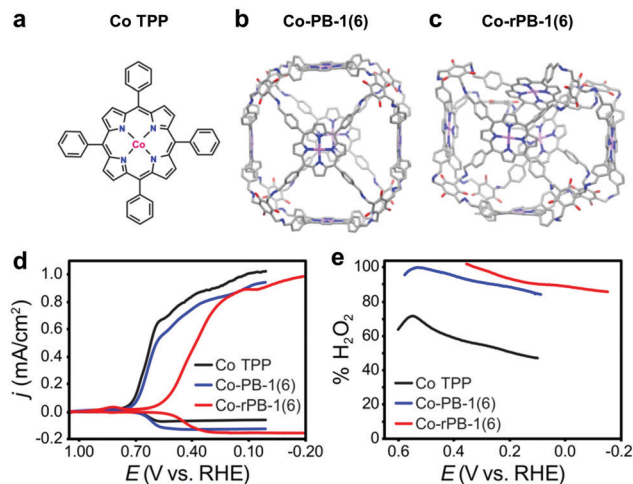
Fig. 23 (a) Molecular structure of Co TPP. Crystal structure of Co-PB-1(6) (b) and Co-rPB-1(6) (c). LSV data measured with RRDE at 250 rpm in PBS (d) and the corresponding yield of H_2O_2 of Co TPP, Co-PB-1(6), and Co-rPB-1(6) (e).[295] Reproduced from ref. 295 with permission from the Wiley-VCH, copyright 2020.

generation. Recently, Cu material has attracted great attention due to the high selectivity for C2 compounds.[397] Yang and co-workers designed a dual-metal Cu–Ag catalyst, which can enhance the production of C2 compounds.[398] CO_2 experienced the first reduction process on Ag from CO_2 to CO, and then the resulting CO experienced carbon coupling on Cu to form C2 compounds. Furthermore, Sargent and co-workers have also demonstrated that Fe porphyrin/Cu composites have high value of FE for ethanol of 41% at −0.82 V (*versus* RHE) due to the synergistic effect of porphyrin and Cu.[345] Therefore, constructing porphyrin-based frameworks grown on Cu substrates is an effective strategy to realize synthetic catalysis of CO_2RR from CO_2 to CO and then to C2 compounds.

4.3 Guidelines for improving stability

Stability is another important factor for electrocatalysis. It has been reported that electron-rich Co and Fe-based porphyrin molecules may decompose and transfer to corresponding oxyhydroxide during the OER process.[399,400] Therefore, fine-tuning the electronic structures of metal porphyrins to improve their stability under oxidative conditions is required. On the other hand, stability of porphyrin-based framework electrocatalysts is not satisfactory due to the phase transition of porphyrin building units, the decomposition of frameworks and the corrosion of by-products. Therefore, developing porphyrin-based frameworks with high chemical stability is also of great importance. Porphyrin-based MOFs connected with Zr, Ti, and Hf nodes usually exhibited excellent structural stability with pH values ranging from 0 to 13.[197,201] Recently, Bao, Jaramillo, and co-workers had also confirmed the excellent stability of PCN-222-Co after electrocatalytic measurements conducted in 0.1 M $HClO_4$.[197] On the other hand, the development of amorphous porphyrin-based frameworks, especially COFs, is also a future research direction.

2570 | *Chem. Soc. Rev.*, 2021, **50**, 2540–2581

This journal is © The Royal Society of Chemistry 2021

4.4 Reaction mechanisms

Reaction mechanism studies are urgently needed to guide the future design of efficient porphyrin-based frameworks, especially for CO_2RR due to the complex byproducts formed by multi-electron reductions. Investigating the structure evolution of porphyrin-based frameworks during the CO_2RR process can be realized with operando measurements such as Raman spectra and X-ray technologies.[401] For example, Kornienko and co-workers investigated electrochemical CO_2RR with *in situ* technologies including UV-vis absorption, resonance Raman, and infrared spectroscopy.[402] In addition, theoretical calculation has also been regarded as a good assistance method for studying reaction pathways. Therefore, developing porphyrin-based frameworks with high activity, excellent selectivity, and long-term durability and understanding the reaction mechanisms of porphyrin-based frameworks by combining *in situ* technologies and theoretical calculations should keep pace with each other.

5. Summary and outlook

At present, developing efficient catalysts for activation of energy-related small molecules is of great significance to meet increasing energy demands. Porphyrin-based frameworks have shown potential and promising applications in oxygen electrocatalysis and catalytic reduction of CO_2 due to intrinsic advantages of diverse metal active sites, tunable crystal structures, and large surface areas. Herein, recent progress in porphyrin-based frameworks in ORR, OER, Zn–air batteries, and CO_2RR are reviewed. For porphyrin-based MOFs and COFs, diverse molecular porphyrin structures as building units are summarized. Both metal active centers and surrounding functional groups of porphyrins can regulate the catalytic activity of resulting frameworks. In addition, different metal cluster nodes of MOFs and organic linkers of COFs endow porphyrin-based frameworks with diverse topologies, morphologies, and pore sizes. Typical synthetic procedures of porphyrin-based frameworks are summarized, such as the hydrothermal method, Schiff based reaction, one-pot strategy and electrochemical polymerization. Related activity measurements and evaluation criteria of energy-related applications are briefly introduced, and a performance comparison of these related porphyrin-based frameworks is also made.

Porphyrin-based frameworks combine the advantages of both homogeneous catalysts and heterogeneous catalysts, which make them promising candidates for related electrocatalysis. Catalytic activity, selectivity, and stability of porphyrin-based framework catalysts are summarized, discussed and evaluated. Catalytic activity is predominantly governed by the nature of metal centers and porphyrins. The selectivity of porphyrin-based frameworks is largely governed not only by types of metals and their surrounding environments, including distance between active sites of neighboring porphyrin molecules, but also by electron transfer and mass diffusion efficiency. Herein, the enhanced electron transfer was achieved by physically mixing porphyrin-based frameworks with conductive materials (*e.g.*, CNT, graphene, carbon black *etc.*), *in situ* growing porphyrin-based frameworks on conductive supports (*e.g.*, FTO, CNTs, Ni foam, graphene *etc.*), and pyrolyzing these frameworks into porous carbon materials at high temperatures. The improvement of mass transfer is attributed to the high porosity of porphyrin-based frameworks with large pore diameters and open hole channels. The stability of these catalysts is primarily governed by the intrinsic structure of porphyrin-based frameworks. Though great efforts have been dedicated to the development of porphyrin-based frameworks, there is still a long way to go to improve the activity, selectively, and stability of these catalysts for electrochemical reactions, including ORR, OER, ORR/OER, Zn–air batteries and CO_2RR *etc.*

According to above discussions, the future development of porphyrin-based framework electrocatalysts is outlooked.

(1) Designing and developing new porphyrin-based framework systems with a high density of metal porphyrins to increase the exposure of catalytic active sites and thus to enhance catalytic performance for oxygen electrocatalysis is highly desired. Currently, the electrocatalytic performance of porphyrin-based frameworks is still far from the level of practical industrialization. The catalytic activity of porphyrin-based frameworks can be improved from the following aspects. First, the mass transfer process of porphyrin-based frameworks can be enhanced through tuning the porosity with more active sites exposed. Second, the electron transfer process can be enhanced through growing porphyrin-based frameworks on conductive substrates, constructing conductive porphyrin-based frameworks, and introducing electron-collecting and donating nodes. Third, creating fewer defects and regulating the coordination number of metals in porphyrin-based frameworks can directly increase intrinsic catalytic activity. Fourth, constructing composite catalytic systems by introducing nanoparticles and molecules to realize synergistic effect between porphyrins and guests is also an effective strategy to enhance activity and selectivity.

(2) In-depth understanding of the structure–activity relationship is of great importance for the design and synthesis of porphyrin-based frameworks. Currently, many factors, such as metal active sites, surrounding functional groups at the *meso-* and β-positions, metal cluster nodes, organic linkers of porphyrin-based frameworks, have been reported to affect the adsorption, reaction and desorption process of reactants, intermediates and products. These obtained frameworks usually have a high symmetry, which, to a great extent, limits their diversity. Therefore, porphyrin building units with unsymmetrical substituents and nodes with unusual connectivity numbers can be introduced to construct new frameworks.[403] Furthermore, combinations of mixed porphyrin building units and flexible organic linkers can result in novel porphyrin-based frameworks with different porosity and topological structures.

(3) Improving structural and mechanical long-term stability of porphyrin-based frameworks is also of great importance due to harsh catalytic conditions in practical applications. Thermal stability and chemical stability of porphyrin-based MOFs can be enhanced by using metal center nodes with high oxidation states such as Zr^{4+}. Zr-based porphyrin MOFs, especially

This journal is © The Royal Society of Chemistry 2021

Chem. Soc. Rev., 2021, **50**, 2540–2581 | **2571**

Zr-chains nodes, are usually very stable in strong acidic and basic solutions. Stability of MOFs in weak acids and bases can be improved by incorporating –CF$_3$ groups in pores.[404] In contrast, porphyrin-based COFs usually have high chemical stability due to covalently linked organic linkers. In addition, due to harsh catalytic reaction conditions, porphyrin-based MOFs with partial decomposition should be the focus of further research to understand reaction mechanisms and real active sites. In particular, the effect of amorphization of porphyrin-based COFs on the catalytic activity and reaction mechanism still remains a great challenge. This is because porphyrin-based COFs, which are usually prepared by one-pot polymerization, are challenging to obtain accurate crystal structures.

(4) Advanced *in situ* technologies (*e.g.*, ECSTM, liquid phase-TEM, scanning probe microscopy, Raman spectra, X-ray absorption spectroscopy, infrared spectroscopy, *etc.*) and *ex situ* technologies (*e.g.*, aberration correction STEM, X-ray photoelectron spectroscopy, XRD, *etc.*) should be applied to shed light on studying catalytic processes, characterizing reaction intermediates, and determining structure evolution of porphyrin-based frameworks. It is a general trend to make full use of computer technology to carry out theoretical investigation on electrocatalytic reaction pathways and their affecting factors. The combination of *in situ* technologies, *ex situ* technologies, and theoretical investigations will be beneficial to the construction of explicit catalytic cycle and structure–activity correlation. These results will provide new insights into the design of more efficient porphyrin-based frameworks.

(5) Reducing synthetic steps is also an important research direction in the future. This is because the cost of porphyrin-based frameworks is one important factor to consider for large-scale industrial applications. At present, the cost of preparing porphyrin-based frameworks is still very high. It is urgent to develop new synthetic methods. Recently, Jiang, Zeng, Wang and co-workers introduced a general imine-exchange strategy to prepare COF-367-Co nanosheets on a large scale and with high yield.[405] This strategy for preparing imine-linked COF nanosheets may be applied to the construction of other bond-linked COFs with promising applications.

Abbreviations

1D	One dimensional
2D	Two dimensional
2e	Two-electron
3D	Three dimensional
4e	Four-electron
AFM	Atomic force microscopy
Al-PMOF	Al$_2$(OH)$_2$(H$_2$TCPP) MOF
Al-PyrMOF	Al$_2$(OH)$_2$(1,3,6,8-tetra(*p*-benzoic acid)pyrene) MOF
BDA	1,4-Benzenedicarboxaldehyde
BPDA	4,4′-Biphenyldicarboxaldehyde
CF	Cu foam
CFP	Carbon fiber paper
CNT	Carbon nanotube
CO$_2$RR	CO$_2$ reduction reaction
Co–Al-PMOF	Co–Al-based TCPP MOF
COFs	Covalent organic frameworks
Co-PCOF	Co porphyrin COF
Co-PMOF	Co porphyrin MOF
CV	Cyclic voltammetry
$E_{1/2}$	Half-wave potential
E_{10}	Potential at $j = 10$ mA cm^{-2}
ECSTM	Electrochemical scanning tunneling microscopy
E_{onset}	Onset potential
Fe$_{SA}$–N–C	Single-atom Fe doped N–C materials
FE	faradaic efficiency
FTO	Fluorine-doped tin oxide
GC	Glassy carbon
η_{10}	Overpotential for OER at $j = 10$ mA cm^{-2}
H$_2$O$_2$	Hydrogen peroxide
HER	Hydrogen evolution reaction
j	Current density
j_K	Kinetic current density
j_L	Diffusion-limited current density
LSV	Linear sweep voltammetry
M^{1}TPyP-M^2	(M^{1}TPyP = Metal-5,10,15,20-tetra(4-pyridyl)-porphyrin; M^1, M^2 = Fe, Co)
M–N–C	Metal–nitrogen–carbon
MOFs	Metal–organic frameworks
n	Electron transfer number
NHE	Normal hydrogen electrode
OER	Oxygen evolution reaction
ORR	Oxygen reduction reaction
PB	Porphyrin box
PBS	Phosphate buffer solution
PCN	Porous coordination network
PEM	Proton exchange membrane
PEMFC	Proton exchange membrane fuel cell
py-G	Pyridine-functionalized graphene
py-rGO	Pyridine-functionalized reduced graphene oxide
RDE	Rotating disk electrode
RHE	Reversible hydrogen electrode
RRDE	Rotating ring-disk electrode
SEM	Scanning electron microscopy
STEM	Scanning transmission electron microscopy
STM	Scanning tunneling microscopy
TABPP	5,10,15,20-Tetra(4-aminobiphenyl)porphyrin
TAPP	5,10,15,20-Tetra(4-aminophenyl)porphyrin
TBBPP	5,10,15,20-Tetra(4-bromobiphenyl)porphyrin
TBPP	5,10,15,20-Tetra(4-bromophenyl)porphyrin
TCPP	5,10,15,20-Tetra(4-carboxyphenyl)porphyrin
TCYP	5,10,15,20-Tetra(carbazol-9-ylphenyl)porphyrin
TCyPP	5,10,15,20-Tetra(4-cyanophenyl)porphyrin
TEM	Transmission electron microscope
TEP	5,10,15,20-Tetraethynylporphyrin
TEPP	5,10,15,20-Tetra(4-ethynylphenyl)porphyrin
TFBM	3,3′,5,5′-Tetra(4-formylphenyl)bimesityl
THBPP	5,10,15,20-Tetra(3,4,5-trihydroxybiphenyl)porphyrin
THPP	5,10,15,20-Tetra(3,4,5-trihydroxyphenyl)porphyrin

2572 | *Chem. Soc. Rev.*, 2021, **50**, 2540–2581

This journal is © The Royal Society of Chemistry 2021

TIPP	5,10,15,20-Tetra(4-(imidazol-1-yl)phenyl)porphyrin
TOF	Turnover frequency
TON	Turnover number
TPFPP	5,10,15,20-Tetra(pentafluorophenyl)porphyrin
TPP	5,10,15,20-Tetra(phenyl)porphyrin
TPTAP	Tetraphenyltrimethylammonium porphyrin
TPyP	5,10,15,20-Tetra(4-pyridyl)porphyrin
TTF	Tetrathiafulvalene
TTP	5,10,15,20-Tetra(2-thienyl)porphyrin
XRD	X-ray diffraction
ΔE	Potential difference of $E_{1/2}$ for ORR and E_{10} for OER
ΔG_{OH}	Adsorption energy of *OH

Conflicts of interest

There are no conflicts to declare.

Acknowledgements

References

1 M. M. Najafpour, G. Renger, M. Hołyńska, A. N. Moghaddam, E.-M. Aro, R. Carpentier, H. Nishihara, J. J. Eaton-Rye, J.-R. Shen and S. I. Allakhverdiev, *Chem. Rev.*, 2016, **116**, 2886–2936.

2 W. Auwärter, D. Écija, F. Klappenberger and J. V. Barth, *Nat. Chem.*, 2015, **7**, 105–120.

3 W. Zhang, W. Lai and R. Cao, *Chem. Rev.*, 2017, **117**, 3717–3797.

4 K. D. Borah and J. Bhuyan, *Dalton Trans.*, 2017, **46**, 6497–6509.

5 X. Huang and J. T. Groves, *Chem. Rev.*, 2018, **118**, 2491–2553.

6 T. L. Poulos, *Chem. Rev.*, 2014, **114**, 3919–3962.

7 B. Meunier, S. P. de Visser and S. Shaik, *Chem. Rev.*, 2004, **104**, 3947–3980.

8 M. Wikström, K. Krab and V. Sharma, *Chem. Rev.*, 2018, **118**, 2469–2490.

9 T. Tsukihara, H. Aoyama, E. Yamashita, T. Tomizaki, H. Yamaguchi, K. Shinzawa-Itoh, R. Nakashima, R. Yaono and S. Yoshikawa, *Science*, 1995, **269**, 1069–1074.

10 S. M. Adam, G. B. Wijeratne, P. J. Rogler, D. E. Diaz, D. A. Quist, J. J. Liu and K. D. Karlin, *Chem. Rev.*, 2018, **118**, 10840–11022.

11 S. Yoshikawa and A. Shimada, *Chem. Rev.*, 2015, **115**, 1936–1989.

12 J. P. Collman, N. K. Devaraj, R. A. Decréau, Y. Yang, Y.-L. Yan, W. Ebina, T. A. Eberspacher and C. E. D. Chidsey, *Science*, 2007, **315**, 1565–1568.

13 S. Samanta, P. K. Das, S. Chatterjee and A. Dey, *J. Porphyrins phthalocyanines*, 2015, **19**, 92–108.

14 J. P. Collman, L. Fu, P. C. Herrmann, Z. Wang, M. Rapta, M. Bröring, R. Schwenninger and B. Boitrel, *Angew. Chem., Int. Ed.*, 1998, **37**, 3397–3400.

15 P. Garrido-Barros, C. Gimbert-Suriñach, R. Matheu, X. Sala and A. Llobet, *Chem. Soc. Rev.*, 2017, **46**, 6088–6098.

16 M. D. Kärkäs, O. Verho, E. V. Johnston and B. Åkermark, *Chem. Rev.*, 2014, **114**, 11863–12001.

17 X. Guo, N. Wang, X. Li, Z. Zhang, J. Zhao, W. Ren, S. Ding, G. Xu, J. Li, U.-P. Apfel, W. Zhang and R. Cao, *Angew. Chem., Int. Ed.*, 2020, **59**, 8941–8946.

18 C. Costentin, G. Passard and J.-M. Savéant, *J. Am. Chem. Soc.*, 2015, **137**, 5461–5467.

19 Y. Han, H. Fang, H. Jing, H. Sun, H. Lei, W. Lai and R. Cao, *Angew. Chem., Int. Ed.*, 2016, **55**, 5457–5462.

20 N. Wang, H. Lei, Z. Zhang, J. Li, W. Zhang and R. Cao, *Chem. Sci.*, 2019, **10**, 2308–2314.

21 H. Lei, Y. Wang, Q. Zhang and R. Cao, *J. Porphyrins phthalocyanines*, 2020, **24**, 1361–1371.

22 H. Lei, H. Fang, Y. Han, W. Lai, X. Fu and R. Cao, *ACS Catal.*, 2015, **5**, 5145–5153.

23 J. M. Park, J. H. Lee and W.-D. Jang, *Coord. Chem. Rev.*, 2020, **407**, 213157.

24 C. W. Machan, *ACS Catal.*, 2020, **10**, 2640–2655.

25 P. Zhang, J. Hu, B. Liu, J. Yang and H. Hou, *Chemosphere*, 2019, **219**, 617–635.

26 V. Artero, M. Chavarot-Kerlidou and M. Fontecave, *Angew. Chem., Int. Ed.*, 2011, **50**, 7238–7266.

27 L. L. Chng, C. J. Chang and D. G. Nocera, *Org. Lett.*, 2003, **5**, 2421–2424.

28 S. Bhunia, A. Rana, P. Roy, D. J. Martin, M. L. Pegis, B. Roy and A. Dey, *J. Am. Chem. Soc.*, 2018, **140**, 9444–9457.

29 K. Sengupta, S. Chatterjee, S. Samanta, S. Bandyopadhyay and A. Dey, *Inorg. Chem.*, 2013, **52**, 2000–2014.

30 K. Mittra, S. Chatterjee, S. Samanta and A. Dey, *Inorg. Chem.*, 2013, **52**, 14317–14325.

31 S. Samanta, K. Sengupta, K. Mittra, S. Bandyopadhyay and A. Dey, *Chem. Commun.*, 2012, **48**, 7631–7633.

32 A. C. Brezny, S. I. Johnson, S. Raugei and J. M. Mayer, *J. Am. Chem. Soc.*, 2020, **142**, 4108–4113.

33 D. J. Wasylenko, C. Rodríguez, M. L. Pegis and J. M. Mayer, *J. Am. Chem. Soc.*, 2014, **136**, 12544–12547.

34 D. J. Martin, C. F. Wise, M. L. Pegis and J. M. Mayer, *Acc. Chem. Res.*, 2020, **53**, 1056–1065.

35 M. L. Pegis, D. J. Martin, C. F. Wise, A. C. Brezny, S. I. Johnson, L. E. Johnson, N. Kumar, S. Raugei and J. M. Mayer, *J. Am. Chem. Soc.*, 2019, **141**, 8315–8326.

36 C. Costentin, H. Dridi and J.-M. Savéant, *J. Am. Chem. Soc.*, 2015, **137**, 13535–13544.

37 Y. Yamada, Y. Fukunishi, S. Yamazaki and S. Fukuzumi, *Chem. Commun.*, 2010, **46**, 7334–7336.

38 Y. H. Hong, J. W. Han, J. Jung, T. Nakagawa, Y.-M. Lee, W. Nam and S. Fukuzumi, *J. Am. Chem. Soc.*, 2019, **141**, 9155–9159.

39 B. Sun, Z. Ou, S. Yang, D. Meng, G. Lu, Y. Fang and K. M. Kadish, *Dalton Trans.*, 2014, **43**, 10809–10815.

40 B. Su, I. Hatay, A. Trojánek, Z. Samec, T. Khoury, C. P. Gros, J.-M. Barbe, A. Daina, P.-A. Carrupt and H. H. Girault, *J. Am. Chem. Soc.*, 2010, **132**, 2655–2662.

41 R. McGuire Jr., D. K. Dogutan, T. S. Teets, J. Suntivich, Y. Shao-Horn and D. G. Nocera, *Chem. Sci.*, 2010, **1**, 411–414.

42 C. J. Chang, Y. Deng, C. Shi, C. K. Chang, F. C. Anson and D. G. Nocera, *Chem. Commun.*, 2000, 1355–1356.

43 P. Peljo, L. Murtomäki, T. Kallio, H.-J. Xu, M. Meyer, C. P. Gros, J.-M. Barbe, H. H. Girault, K. Laasonen and K. Kontturi, *J. Am. Chem. Soc.*, 2012, **134**, 5974–5984.

44 Y. Liu, G. Zhou, Z. Zhang, H. Lei, Z. Yao, J. Li, J. Lin and R. Cao, *Chem. Sci.*, 2020, **11**, 87–96.

45 M. L. Pegis, C. F. Wise, D. J. Martin and J. M. Mayer, *Chem. Rev.*, 2018, **118**, 2340–2391.

46 G. Passard, D. K. Dogutan, M. Qiu, C. Costentin and D. G. Nocera, *ACS Catal.*, 2018, **8**, 8671–8679.

47 M. L. Pegis, B. A. McKeown, N. Kumar, K. Lang, D. J. Wasylenko, X. P. Zhang, S. Raugei and J. M. Mayer, *ACS Cent. Sci.*, 2016, **2**, 850–856.

48 H. Lei, X. Li, J. Meng, H. Zheng, W. Zhang and R. Cao, *ACS Catal.*, 2019, **9**, 4320–4344.

49 Y. Fang, Z. Ou and K. M. Kadish, *Chem. Rev.*, 2017, **117**, 3377–3419.

50 J. P. Collman, M. Kaplun and R. A. Decréau, *Dalton Trans.*, 2006, 554–559.

51 Z. Ou, A. Lü, D. Meng, S. Huang, Y. Fang, G. Lu and K. M. Kadish, *Inorg. Chem.*, 2012, **51**, 8890–8896.

52 S. Sun, N. Jiang and D. Xia, *J. Phys. Chem. C*, 2011, **115**, 9511–9517.

53 A. Morozan, S. Campidelli, A. Filoramo, B. Jousselme and S. Palacin, *Carbon*, 2011, **49**, 4839–4847.

54 W. Li, A. Yu, D. C. Higgins, B. G. Llanos and Z. Chen, *J. Am. Chem. Soc.*, 2010, **132**, 17056–17058.

55 Z. Wang, H. Lei, R. Cao and M. Zhang, *Electrochim. Acta*, 2015, **171**, 81–88.

56 J. Masa and W. Schuhmann, *Chem. – Eur. J.*, 2013, **19**, 9644–9654.

57 G. Tei, T. Tamaki, T. Hayashi, K. Nakajima, A. Sakai, S. Yotsuhashi and T. Ogawa, *Eur. J. Inorg. Chem.*, 2017, 3229–3232.

58 A. Han, H. Jia, H. Ma, S. Ye, H. Wu, H. Lei, Y. Han, R. Cao and P. Du, *Phys. Chem. Chem. Phys.*, 2014, **16**, 11224–11232.

59 T. Nakazono, A. R. Parent and K. Sakai, *Chem. Commun.*, 2013, **49**, 6325–6327.

60 D. Wang and J. T. Groves, *Proc. Natl. Acad. Sci. U. S. A.*, 2013, **110**, 15579–15584.

61 Y. Naruta, M. Sasayama and T. Sasaki, *Angew. Chem., Int. Ed. Engl.*, 1994, **33**, 1839–1841.

62 M. Suga, F. Akita, K. Hirata, G. Ueno, H. Murakami, Y. Nakajima, T. Shimizu, K. Yamashita, M. Yamamoto, H. Ago and J.-R. Shen, *Nature*, 2015, **517**, 99–103.

63 K. N. Ferreira, T. M. Iverson, K. Maghlaoui, J. Barber and S. Iwata, *Science*, 2004, **303**, 1831–1838.

64 X.-P. Zhang, H.-Y. Wang, H. Zheng, W. Zhang and R. Cao, *Chin. J. Catal.*, DOI: 10.1016/S1872-2067(20)63681-6.

65 Y. Liu, Y. Han, Z. Zhang, W. Zhang, W. Lai, Y. Wang and R. Cao, *Chem. Sci.*, 2019, **10**, 2613–2622.

66 Y. Han, Y. Wu, W. Lai and R. Cao, *Inorg. Chem.*, 2015, **54**, 5604–5613.

67 M. Guo, Y.-M. Lee, R. Gupta, M. S. Seo, T. Ohta, H.-H. Wang, H.-Y. Liu, S. N. Dhuri, R. Sarangi, S. Fukuzumi and W. Nam, *J. Am. Chem. Soc.*, 2017, **139**, 15858–15867.

68 H. Lei, A. Han, F. Li, M. Zhang, Y. Han, P. Du, W. Lai and R. Cao, *Phys. Chem. Chem. Phys.*, 2014, **16**, 1883–1893.

69 L. Xu, H. Lei, Z. Zhang, Z. Yao, J. Li, Z. Yu and R. Cao, *Phys. Chem. Chem. Phys.*, 2017, **19**, 9755–9761.

70 D. K. Dogutan, R. McGuire, Jr. and D. G. Nocera, *J. Am. Chem. Soc.*, 2011, **133**, 9178–9180.

71 H. Sun, Y. Han, H. Lei, M. Chen and R. Cao, *Chem. Commun.*, 2017, **53**, 6195–6198.

72 W. Lai, R. Cao, G. Dong, S. Shaik, J. Yao and H. Chen, *J. Phys. Chem. Lett.*, 2012, **3**, 2315–2319.

73 Y. Wu, Z. Jiang, X. Lu, Y. Liang and H. Wang, *Nature*, 2019, **575**, 639–642.

74 R. Francke, B. Schille and M. Roemelt, *Chem. Rev.*, 2018, **118**, 4631–4701.

75 A. M. Appel, J. E. Bercaw, A. B. Bocarsly, H. Dobbek, D. L. DuBois, M. Dupuis, J. G. Ferry, E. Fujita, R. Hille, P. J. A. Kenis, C. A. Kerfeld, R. H. Morris, C. H. F. Peden, A. R. Portis, S. W. Ragsdale, T. B. Rauchfuss, J. N. H. Reek, L. C. Seefeldt, R. K. Thauer and G. L. Waldrop, *Chem. Rev.*, 2013, **113**, 6621–6658.

76 C. Costentin, M. Robert and J.-M. Savéant, *Chem. Soc. Rev.*, 2013, **42**, 2423–2436.

77 P. Gotico, Z. Halime and A. Aukauloo, *Dalton Trans.*, 2020, **49**, 2381–2396.

78 K. Elouarzaki, V. Kannan, V. Jose, H. S. Sabharwal and J.-M. Lee, *Adv. Energy Mater.*, 2019, **9**, 1900090.

79 C. Costentin, S. Drouet, M. Robert and J.-M. Savéant, *Science*, 2012, **338**, 90–94.

80 I. Azcarate, C. Costentin, M. Robert and J.-M. Savéant, *J. Am. Chem. Soc.*, 2016, **138**, 16639–16644.

81 C. Costentin, M. Robert and J.-M. Savéant, *Acc. Chem. Res.*, 2015, **48**, 2996–3006.

82 P. Sen, B. Mondal, D. Saha, A. Rana and A. Dey, *Dalton Trans.*, 2019, **48**, 5965–5977.

83 A. Ghatak, S. Bhakta, S. Bhunia and A. Dey, *Chem. Sci.*, 2019, **10**, 9692–9698.

84 B. Mondal, P. Sen, A. Rana, D. Saha, P. Das and A. Dey, *ACS Catal.*, 2019, **9**, 3895–3899.

85 C. G. Margarit, C. Schnedermann, N. G. Asimow and D. G. Nocera, *Organometallics*, 2019, **38**, 1219–1223.

86 C. G. Margarit, N. G. Asimow, M. I. Gonzalez and D. G. Nocera, *J. Phys. Chem. Lett.*, 2020, **11**, 1890–1895.

87 K. Guo, X. Li, H. Lei, W. Zhang and R. Cao, *ChemCatChem*, 2020, **12**, 1591–1595.

88 B. Zhao, H. Lei, N. Wang, G. Xu, W. Zhang and R. Cao, *Chem. – Eur. J.*, 2020, **26**, 4007–4012.

2574 | *Chem. Soc. Rev.*, 2021, **50**, 2540–2581

This journal is © The Royal Society of Chemistry 2021

89 Z. N. Zahran, E. A. Mohamed and Y. Naruta, *Sci. Rep.*, 2016, **6**, 24533.

90 M. Abdinejad, A. Seifitokaldani, C. Dao, E. H. Sargent, X.-A. Zhang and H. B. Kraatz, *ACS Appl. Energy Mater.*, 2019, **2**, 1330–1335.

91 Y.-Q. Zhang, J.-Y. Chen, P. E. M. Siegbahn and R.-Z. Liao, *ACS Catal.*, 2020, **10**, 6332–6345.

92 P. Gotico, B. Boitrel, R. Guillot, M. Sircoglou, A. Quaranta, Z. Halime, W. Leibl and A. Aukauloo, *Angew. Chem., Int. Ed.*, 2019, **58**, 4504–4509.

93 K. Torbensen, C. Han, B. Boudy, N. von Wolff, C. Bertail, W. Braun and M. Robert, *Chem. – Eur. J.*, 2020, **26**, 3034–3038.

94 K. Takahashi, K. Hiratsuka, H. Sasaki and S. Toshima, *Chem. Lett.*, 1979, 305–308.

95 K. Hiratsuka, K. Takahashi, H. Sasaki and S. Toshima, *Chem. Lett.*, 1977, 1137–1140.

96 Z. Weng, J. Jiang, Y. Wu, Z. Wu, X. Guo, K. L. Materna, W. Liu, V. S. Batista, G. W. Brudvig and H. Wang, *J. Am. Chem. Soc.*, 2016, **138**, 8076–8079.

97 G. F. Manbeck and E. Fujita, *J. Porphyrins phthalocyanines*, 2015, **19**, 45–64.

98 J. D. Froehlich and C. P. Kubiak, *Inorg. Chem.*, 2012, **51**, 3932–3934.

99 J. D. Froehlich and C. P. Kubiak, *J. Am. Chem. Soc.*, 2015, **137**, 3565–3573.

100 X. Wang, Z.-F. Cai, Y.-Q. Wang, Y.-C. Feng, H.-J. Yan, D. Wang and L.-J. Wan, *Angew. Chem., Int. Ed.*, 2020, **59**, 16098–16103.

101 K. Leung, I. M. B. Nielsen, N. Sai, C. Medforth and J. A. Shelnutt, *J. Phys. Chem. A*, 2010, **114**, 10174–10184.

102 J. Shen, M. J. Kolb, A. J. Göttle and M. T. M. Koper, *J. Phys. Chem. C*, 2016, **120**, 15714–15721.

103 B. Zhang and L. Sun, *Chem. Soc. Rev.*, 2019, **48**, 2216–2264.

104 S. Zhang, Q. Fan, R. Xia and T. J. Meyer, *Acc. Chem. Res.*, 2020, **53**, 255–264.

105 S. Dey, B. Mondal, S. Chatterjee, A. Rana, S. Amanullah and A. Dey, *Nat. Rev. Chem.*, 2017, **1**, 0098.

106 X. Li, H. Lei, X. Guo, X. Zhao, S. Ding, X. Gao, W. Zhang and R. Cao, *ChemSusChem*, 2017, **10**, 4632–4641.

107 H. Li, X. Li, H. Lei, G. Zhou, W. Zhang and R. Cao, *ChemSusChem*, 2019, **12**, 801–806.

108 L. Xie, J. Tian, Y. Ouyang, X. Guo, W. Zhang, U.-P. Apfel, W. Zhang and R. Cao, *Angew. Chem., Int. Ed.*, 2020, **59**, 15844–15848.

109 J. Meng, H. T. Lei, X. L. Li, W. Zhang and R. Cao, *J. Phys. Chem. C*, 2020, **124**, 16324–16331.

110 M. Garrido, M. K. Volland, P. W. Münich, L. Rodríguez-Pérez, J. Calbo, E. Ortí, M. Á. Herranz, N. Martín and D. M. Guldi, *J. Am. Chem. Soc.*, 2020, **142**, 1895–1903.

111 H. Lei, C. Liu, Z. Wang, Z. Zhang, M. Zhang, X. Chang, W. Zhang and R. Cao, *ACS Catal.*, 2016, **6**, 6429–6437.

112 L. Xie, X. Li, B. Wang, J. Meng, H. Lei, W. Zhang and R. Cao, *Angew. Chem., Int. Ed.*, 2019, **58**, 18883–18887.

113 A. N. Marianov and Y. Jiang, *ACS Sustainable Chem. Eng.*, 2019, **7**, 3838–3848.

114 J. Meng, H. Lei, X. Li, J. Qi, W. Zhang and R. Cao, *ACS Catal.*, 2019, **9**, 4551–4560.

115 D. Dasler, R. A. Schäfer, M. B. Minameyer, J. F. Hitzenberger, F. Hauke, T. Drewello and A. Hirsch, *J. Am. Chem. Soc.*, 2017, **139**, 11760–11765.

116 X. Li, H. Lei, J. Liu, X. Zhao, S. Ding, Z. Zhang, X. Tao, W. Zhang, W. Wang, X. Zheng and R. Cao, *Angew. Chem., Int. Ed.*, 2018, **57**, 15070–15075.

117 W.-Y. Gao, M. Chrzanowski and S. Ma, *Chem. Soc. Rev.*, 2014, **43**, 5841–5866.

118 G. Xu, H. Lei, G. Zhou, C. Zhang, L. Xie, W. Zhang and R. Cao, *Chem. Commun.*, 2019, **55**, 12647–12650.

119 X. F. Lu, B. Y. Xia, S.-Q. Zang and X. W. Lou, *Angew. Chem., Int. Ed.*, 2020, **59**, 4634–4650.

120 O. M. Yaghi, G. Li and H. Li, *Nature*, 1995, **378**, 703–706.

121 A. Kirchon, L. Feng, H. F. Drake, E. A. Joseph and H.-C. Zhou, *Chem. Soc. Rev.*, 2018, **47**, 8611–8638.

122 Q.-L. Zhu and Q. Xu, *Chem. Soc. Rev.*, 2014, **43**, 5468–5512.

123 N. Stock and S. Biswas, *Chem. Rev.*, 2012, **112**, 933–969.

124 H. Furukawa, K. E. Cordova, M. O'Keeffe and O. M. Yaghi, *Science*, 2013, **341**, 1230444.

125 S. Kandambeth, K. Dey and R. Banerjee, *J. Am. Chem. Soc.*, 2019, **141**, 1807–1822.

126 C. S. Diercks and O. M. Yaghi, *Science*, 2017, **355**, eaal1585.

127 S.-Y. Ding and W. Wang, *Chem. Soc. Rev.*, 2013, **42**, 548–568.

128 A. P. Côté, A. I. Benin, N. W. Ockwig, M. O'Keeffe, A. J. Matzger and O. M. Yaghi, *Science*, 2005, **310**, 1166–1170.

129 J. Li, X. Jing, Q. Li, S. Li, X. Gao, X. Feng and B. Wang, *Chem. Soc. Rev.*, 2020, **49**, 3565–3604.

130 H. B. Wu and X. W. Lou, *Sci. Adv.*, 2017, **3**, eaap9252.

131 Y. Song, Q. Sun, B. Aguila and S. Ma, *Adv. Sci.*, 2019, **6**, 1801410.

132 R. Zhao, Z. Liang, R. Zou and Q. Xu, *Joule*, 2018, **2**, 2235–2259.

133 P. Peng, Z. Zhou, J. Guo and Z. Xiang, *ACS Energy Lett.*, 2017, **2**, 1308–1314.

134 Y. Zhao, Z. Song, X. Li, Q. Sun, N. Cheng, S. Lawes and X. Sun, *Energy Storage Mater.*, 2016, **2**, 35–62.

135 W. Xia, A. Mahmood, R. Zou and Q. Xu, *Energy Environ. Sci.*, 2015, **8**, 1837–1866.

136 H. Wang, Q.-L. Zhu, R. Zou and Q. Xu, *Chem*, 2017, **2**, 52–80.

137 H. Wang, Z. Zeng, P. Xu, L. Li, G. Zeng, R. Xiao, Z. Tang, D. Huang, L. Tang, C. Lai, D. Jiang, Y. Liu, H. Yi, L. Qin, S. Ye, X. Ren and W. Tang, *Chem. Soc. Rev.*, 2019, **48**, 488–516.

138 N. L. Rosi, J. Eckert, M. Eddaoudi, D. T. Vodak, J. Kim, M. O'Keeffe and O. M. Yaghi, *Science*, 2003, **300**, 1127–1129.

139 H. B. Aiyappa, J. Masa, C. Andronescu, M. Muhler, R. A. Fischer and W. Schuhmann, *Small Methods*, 2019, **3**, 1800415.

140 P.-Q. Liao, J.-Q. Shen and J.-P. Zhang, *Coord. Chem. Rev.*, 2018, **373**, 22–48.

This journal is © The Royal Society of Chemistry 2021

Chem. Soc. Rev., 2021, **50**, 2540–2581 | **2575**

141 K. Sumida, D. L. Rogow, J. A. Mason, T. M. McDonald, E. D. Bloch, Z. R. Herm, T.-H. Bae and J. R. Long, *Chem. Rev.*, 2012, **112**, 724–781.

142 L. Kong, M. Zhong, W. Shuang, Y. Xu and X.-H. Bu, *Chem. Soc. Rev.*, 2020, **49**, 2378–2407.

143 J.-R. Li, J. Sculley and H.-C. Zhou, *Chem. Rev.*, 2012, **112**, 869–932.

144 H. Wang, H. Wang, Z. Wang, L. Tang, G. Zeng, P. Xu, M. Chen, T. Xiong, C. Zhou, X. Li, D. Huang, Y. Zhu, Z. Wang and J. Tang, *Chem. Soc. Rev.*, 2020, **49**, 4135–4165.

145 Q. Yang, Q. Xu and H.-L. Jiang, *Chem. Soc. Rev.*, 2017, **46**, 4774–4808.

146 T. Rasheed, K. Rizwan, M. Bilal and H. M. N. Iqbal, *Molecules*, 2020, **25**, 1598.

147 J. Zhou and B. Wang, *Chem. Soc. Rev.*, 2017, **46**, 6927–6945.

148 Y. Chen, D. Wang, X. Deng and Z. Li, *Catal. Sci. Technol.*, 2017, **7**, 4893–4904.

149 L. Jiao, Y. Wang, H.-L. Jiang and Q. Xu, *Adv. Mater.*, 2018, **30**, 1703663.

150 W. Cheng, X. Zhao, H. Su, F. Tang, W. Che, H. Zhang and Q. Liu, *Nat. Energy*, 2019, **4**, 115–122.

151 F. Yang, G. Xu, Y. Dou, B. Wang, H. Zhang, H. Wu, W. Zhou, J.-R. Li and B. Chen, *Nat. Energy*, 2017, **2**, 877–883.

152 H. Zheng, Y. Zhang, L. Liu, W. Wan, P. Guo, A. M. Nyström and X. Zou, *J. Am. Chem. Soc.*, 2016, **138**, 962–968.

153 M.-X. Wu and Y.-W. Yang, *Adv. Mater.*, 2017, **29**, 1606134.

154 B. F. Abrahams, B. F. Hoskins and R. Robson, *J. Am. Chem. Soc.*, 1991, **113**, 3606–3607.

155 D. Micheroni, G. Lan and W. Lin, *J. Am. Chem. Soc.*, 2018, **140**, 15591–15595.

156 K. S. Suslick, P. Bhyrappa, J.-H. Chou, M. E. Kosal, S. Nakagaki, D. W. Smithenry and S. R. Wilson, *Acc. Chem. Res.*, 2005, **38**, 283–291.

157 O. K. Farha, A. M. Shultz, A. A. Sarjeant, S. T. Nguyen and J. T. Hupp, *J. Am. Chem. Soc.*, 2011, **133**, 5652–5655.

158 J. Cheng, S. Chen, D. Chen, L. Dong, J. Wang, T. Zhang, T. Jiao, B. Liu, H. Wang, J.-J. Kai, D. Zhang, G. Zheng, L. Zhi, F. Kang and W. Zhang, *J. Mater. Chem. A*, 2018, **6**, 20254–20266.

159 B. F. Abrahams, B. F. Hoskins, D. M. Michail and R. Robson, *Nature*, 1994, **369**, 727–729.

160 C. Zou and C.-D. Wu, *Dalton Trans.*, 2012, **41**, 3879–3888.

161 N. Keller, M. Calik, D. Sharapa, H. R. Soni, P. M. Zehetmaier, S. Rager, F. Auras, A. C. Jakowetz, A. Görling, T. Clark and T. Bein, *J. Am. Chem. Soc.*, 2018, **140**, 16544–16552.

162 M. H. Beyzavi, N. A. Vermeulen, A. J. Howarth, S. Tussupbayev, A. B. League, N. M. Schweitzer, J. R. Gallagher, A. E. Platero-Prats, N. Hafezi, A. A. Sarjeant, J. T. Miller, K. W. Chapman, J. F. Stoddart, C. J. Cramer, J. T. Hupp and O. K. Farha, *J. Am. Chem. Soc.*, 2015, **137**, 13624–13631.

163 G. Zhou, B. Wang and R. Cao, *J. Am. Chem. Soc.*, 2020, **142**, 14848–14853.

164 S.-Y. Ding, M. Dong, Y.-W. Wang, Y.-T. Chen, H.-Z. Wang, C.-Y. Su and W. Wang, *J. Am. Chem. Soc.*, 2016, **138**, 3031–3037.

165 W. Hao, D. Chen, Y. Li, Z. Yang, G. Xing, J. Li and L. Chen, *Chem. Mater.*, 2019, **31**, 8100–8105.

166 C. F. Pereira, M. M. Q. Simões, J. P. C. Tomé and F. A. Almeida Paz, *Molecules*, 2016, **21**, 1348.

167 Z. Zhao-Karger, P. Gao, T. Ebert, S. Klyatskaya, Z. Chen, M. Ruben and M. Fichtner, *Adv. Mater.*, 2019, **31**, 1806599.

168 C. Liu, C. Wang, H. Wang, T. Wang and J. Jiang, *Eur. J. Inorg. Chem.*, 2019, 4815–4819.

169 H.-Q. Xu, J. Hu, D. Wang, Z. Li, Q. Zhang, Y. Luo, S.-H. Yu and H.-L. Jiang, *J. Am. Chem. Soc.*, 2015, **137**, 13440–13443.

170 T. He, S. Chen, B. Ni, Y. Gong, Z. Wu, L. Song, L. Gu, W. Hu and X. Wang, *Angew. Chem., Int. Ed.*, 2018, **57**, 3493–3498.

171 H. Zhang, J. Wei, J. Dong, G. Liu, L. Shi, P. An, G. Zhao, J. Kong, X. Wang, X. Meng, J. Zhang and J. Ye, *Angew. Chem., Int. Ed.*, 2016, **55**, 14310–14314.

172 J. Chen, Y. Zhu and S. Kaskel, *Angew. Chem., Int. Ed.*, 2020, DOI: 10.1002/anie.201909880.

173 S. A. Younis, D.-K. Lim, K.-H. Kim and A. Deep, *Adv. Colloid Interface Sci.*, 2020, **277**, 102108.

174 L. Feng, Y. Wang, S. Yuan, K.-Y. Wang, J.-L. Li, G. S. Day, D. Qiu, L. Cheng, W.-M. Chen, S. T. Madrahimov and H.-C. Zhou, *ACS Catal.*, 2019, **9**, 5111–5118.

175 W. Chen, J. Akhigbe, C. Brückner, C. M. Li and Y. Lei, *J. Phys. Chem. C*, 2010, **114**, 8633–8638.

176 S. Huh, S.-J. Kim and Y. Kim, *CrystEngComm*, 2016, **18**, 345–368.

177 W. Morris, B. Volosskiy, S. Demir, F. Gándara, P. L. McGrier, H. Furukawa, D. Cascio, J. F. Stoddart and O. M. Yaghi, *Inorg. Chem.*, 2012, **51**, 6443–6445.

178 D. Feng, W.-C. Chung, Z. Wei, Z.-Y. Gu, H.-L. Jiang, Y.-P. Chen, D. J. Darensbourg and H.-C. Zhou, *J. Am. Chem. Soc.*, 2013, **135**, 17105–17110.

179 D. Feng, Z.-Y. Gu, Y.-P. Chen, J. Park, Z. Wei, Y. Sun, M. Bosch, S. Yuan and H.-C. Zhou, *J. Am. Chem. Soc.*, 2014, **136**, 17714–17717.

180 D. Feng, Z.-Y. Gu, J.-R. Li, H.-L. Jiang, Z. Wei and H.-C. Zhou, *Angew. Chem., Int. Ed.*, 2012, **51**, 10307–10310.

181 I. Hod, M. D. Sampson, P. Deria, C. P. Kubiak, O. K. Farha and J. T. Hupp, *ACS Catal.*, 2015, **5**, 6302–6309.

182 B.-X. Dong, S.-L. Qian, F.-Y. Bu, Y.-C. Wu, L.-G. Feng, Y.-L. Teng, W.-L. Liu and Z.-W. Li, *ACS Appl. Energy Mater.*, 2018, **1**, 4662–4669.

183 P. M. Usov, S. R. Ahrenholtz, W. A. Maza, B. Stratakes, C. C. Epley, M. C. Kessinger, J. Zhu and A. J. Morris, *J. Mater. Chem. A*, 2016, **4**, 16818–16823.

184 P. M. Usov, B. Huffman, C. C. Epley, M. C. Kessinger, J. Zhu, W. A. Maza and A. J. Morris, *ACS Appl. Mater. Interfaces*, 2017, **9**, 33539–33543.

185 A. Fateeva, P. A. Chater, C. P. Ireland, A. A. Tahir, Y. Z. Khimyak, P. V. Wiper, J. R. Darwent and M. J. Rosseinsky, *Angew. Chem., Int. Ed.*, 2012, **51**, 7440–7444.

186 N. Kornienko, Y. Zhao, C. S. Kley, C. Zhu, D. Kim, S. Lin, C. J. Chang, O. M. Yaghi and P. Yang, *J. Am. Chem. Soc.*, 2015, **137**, 14129–14135.

187 M. Lions, J.-B. Tommasino, R. Chattot, B. Abeykoon, N. Guillou, T. Devic, A. Demessence, L. Cardenas,

2576 | *Chem. Soc. Rev.*, 2021, **50**, 2540–2581

This journal is © The Royal Society of Chemistry 2021

F. Maillard and A. Fateeva, *Chem. Commun.*, 2017, **53**, 6496–6499.

188 S. Lin, C. S. Diercks, Y.-B. Zhang, N. Kornienko, E. M. Nichols, Y. Zhao, A. R. Paris, D. Kim, P. Yang, O. M. Yaghi and C. J. Chang, *Science*, 2015, **349**, 1208–1213.

189 C. S. Diercks, S. Lin, N. Kornienko, E. A. Kapustin, E. M. Nichols, C. Zhu, Y. Zhao, C. J. Chang and O. M. Yaghi, *J. Am. Chem. Soc.*, 2018, **140**, 1116–1122.

190 B.-Q. Li, S.-Y. Zhang, B. Wang, Z.-J. Xia, C. Tang and Q. Zhang, *Energy Environ. Sci.*, 2018, **11**, 1723–1729.

191 B.-Q. Li, S.-Y. Zhang, X. Chen, C.-Y. Chen, Z.-J. Xia and Q. Zhang, *Adv. Funct. Mater.*, 2019, **29**, 1901301.

192 H. Huang, F. Li, Y. Zhang and Y. Chen, *J. Mater. Chem. A*, 2019, **7**, 5575–5582.

193 I. Hijazi, T. Bourgeteau, R. Cornut, A. Morozan, A. Filoramo, J. Leroy, V. Derycke, B. Jousselme and S. Campidelli, *J. Am. Chem. Soc.*, 2014, **136**, 6348–6354.

194 H. Jia, Z. Sun, D. Jiang, S. Yang and P. Du, *Inorg. Chem. Front.*, 2016, **3**, 821–827.

195 E. Tavakoli, A. Kakekhani, S. Kaviani, P. Tan, M. M. Ghaleni, M. A. Zaeem, A. M. Rappe and S. Nejati, *J. Am. Chem. Soc.*, 2019, **141**, 19560–19564.

196 Y.-R. Wang, Q. Huang, C.-T. He, Y. Chen, J. Liu, F.-C. Shen and Y.-Q. Lan, *Nat. Commun.*, 2018, **9**, 4466.

197 G. Chen, M. B. Stevens, Y. Liu, L. A. King, J. Park, T. R. Kim, R. Sinclair, T. F. Jaramillo and Z. Bao, *Small Methods*, 2020, **4**, 2000085.

198 F. Dai, F. Fan, J. Bi, P. Jiang, D. Liu, X. Zhang, H. Lin, C. Gong, R. Wang, L. Zhang and D. Sun, *Dalton Trans.*, 2016, **45**, 61–65.

199 Y. Liu, X. Yan, T. Li, W.-D. Zhang, Q.-T. Fu, H.-S. Lu, X. Wang and Z.-G. Gu, *New J. Chem.*, 2019, **43**, 16907–16914.

200 S. Sohrabi, S. Dehghanpour and M. Ghalkhani, *J. Mater. Sci.*, 2018, **53**, 3624–3639.

201 M. O. Cichocka, Z. Liang, D. Feng, S. Back, S. Siahrostami, X. Wang, L. Samperisi, Y. Sun, H. Xu, N. Hedin, H. Zheng, X. Zou, H.-C. Zhou and Z. Huang, *J. Am. Chem. Soc.*, 2020, **142**, 15386–15395.

202 Z. Xin, Y.-R. Wang, Y. Chen, W.-L. Li, L.-Z. Dong and Y.-Q. Lan, *Nano Energy*, 2020, **67**, 104233.

203 P. L. Cheung, S. K. Lee and C. P. Kubiak, *Chem. Mater.*, 2019, **31**, 1908–1919.

204 X. Gong, Y. Shu, Z. Jiang, L. Lu, X. Xu, C. Wang and H. Deng, *Angew. Chem., Int. Ed.*, 2020, **59**, 5326–5331.

205 E.-X. Chen, M. Qiu, Y.-F. Zhang, Y.-S. Zhu, L.-Y. Liu, Y.-Y. Sun, X. Bu, J. Zhang and Q. Lin, *Adv. Mater.*, 2018, **30**, 1704388.

206 N. U. Day, C. C. Wamser and M. G. Walter, *Polym. Int.*, 2015, **64**, 833–857.

207 H. Sahabudeen, H. Qi, B. A. Glatz, D. Tranca, R. Dong, Y. Hou, T. Zhang, C. Kuttner, T. Lehnert, G. Seifert, U. Kaiser, A. Fery, Z. Zheng and X. Feng, *Nat. Commun.*, 2016, **7**, 13461.

208 J. L. Segura, M. J. Mancheño and F. Zamora, *Chem. Soc. Rev.*, 2016, **45**, 5635–5671.

209 G. Lin, H. Ding, R. Chen, Z. Peng, B. Wang and C. Wang, *J. Am. Chem. Soc.*, 2017, **139**, 8705–8709.

210 X.-M. Hu, Z. Salmi, M. Lillethorup, E. B. Pedersen, M. Robert, S. U. Pedersen, T. Skrydstrup and K. Daasbjerg, *Chem. Commun.*, 2016, **52**, 5864–5867.

211 R. Dong, T. Zhang and X. Feng, *Chem. Rev.*, 2018, **118**, 6189–6235.

212 Z.-S. Wu, L. Chen, J. Liu, K. Parvez, H. Liang, J. Shu, H. Sachdev, R. Graf, X. Feng and K. Müllen, *Adv. Mater.*, 2014, **26**, 1450–1455.

213 Z. Xiang, Y. Xue, D. Cao, L. Huang, J.-F. Chen and L. Dai, *Angew. Chem., Int. Ed.*, 2014, **53**, 2433–2437.

214 Y. Han, Y.-G. Wang, W. Chen, R. Xu, L. Zheng, J. Zhang, J. Luo, R.-A. Shen, Y. Zhu, W.-C. Cheong, C. Chen, Q. Peng, D. Wang and Y. Li, *J. Am. Chem. Soc.*, 2017, **139**, 17269–17272.

215 R. Makiura, S. Motoyama, Y. Umemura, H. Yamanaka, O. Sakata and H. Kitagawa, *Nat. Mater.*, 2010, **9**, 565–571.

216 J. Liu and C. Wöll, *Chem. Soc. Rev.*, 2017, **46**, 5730–5770.

217 S. Park, Z. Liao, B. Ibarlucea, H. Qi, H.-H. Lin, D. Becker, J. Melidonie, T. Zhang, H. Sahabudeen, L. Baraban, C.-K. Baek, Z. Zheng, E. Zschech, A. Fery, T. Heine, U. Kaiser, G. Cuniberti, R. Dong and X. Feng, *Angew. Chem., Int. Ed.*, 2020, **59**, 8218–8224.

218 M. Zhao, Y. Wang, Q. Ma, Y. Huang, X. Zhang, J. Ping, Z. Zhang, Q. Lu, Y. Yu, H. Xu, Y. Zhao and H. Zhang, *Adv. Mater.*, 2015, **27**, 7372–7378.

219 Y. Wang, M. Zhao, J. Ping, B. Chen, X. Cao, Y. Huang, C. Tan, Q. Ma, S. Wu, Y. Yu, Q. Lu, J. Chen, W. Zhao, Y. Ying and H. Zhang, *Adv. Mater.*, 2016, **28**, 4149–4155.

220 X. Wang, Z. Li, Y. Qu, T. Yuan, W. Wang, Y. Wu and Y. Li, *Chem*, 2019, **5**, 1486–1511.

221 L. Yang, J. Shui, L. Du, Y. Shao, J. Liu, L. Dai and Z. Hu, *Adv. Mater.*, 2019, **31**, 1804799.

222 M. A. Zeb Gul Sial, M. A. Ud Din and X. Wang, *Chem. Soc. Rev.*, 2018, **47**, 6175–6200.

223 W. Wang, F. Lv, B. Lei, S. Wan, M. Luo and S. Guo, *Adv. Mater.*, 2016, **28**, 10117–10141.

224 M. K. Debe, *Nature*, 2012, **486**, 43–51.

225 X. X. Wang, V. Prabhakaran, Y. He, Y. Shao and G. Wu, *Adv. Mater.*, 2019, **31**, 1805126.

226 A. Kulkarni, S. Siahrostami, A. Patel and J. K. Nørskov, *Chem. Rev.*, 2018, **118**, 2302–2312.

227 C. Tang, Y. Jiao, B. Shi, J.-N. Liu, Z. Xie, X. Chen, Q. Zhang and S.-Z. Qiao, *Angew. Chem., Int. Ed.*, 2020, **59**, 9171–9176.

228 S. Fukuzumi, Y. Yamada and K. D. Karlin, *Electrochim. Acta*, 2012, **82**, 493–511.

229 R. Cao, J.-S. Lee, M. Liu and J. Cho, *Adv. Energy Mater.*, 2012, **2**, 816–829.

230 H.-F. Wang and Q. Xu, *Matter*, 2019, **1**, 565–595.

231 Y. Li and J. Lu, *ACS Energy Lett.*, 2017, **2**, 1370–1377.

232 J. Ryu, M. Park and J. Cho, *Adv. Mater.*, 2019, **31**, 1804784.

233 J.-S. Lee, S. T. Kim, R. Cao, N.-S. Choi, M. Liu, K. T. Lee and J. Cho, *Adv. Energy Mater.*, 2011, **1**, 34–50.

234 H.-F. Wang, C. Tang and Q. Zhang, *Adv. Funct. Mater.*, 2018, **28**, 1803329.

This journal is © The Royal Society of Chemistry 2021

Chem. Soc. Rev., 2021, **50**, 2540–2581 | **2577**

235 J. Fu, Z. P. Cano, M. G. Park, A. Yu, M. Fowler and Z. Chen, *Adv. Mater.*, 2017, **29**, 1604685.

236 Y. Zhong, X. Xu, W. Wang and Z. Shao, *Batteries Supercaps*, 2019, **2**, 272–289.

237 J. Yi, P. Liang, X. Liu, K. Wu, Y. Liu, Y. Wang, Y. Xia and J. Zhang, *Energy Environ. Sci.*, 2018, **11**, 3075–3095.

238 Y. Li and H. Dai, *Chem. Soc. Rev.*, 2014, **43**, 5257–5275.

239 H. Luo, W.-J. Jiang, S. Niu, X. Zhang, Y. Zhang, L.-P. Yuan, C. He and J.-S. Hu, *Small*, 2020, **16**, 2001171.

240 Y. Li, M. Gong, Y. Liang, J. Feng, J.-E. Kim, H. Wang, G. Hong, B. Zhang and H. Dai, *Nat. Commun.*, 2013, **4**, 1805.

241 X. Cai, L. Lai, J. Lin and Z. Shen, *Mater. Horiz.*, 2017, **4**, 945–976.

242 M. B. Ross, P. De Luna, Y. Li, C.-T. Dinh, D. Kim, P. Yang and E. H. Sargent, *Nat. Catal.*, 2019, **2**, 648–658.

243 W. Ma, S. Xie, T. Liu, Q. Fan, J. Ye, F. Sun, Z. Jiang, Q. Zhang, J. Cheng and Y. Wang, *Nat. Catal.*, 2020, **3**, 478–487.

244 D. Gao, R. M. Arán-Ais, H. S. Jeon and B. R. Cuenya, *Nat. Catal.*, 2019, **2**, 198–210.

245 J. Li, G. Chen, Y. Zhu, Z. Liang, A. Pei, C.-L. Wu, H. Wang, H. R. Lee, K. Liu, S. Chu and Y. Cui, *Nat. Catal.*, 2018, **1**, 592–600.

246 Y. Y. Birdja, E. Pérez-Gallent, M. C. Figueiredo, A. J. Göttle, F. Calle-Vallejo and M. T. M. Koper, *Nat. Energy*, 2019, **4**, 732–745.

247 L. Sun, V. Reddu, A. C. Fisher and X. Wang, *Energy Environ. Sci.*, 2020, **13**, 374–403.

248 D. D. Zhu, J. L. Liu and S. Z. Qiao, *Adv. Mater.*, 2016, **28**, 3423–3452.

249 D. M. Weekes, D. A. Salvatore, A. Reyes, A. Huang and C. P. Berlinguette, *Acc. Chem. Res.*, 2018, **51**, 910–918.

250 A. A. Gewirth, J. A. Varnell and A. M. DiAscro, *Chem. Rev.*, 2018, **118**, 2313–2339.

251 H. Jin, C. Guo, X. Liu, J. Liu, A. Vasileff, Y. Jiao, Y. Zheng and S.-Z. Qiao, *Chem. Rev.*, 2018, **118**, 6337–6408.

252 W. Xia, A. Mahmood, Z. Liang, R. Zou and S. Guo, *Angew. Chem., Int. Ed.*, 2016, **55**, 2650–2676.

253 S. Zhao, L. Yan, H. Luo, W. Mustain and H. Xu, *Nano Energy*, 2018, **47**, 172–198.

254 Z. Liang, H. Zheng and R. Cao, *ChemElectroChem*, 2019, **6**, 2600–2614.

255 G. Zhong, S. Xu, L. Liu, C. Z. Zheng, J. Dou, F. Wang, X. Fu, W. Liao and H. Wang, *ChemElectroChem*, 2020, **7**, 1107–1114.

256 Y. Liang, Y. Li, H. Wang, J. Zhou, J. Wang, T. Regier and H. Dai, *Nat. Mater.*, 2011, **10**, 780–786.

257 X. Ren, Q. Lv, L. Liu, B. Liu, Y. Wang, A. Liu and G. Wu, *Sustainable Energy Fuels*, 2020, **4**, 15–30.

258 Y.-J. Wang, N. Zhao, B. Fang, H. Li, X. T. Bi and H. Wang, *Chem. Rev.*, 2015, **115**, 3433–3467.

259 M. Shao, Q. Chang, J.-P. Dodelet and R. Chenitz, *Chem. Rev.*, 2016, **116**, 3594–3657.

260 R. Lin, X. Cai, H. Zeng and Z. Yu, *Adv. Mater.*, 2018, **30**, 1705332.

261 X. X. Wang, M. T. Swihart and G. Wu, *Nat. Catal.*, 2019, **2**, 578–589.

262 H. Wan, A. W. Jensen, M. Escudero-Escribano and J. Rossmeisl, *ACS Catal.*, 2020, **10**, 5979–5989.

263 Z.-F. Cai, X. Wang, D. Wang and L.-J. Wan, *ChemElectroChem*, 2016, **3**, 2048–2051.

264 G. Lu, H. Yang, Y. Zhu, T. Huggins, Z. J. Ren, Z. Liu and W. Zhang, *J. Mater. Chem. A*, 2015, **3**, 4954–4959.

265 X. Zhou, J. Qiao, L. Yang and J. Zhang, *Adv. Energy Mater.*, 2014, **4**, 1301523.

266 C.-X. Zhao, B.-Q. Li, J.-N. Liu, J.-Q. Huang and Q. Zhang, *Chin. Chem. Lett.*, 2019, **30**, 911–914.

267 J. Guo, C.-Y. Lin, Z. Xia and Z. Xiang, *Angew. Chem., Int. Ed.*, 2018, **57**, 12567–12572.

268 M. Jahan, Q. Bao and K. P. Loh, *J. Am. Chem. Soc.*, 2012, **134**, 6707–6713.

269 Q. Zuo, G. Cheng and W. Luo, *Dalton Trans.*, 2017, **46**, 9344–9348.

270 S. Sohrabi, S. Dehghanpour and M. Ghalkhani, *ChemCatChem*, 2016, **8**, 2356–2366.

271 Y. He, Q. Tan, L. Lu, J. Sokolowski and G. Wu, *Electrochem. Energy Rev.*, 2019, **2**, 231–251.

272 W. Wang, Q. Jia, S. Mukerjee and S. Chen, *ACS Catal.*, 2019, **9**, 10126–10141.

273 Z. Liang, X. Fan, H. Lei, J. Qi, Y. Li, J. Gao, M. Huo, H. Yuan, W. Zhang, H. Lin, H. Zheng and R. Cao, *Angew. Chem., Int. Ed.*, 2018, **57**, 13187–13191.

274 C. Zhang, H. Yang, D. Zhong, Y. Xu, Y. Wang, Q. Yuan, Z. Liang, B. Wang, W. Zhang, H. Zheng, T. Cheng and R. Cao, *J. Mater. Chem. A*, 2020, **8**, 9536–9544.

275 Z. Liang, C. Zhang, H. Yuan, W. Zhang, H. Zheng and R. Cao, *Chem. Commun.*, 2018, **54**, 7519–7522.

276 M. Shen, C. Wei, K. Ai and L. Lu, *Nano Res.*, 2017, **10**, 1449–1470.

277 C. Zhu, H. Li, S. Fu, D. Du and Y. Lin, *Chem. Soc. Rev.*, 2016, **45**, 517–531.

278 Z. Liang, H. Zheng and R. Cao, *Sustainable Energy Fuels*, 2020, **4**, 3848–3870.

279 J. H. Zagal and M. T. M. Koper, *Angew. Chem., Int. Ed.*, 2016, **55**, 14510–14521.

280 H. Xu, D. Cheng, D. Cao and X. C. Zeng, *Nat. Catal.*, 2018, **1**, 339–348.

281 N. M. Cantillo, G. A. Goenaga, W. Gao, K. Williams, C. A. Neal, S. Ma, K. L. More and T. A. Zawodzinski Jr., *J. Mater. Chem. A*, 2016, **4**, 15621–15630.

282 Y. Ji, Z. Li, S. Wang, G. Xu, D. Li and X. Yu, *J. Electrochem. Soc.*, 2011, **158**, B139–B142.

283 W. Ma, P. Yu, T. Ohsaka and L. Mao, *Electrochem. Commun.*, 2015, **52**, 53–57.

284 H. Huang, K. Shen, F. Chen and Y. Li, *ACS Catal.*, 2020, **10**, 6579–6586.

285 X. Fang, Q. Shang, Y. Wang, L. Jiao, T. Yao, Y. Li, Q. Zhang, Y. Luo and H.-L. Jiang, *Adv. Mater.*, 2018, **30**, 1705112.

286 Q. Zuo, T. Liu, C. Chen, Y. Ji, X. Gong, Y. Mai and Y. Zhou, *Angew. Chem., Int. Ed.*, 2019, **58**, 10198–10203.

2578 | *Chem. Soc. Rev.*, 2021, **50**, 2540–2581

This journal is © The Royal Society of Chemistry 2021

287 L. Jiao, G. Wan, R. Zhang, H. Zhou, S.-H. Yu and H.-L. Jiang, *Angew. Chem., Int. Ed.*, 2018, **57**, 8525–8529.

288 J.-D. Yi, R. Xu, Q. Wu, T. Zhang, K.-T. Zang, J. Luo, Y.-L. Liang, Y.-B. Huang and R. Cao, *ACS Energy Lett.*, 2018, **3**, 883–889.

289 C.-C. Hou, H.-F. Wang, C. Li and Q. Xu, *Energy Environ. Sci.*, 2020, **13**, 1658–1693.

290 A. Wang, J. Li and T. Zhang, *Nat. Rev. Chem.*, 2018, **2**, 65–81.

291 Y. Chen, S. Ji, C. Chen, Q. Peng, D. Wang and Y. Li, *Joule*, 2018, **2**, 1242–1264.

292 L. Jiao, R. Zhang, G. Wan, W. Yang, X. Wan, H. Zhou, J. Shui, S.-H. Yu and H.-L. Jiang, *Nat. Commun.*, 2020, **11**, 2831.

293 H. Zhang, W. Tian, X. Duan, H. Sun, S. Liu and S. Wang, *Adv. Mater.*, 2020, **32**, 1904037.

294 Q. Lin, X. Bu, A. Kong, C. Mao, F. Bu and P. Feng, *Adv. Mater.*, 2015, **27**, 3431–3436.

295 P. T. Smith, Y. Kim, B. P. Benke, K. Kim and C. J. Chang, *Angew. Chem., Int. Ed.*, 2020, **59**, 4902–4907.

296 G. Cai, L. Zeng, L. He, S. Sun, Y. Tong and J. Zhang, *Chem. – Asian J.*, 2020, **15**, 1963–1969.

297 H. Qin, Y. Wang, B. Wang, X. Duan, H. Lei, X. Zhang, H. Zheng, W. Zhang and R. Cao, *J. Energy Chem.*, 2021, **53**, 77–81.

298 H. Zhong, K. H. Ly, M. Wang, Y. Krupskaya, X. Han, J. Zhang, J. Zhang, V. Kataev, B. Büchner, I. M. Weidinger, S. Kaskel, P. Liu, M. Chen, R. Dong and X. Feng, *Angew. Chem., Int. Ed.*, 2019, **58**, 10677–10682.

299 T. Reier, M. Oezaslan and P. Strasser, *ACS Catal.*, 2012, **2**, 1765–1772.

300 D. Zhao, Z. Zhuang, X. Cao, C. Zhang, Q. Peng, C. Chen and Y. Li, *Chem. Soc. Rev.*, 2020, **49**, 2215–2264.

301 N.-T. Suen, S.-F. Hung, Q. Quan, N. Zhang, Y.-J. Xu and H. M. Chen, *Chem. Soc. Rev.*, 2017, **46**, 337–365.

302 J. Wang, W. Cui, Q. Liu, Z. Xing, A. M. Asiri and X. Sun, *Adv. Mater.*, 2016, **28**, 215–230.

303 Z. Liang, Z. Huang, H. Yuan, Z. Yang, C. Zhang, Y. Xu, W. Zhang, H. Zheng and R. Cao, *Chem. Sci.*, 2018, **9**, 6961–6968.

304 Z. Liang, Z. Yang, Z. Huang, J. Qi, M. Chen, W. Zhang, H. Zheng, J. Sun and R. Cao, *Electrochim. Acta*, 2018, **271**, 526–536.

305 Z. Liang, C. Zhang, Y. Xu, W. Zhang, H. Zheng and R. Cao, *ACS Sustainable Chem. Eng.*, 2019, **7**, 3527–3535.

306 H. B. Aiyappa, J. Thote, D. B. Shinde, R. Banerjee and S. Kurungot, *Chem. Mater.*, 2016, **28**, 4375–4379.

307 A. Grimaud, O. Diaz-Morales, B. Han, W. T. Hong, Y.-L. Lee, L. Giordano, K. A. Stoerzinger, M. T. M. Koper and Y. Shao-Horn, *Nat. Chem.*, 2017, **9**, 457–465.

308 Z.-F. Huang, J. Song, Y. Du, S. Xi, S. Dou, J. M. V. Nsanzimana, C. Wang, Z. J. Xu and X. Wang, *Nat. Energy*, 2019, **4**, 329–338.

309 T. Nakazono, A. R. Parent and K. Sakai, *Chem. – Eur. J.*, 2015, **21**, 6723–6726.

310 X. Wang, Z.-F. Cai, D. Wang and L.-J. Wan, *J. Am. Chem. Soc.*, 2019, **141**, 7665–7669.

311 Z. Huang, M. Zhang, H. Lin, S. Ding, B. Dong, D. Liu, H. Wang, F. Dai and D. Sun, *RSC Adv.*, 2018, **8**, 40054–40059.

312 A. Wang, L. Cheng, W. Zhao, X. Shen and W. Zhu, *J. Colloid Interface Sci.*, 2020, **579**, 598–606.

313 S. Bhunia, K. Bhunia, B. C. Patra, S. K. Das, D. Pradhan, A. Bhaumik, A. Pradhan and S. Bhattacharya, *ACS Appl. Mater. Interfaces*, 2019, **11**, 1520–1528.

314 A. Wang, L. Cheng, X. Shen, W. Zhu and L. Li, *Dyes Pigm.*, 2020, **181**, 108568.

315 H. Jia, Z. Sun, D. Jiang and P. Du, *Chem. Mater.*, 2015, **27**, 4586–4593.

316 B. Wurster, D. Grumelli, D. Hötger, R. Gutzler and K. Kern, *J. Am. Chem. Soc.*, 2016, **138**, 3623–3626.

317 J. Meng, Y. Zhou, H. Chi, K. Li, J. Wan and Z. Hu, *ChemistrySelect*, 2019, **4**, 8661–8670.

318 H. Jia, Y. Yao, J. Zhao, Y. Gao, Z. Luo and P. Du, *J. Mater. Chem. A*, 2018, **6**, 1188–1195.

319 J. Liu, Y. Ji, J. Nai, X. Niu, Y. Luo, L. Guo and S. Yang, *Energy Environ. Sci.*, 2018, **11**, 1736–1741.

320 Y. Tan, H. Wang, P. Liu, Y. Shen, C. Cheng, A. Hirata, T. Fujita, Z. Tang and M. Chen, *Energy Environ. Sci.*, 2016, **9**, 2257–2261.

321 E. Davari and D. G. Ivey, *Sustainable Energy Fuels*, 2018, **2**, 39–67.

322 P. Peng, L. Shi, F. Huo, C. Mi, X. Wu, S. Zhang and Z. Xiang, *Sci. Adv.*, 2019, **5**, eaaw2322.

323 J.-N. Liu, B.-Q. Li, C.-X. Zhao, J. Yu and Q. Zhang, *ChemSusChem*, 2020, **13**, 1529–1536.

324 X. Fan, F. Kong, A. Kong, A. Chen, Z. Zhou and Y. Shan, *ACS Appl. Mater. Interfaces*, 2017, **9**, 32840–32850.

325 B.-Q. Li, C.-X. Zhao, S. Chen, J.-N. Liu, X. Chen, L. Song and Q. Zhang, *Adv. Mater.*, 2019, **31**, 1900592.

326 Y. Li, X. Tao, J. Wei, X. Lv and H.-G. Wang, *Chem. – Asian J.*, 2020, **15**, 1970–1975.

327 S. Xu, Z. Li, Y. Ji, S. Wang, X. Yin and Y. Wang, *Int. J. Hydrogen Energy*, 2014, **39**, 20171–20182.

328 B.-Q. Li, S.-Y. Zhang, L. Kong, H.-J. Peng and Q. Zhang, *Adv. Mater.*, 2018, **30**, 1707483.

329 X. Hu, J. Jian, Z. Fang, L. Zhong, Z. Yuan, M. Yang, S. Ren, Q. Zhang, X. Chen and D. Yu, *Energy Storage Mater.*, 2019, **22**, 40–47.

330 M. Luo, Z. Zhao, Y. Zhang, Y. Sun, Y. Xing, F. Lv, Y. Yang, X. Zhang, S. Hwang, Y. Qin, J.-Y. Ma, F. Lin, D. Su, G. Lu and S. Guo, *Nature*, 2019, **574**, 81–85.

331 D.-H. Nam, P. De Luna, A. Rosas-Hernández, A. Thevenon, F. Li, T. Agapie, J. C. Peters, O. Shekhah, M. Eddaoudi and E. H. Sargent, *Nat. Mater.*, 2020, **19**, 266–276.

332 L. Wang, W. Chen, D. Zhang, Y. Du, R. Amal, S. Qiao, J. Wu and Z. Yin, *Chem. Soc. Rev.*, 2019, **48**, 5310–5349.

333 C. Yang, S. Li, Z. Zhang, H. Wang, H. Liu, F. Jiao, Z. Guo, X. Zhang and W. Hu, *Small*, 2020, **16**, 2001847.

334 S. Fukuzumi, Y.-M. Lee, H. S. Ahn and W. Nam, *Chem. Sci.*, 2018, **9**, 6017–6034.

335 R. De, S. Gonglach, S. Paul, M. Haas, S. S. Sreejith, P. Gerschel, U.-P. Apfel, T. H. Vuong, J. Rabeah, S. Roy

This journal is © The Royal Society of Chemistry 2021

Chem. Soc. Rev., 2021, **50**, 2540–2581 | **2579**

and W. Schöfberger, *Angew. Chem., Int. Ed.*, 2020, **59**, 10527–10534.

336 A. Maurin and M. Robert, *J. Am. Chem. Soc.*, 2016, **138**, 2492–2495.

337 S. Gonglach, S. Paul, M. Haas, F. Pillwein, S. S. Sreejith, S. Barman, R. De, S. Müllegger, P. Gerschel, U.-P. Apfel, H. Coskun, A. Aljabour, P. Stadler, W. Schöfberger and S. Roy, *Nat. Commun.*, 2019, **10**, 3864.

338 J. Choi, J. Kim, P. Wagner, S. Gambhir, R. Jalili, S. Byun, S. Sayyar, Y. M. Lee, D. R. MacFarlane, G. G. Wallace and D. L. Officer, *Energy Environ. Sci.*, 2019, **12**, 747–755.

339 M. Abdinejad, C. Dao, B. Deng, M. E. Sweeney, F. Dielmann, X.-A. Zhang and H. B. Kraatz, *ChemistrySelect*, 2020, **5**, 979–984.

340 X.-M. Hu, M. H. Rønne, S. U. Pedersen, T. Skrydstrup and K. Daasbjerg, *Angew. Chem., Int. Ed.*, 2017, **56**, 6468–6472.

341 M. Zhu, J. Chen, L. Huang, R. Ye, J. Xu and Y.-F. Han, *Angew. Chem., Int. Ed.*, 2019, **58**, 6595–6599.

342 A. Maurin and M. Robert, *Chem. Commun.*, 2016, **52**, 12084–12087.

343 J. Choi, P. Wagner, R. Jalili, J. Kim, D. R. MacFarlane, G. G. Wallace and D. L. Officer, *Adv. Energy Mater.*, 2018, **8**, 1801280.

344 Y. Guo, W. Shi, H. Yang, Q. He, Z. Zeng, J.-Y. Ye, X. He, R. Huang, C. Wang and W. Lin, *J. Am. Chem. Soc.*, 2019, **141**, 17875–17883.

345 F. Li, Y. C. Li, Z. Wang, J. Li, D.-H. Nam, Y. Lum, M. Luo, X. Wang, A. Ozden, S.-F. Hung, B. Chen, Y. Wang, J. Wicks, Y. Xu, Y. Li, C. M. Gabardo, C.-T. Dinh, Y. Wang, T.-T. Zhuang, D. Sinton and E. H. Sargent, *Nat. Catal.*, 2020, **3**, 75–82.

346 M. S. Xie, B. Y. Xia, Y. Li, Y. Yan, Y. Yang, Q. Sun, S. H. Chan, A. Fisher and X. Wang, *Energy Environ. Sci.*, 2016, **9**, 1687–1695.

347 S. Ren, D. Joulié, D. Salvatore, K. Torbensen, M. Wang, M. Robert and C. P. Berlinguette, *Science*, 2019, **365**, 367–369.

348 H.-J. Zhu, M. Lu, Y.-R. Wang, S.-J. Yao, M. Zhang, Y.-H. Kan, J. Liu, Y. Chen, S.-L. Li and Y.-Q. Lan, *Nat. Commun.*, 2020, **11**, 497.

349 C. Lu, J. Yang, S. Wei, S. Bi, Y. Xia, M. Chen, Y. Hou, M. Qiu, C. Yuan, Y. Su, F. Zhang, H. Liang and X. Zhuang, *Adv. Funct. Mater.*, 2019, **29**, 1806884.

350 J. Han, P. An, S. Liu, X. Zhang, D. Wang, Y. Yuan, J. Guo, X. Qiu, K. Hou, L. Shi, Y. Zhang, S. Zhao, C. Long and Z. Tang, *Angew. Chem., Int. Ed.*, 2019, **58**, 12711–12716.

351 J. Liu, Y.-Z. Fan, K. Zhang, L. Zhang and C.-Y. Su, *J. Am. Chem. Soc.*, 2020, **142**, 14548–14556.

352 F. Mao, Y.-H. Jin, P. F. Liu, P. Yang, L. Zhang, L. Chen, X.-M. Cao, J. Gu and H. G. Yang, *J. Mater. Chem. A*, 2019, **7**, 23055–23063.

353 Y. Lu, J. Zhang, W. Wei, D.-D. Ma, X.-T. Wu and Q.-L. Zhu, *ACS Appl. Mater. Interfaces*, 2020, **12**, 37986–37992.

354 Q. Wu, R.-K. Xie, M.-J. Mao, G.-L. Chai, J.-D. Yi, S.-S. Zhao, Y.-B. Huang and R. Cao, *ACS Energy Lett.*, 2020, **5**, 1005–1012.

355 J.-X. Wu, S.-Z. Hou, X.-D. Zhang, M. Xu, H.-F. Yang, P.-S. Cao and Z.-Y. Gu, *Chem. Sci.*, 2019, **10**, 2199–2205.

356 D. Yang, S. Zuo, H. Yang, Y. Zhou and X. Wang, *Angew. Chem., Int. Ed.*, 2020, **59**, 18954–18959.

357 B. Wang, F. Yang, Y. Dong, Y. Cao, J. Wang, B. Yang, Y. Wei, W. Wan, J. Chen and H. Jing, *Chem. Eng. J.*, 2020, **396**, 125255.

358 L. Jiao, W. Yang, G. Wan, R. Zhang, X. Zheng, H. Zhou, S.-H. Yu and H.-L. Jiang, *Angew. Chem., Int. Ed.*, 2020, **59**, 20589–20595.

359 R. Schlögl, *Angew. Chem., Int. Ed.*, 2015, **54**, 3465–3520.

360 S. Feng, W. Zheng, J. Zhu, Z. Li, B. Yang, Z. Wen, J. Lu, L. Lei, S. Wang and Y. Hou, *Appl. Catal., B*, 2020, **270**, 118908.

361 Y. Hou, Y.-B. Huang, Y.-L. Liang, G.-L. Chai, J.-D. Yi, T. Zhang, K.-T. Zang, J. Luo, R. Xu, H. Lin, S.-Y. Zhang, H.-M. Wang and R. Cao, *CCS Chem.*, 2019, **1**, 384–395.

362 H.-J. Son, S. Jin, S. Patwardhan, S. J. Wezenberg, N. C. Jeong, M. So, C. E. Wilmer, A. A. Sarjeant, G. C. Schatz, R. Q. Snurr, O. K. Farha, G. P. Wiederrecht and J. T. Hupp, *J. Am. Chem. Soc.*, 2013, **135**, 862–869.

363 Z.-B. Fang, T.-T. Liu, J. Liu, S. Jin, X.-P. Wu, X.-Q. Gong, K. Wang, Q. Yin, T.-F. Liu, R. Cao and H.-C. Zhou, *J. Am. Chem. Soc.*, 2020, **142**, 12515–12523.

364 Y.-N. Gong, W. Zhong, Y. Li, Y. Qiu, L. Zheng, J. Jiang and H.-L. Jiang, *J. Am. Chem. Soc.*, 2020, **142**, 16723–16731.

365 J. Wu, Y. Huang, W. Ye and Y. Li, *Adv. Sci.*, 2017, **4**, 1700194.

366 S.-S. Wang, H.-H. Huang, M. Liu, S. Yao, S. Guo, J.-W. Wang, Z.-M. Zhang and T.-B. Lu, *Inorg. Chem.*, 2020, **59**, 6301–6307.

367 Q. Wang, Y. Zhang, H. Lin and J. Zhu, *Chem. – Eur. J.*, 2019, **25**, 14026–14035.

368 X. Zhang, Z. Wu, X. Zhang, L. Li, Y. Li, H. Xu, X. Li, X. Yu, Z. Zhang, Y. Liang and H. Wang, *Nat. Commun.*, 2017, **8**, 14675.

369 P. T. Smith, B. P. Benke, Z. Cao, Y. Kim, E. M. Nichols, K. Kim and C. J. Chang, *Angew. Chem., Int. Ed.*, 2018, **57**, 9684–9688.

370 D. Gao, H. Zhou, J. Wang, S. Miao, F. Yang, G. Wang, J. Wang and X. Bao, *J. Am. Chem. Soc.*, 2015, **137**, 4288–4291.

371 Q. Lu, J. Rosen, Y. Zhou, G. S. Hutchings, Y. C. Kimmel, J. G. Chen and F. Jiao, *Nat. Commun.*, 2014, **5**, 3242.

372 W. Zhu, Y.-J. Zhang, H. Zhang, H. Lv, Q. Li, R. Michalsky, A. A. Peterson and S. Sun, *J. Am. Chem. Soc.*, 2014, **136**, 16132–16135.

373 C. Costentin and J.-M. Savéant, *Nat. Rev. Chem.*, 2017, **1**, 0087.

374 S. Wannakao, T. Maihom, K. Kongpatpanich, J. Limtrakul and V. Promarak, *Phys. Chem. Chem. Phys.*, 2017, **19**, 29540–29548.

375 N. Huang, S. Yuan, H. Drake, X. Yang, J. Pang, J. Qin, J. Li, Y. Zhang, Q. Wang, D. Jiang and H.-C. Zhou, *J. Am. Chem. Soc.*, 2017, **139**, 18590–18597.

376 Y. Zhou, Y.-F. Xing, J. Wen, H.-B. Ma, F.-B. Wang and X.-H. Xia, *Sci. Bull.*, 2019, **64**, 1158–1166.

377 I. Liberman, R. Shimoni, R. Ifraemov, I. Rozenberg, C. Singh and I. Hod, *J. Am. Chem. Soc.*, 2020, **142**, 1933–1940.

378 C. J. Chang, L. L. Chng and D. G. Nocera, *J. Am. Chem. Soc.*, 2003, **125**, 1866–1876.

379 S. Wannakao, W. Jumpathong and K. Kongpatpanich, *Inorg. Chem.*, 2017, **56**, 7200–7209.

380 P. Gotico, L. Roupnel, R. Guillot, M. Sircoglou, W. Leibl, Z. Halime and A. Aukauloo, *Angew. Chem., Int. Ed.*, 2020, **59**, 22451–22455.

381 R. Zhang and J. J. Warren, *J. Am. Chem. Soc.*, 2020, **142**, 13426–13434.

382 K. M. Kadish, L. Frémond, F. Burdet, J.-M. Barbe, C. P. Gros and R. Guilard, *J. Inorg. Biochem.*, 2006, **100**, 858–868.

383 Y. Shimazaki, T. Nagano, H. Takesue, B.-H. Ye, F. Tani and Y. Naruta, *Angew. Chem., Int. Ed.*, 2004, **43**, 98–100.

384 T. C. Wang, I. Hod, C. O. Audu, N. A. Vermeulen, S. T. Nguyen, O. K. Farha and J. T. Hupp, *ACS Appl. Mater. Interfaces*, 2017, **9**, 12584–12591.

385 C.-W. Kung, K. Otake, C. T. Buru, S. Goswami, Y. Cui, J. T. Hupp, A. M. Spokoyny and O. K. Farha, *J. Am. Chem. Soc.*, 2018, **140**, 3871–3875.

386 A. A. Talin, A. Centrone, A. C. Ford, M. E. Foster, V. Stavila, P. Haney, R. A. Kinney, V. Szalai, F. El Gabaly, H. P. Yoon, F. Léonard and M. D. Allendorf, *Science*, 2014, **343**, 66–69.

387 W.-H. Li, W.-H. Deng, G.-E. Wang and G. Xu, *EnergyChem*, 2020, **2**, 100029.

388 S. Takaishi, M. Hosoda, T. Kajiwara, H. Miyasaka, M. Yamashita, Y. Nakanishi, Y. Kitagawa, K. Yamaguchi, A. Kobayashi and H. Kitagawa, *Inorg. Chem.*, 2009, **48**, 9048–9050.

389 E. M. Miner, S. Gul, N. D. Ricke, E. Pastor, J. Yano, V. K. Yachandra, T. Van Voorhis and M. Dincă, *ACS Catal.*, 2017, **7**, 7726–7731.

390 E. M. Miner, T. Fukushima, D. Sheberla, L. Sun, Y. Surendranath and M. Dincă, *Nat. Commun.*, 2016, **7**, 10942.

391 L. Sun, M. G. Campbell and M. Dincă, *Angew. Chem., Int. Ed.*, 2016, **55**, 3566–3579.

392 G. Xu, K. Otsubo, T. Yamada, S. Sakaida and H. Kitagawa, *J. Am. Chem. Soc.*, 2013, **135**, 7438–7441.

393 P. G. Boyd, A. Chidambaram, E. García-Díez, C. P. Ireland, T. D. Daff, R. Bounds, A. Gładysiak, P. Schouwink, S. M. Moosavi, M. M. Maroto-Valer, J. A. Reimer, J. A. R. Navarro, T. K. Woo, S. Garcia, K. C. Stylianou and B. Smit, *Nature*, 2019, **576**, 253–256.

394 A. N. Oldacre, A. E. Friedman and T. R. Cook, *J. Am. Chem. Soc.*, 2017, **139**, 1424–1427.

395 A. N. Oldacre, M. R. Crawley, A. E. Friedman and T. R. Cook, *Chem. – Eur. J.*, 2018, **24**, 10984–10987.

396 R. D. Mukhopadhyay, Y. Kim, J. Koo and K. Kim, *Acc. Chem. Res.*, 2018, **51**, 2730–2738.

397 Z. Han, R. Kortlever, H.-Y. Chen, J. C. Peters and T. Agapie, *ACS Cent. Sci.*, 2017, **3**, 853–859.

398 C. Chen, Y. Li, S. Yu, S. Louisia, J. Jin, M. Li, M. B. Ross and P. Yang, *Joule*, 2020, **4**, 1688–1699.

399 D. Hötger, M. Etzkorn, C. Morchutt, B. Wurster, J. Dreiser, S. Stepanow, D. Grumelli, R. Gutzler and K. Kern, *Phys. Chem. Chem. Phys.*, 2019, **21**, 2587–2594.

400 Q. Daniel, R. B. Ambre, B. Zhang, B. Philippe, H. Chen, F. Li, K. Fan, S. Ahmadi, H. Rensmo and L. Sun, *ACS Catal.*, 2017, **7**, 1143–1149.

401 A. D. Handoko, F. Wei, Jenndy, B. S. Yeo and Z. W. Seh, *Nat. Catal.*, 2018, **1**, 922–934.

402 N. Heidary, M. Morency, D. Chartrand, K. H. Ly, R. Iftimie and N. Kornienko, *J. Am. Chem. Soc.*, 2020, **142**, 12382–12393.

403 L. Feng, K.-Y. Wang, E. Joseph and H.-C. Zhou, *Trends Chem.*, 2020, **2**, 555–568.

404 X. Chen, H. Jiang, B. Hou, W. Gong, Y. Liu and Y. Cui, *J. Am. Chem. Soc.*, 2017, **139**, 13476–13482.

405 W. Liu, X. Li, C. Wang, H. Pan, W. Liu, K. Wang, Q. Zeng, R. Wang and J. Jiang, *J. Am. Chem. Soc.*, 2019, **141**, 17431–17440.